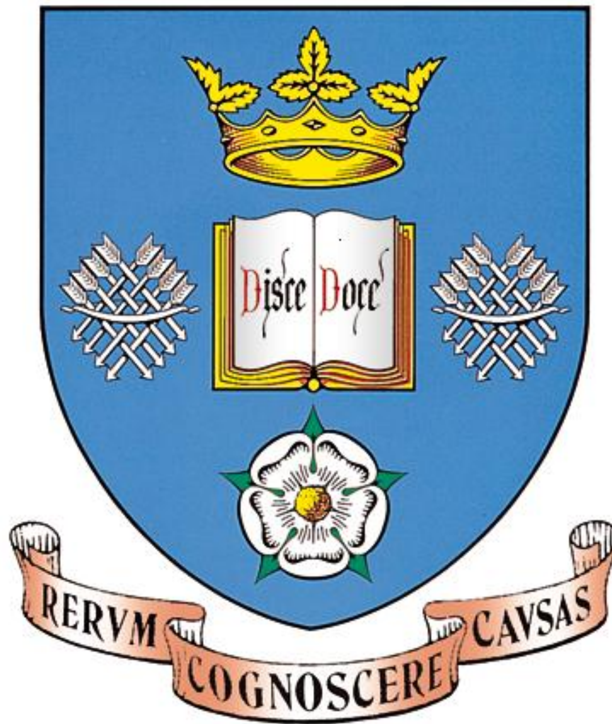

Gain Characterisation of 1.3µm GaAs Quantum Dot lasers

By

Hifsa Shahid

Department of Electronic and Electrical Engineering

THESIS
Submitted to the University of Sheffield in partial fulfilment of the degree of Doctor of Philosophy

December, 2012

Intentionally Blank

Abstract

Gain characterisation of a laser device is of fundamental importance to assist in the physical understanding of laser materials. Not only does it determine important parameters such as threshold, material loss and transparency current density, but is also a vital source of information regarding the evolution of states as a function of current density and temperature. The differential gain (dg/dn) is of key importance in determining the dynamic performance of a laser. Hence, the important role of gain characterisation has driven researchers to devise improved techniques for spectral gain measurement.

This thesis discusses the gain characterisation of 1.3μm quantum dot, commercial Innolume material and bi-layer laser devices. Initially, different gain measurement techniques are reviewed. High resolution spectroscopy and variable stripe length methods are analysed and compared in detail. A technical review is presented for the first time for the commonly used Hakki and Paoli, segmented contact and a new "integrated mode filter" method for gain measurement.

Then the Hakki and Paoli method is used to perform high current density analysis of the gain spectrum of 1.3μm Innolume, quantum dot laser material under continuous wave drive conditions. The device is characterised with and without self-heating effects. The elimination of self-heating effects is achieved by using a longitudinal mode as a junction temperature monitor to keep the junction temperature constant. This allowed an unambiguous study of the continuous wave gain spectrum at average dot occupancy levels up to ~8 e-h pairs per quantum dot. A negative differential gain is observed in both cases. This is shown to be predominantly due to the free carrier effects. As a result, free-carrier related negative differential gain is observed for the first time.

A variant to the segmented contact method, which utilises an integrated amplifier and mode filter is demonstrated for the first time. The measurement of the gain/absorption spectrum is

critically compared under identical data acquisition conditions as for the integrated mode filter and segmented contact methods. By driving the amplifier section, it is possible to achieve ~3-dB of signal amplification. As a result the measurement of the gain spectrum is achieved over a broader spectral range. Further, it is shown that the integrated amplifier method enables gain measurements at lower current densities as compared to the standard technique.

Lastly, the effect of inhomogeneous line width on the lasing line width of ~ 1.3μm quantum dot lasers is studied, as the line width of the transmitter is one of the key factors to determine the dispersion limit for optical communication systems. Two samples, with different inhomogeneous line width are compared under conditions where it is hoped that the effects of homogeneous line width and spectral hole burning are maintained at a constant level. This allows the effects of inhomogeneous line width alone to be studied. A ~30% reduction in inhomogeneous line width is shown to have a significant impact in reducing the lasing line width.

Dedicated to:

To my mother, late father,
&
brother

Intentional Blank

ACKNOWLEDGEMENTS

I would like to thank

God Almighty

Professor Richard A. Hogg: With his supervision and valuable discussions, I was able to complete my thesis.

Dr. Benjamin James Stevens, Dr. Mohammed Abdul Majid: For their samples to perform characterisation.

Dr. David Childs: For sorting out my experimental/equipment requirements (especially the multi-probes)

My Family: For their moral support.

Gordon, Taz , Negin Peyvast, Richard James Edward Taylor, Andrew John Vassilios Griffiths, Omar MS Ghazal: Always inspiring and smiling to get me relieved from the work stress.

Table of Contents

Abstract…… ii
Acknowledgement…… iv

Chapter 1: Historical perspective of semiconductor quantum dot lasers…. 1
1.1: Introduction…… 1
1.2: Evolution of Double Hetero-structures…… 1
1.2.1: Double Hetero-structures…… 2
1.2.2: Active Region Engineering…… 3
1.2.3: Density of states…… 4
1.3: Molecular Beam Epitaxy (MBE)…… 7
1.4: Historical Review of Quantum Dot Lasers…… 9
1.5: Transition Processes in Laser device…… 11
1.5.1: Gain of a Fabry-Pérot laser…… 13
1.5.2: Population Inversion…… 13
1.5.3: Threshold Gain…… 14
1.6: Significance of Gain Measurement…… 15
1.7: Thesis Outline…… 16
References…… 18

Chapter 2: Review of Gain Measurement Techniques…… 20
2.1: Introduction…… 20
2.2: Chapter outline…… 20
2.3: History of Gain measurement Techniques…… 21
2.4: High Resolution Spectroscopy…… 22
2.4.1: Hakki and Paoli Method…… 22
2.4.2: Cassidy and Improved Cassidy Method…… 23
2.4.3: Modal Spacing and resolution…… 24
2.4.4: Device Requirements…… 25
2.4.1.1: Technical Review: Hakki and Paoli Method…… 25
2.4.1.2: Apparatus…… 26
2.4.1.3: Experimental Issues: Trade-offs with Resolution…… 27
2.4.1.4: Experimental Issues: Fidelity of Gain Spectrum for Low Signals…… 28
2.4.1.5: Maintaining a Constant Junction Temperature…… 30
2.5: Variable Stripe Length Techniques…… 30
2.5.1: Shaklee and Lehney Method…… 30
2.5.2: Variable Stripe Length Method…… 30
2.5.3: Segmented Contact Method…… 31
2.5.3.1: Technical Review: Segmented Contact Method…… 33
2.5.3.2: Apparatus…… 34
2.5.3.3: Experimental Issues: Trade-offs with Resolution…… 35
2.5.3.4: Experimental Issues: Fidelity of Gain Spectrum for Low Signals…… 36
2.5.4: Integrated Mode Filter Technique…… 38

2.5.4.1: Technical Review…… 38
2.6: Self Heating Issues…… 40
2.7: Comparison of Gain Measurement Methods…… 40
2.8: Summary…… 42
References…… 43

Chapter 3: Free Carrier Effects in 1.3µm Quantum Dot Lasers…… 45
3.1: Introduction…… 45
3.2: Outline…… 46
3.3: Device Epitaxy and Fabrication…… 47
3.4: Apparatus…… 48
3.5: Device Characteristics…… 48
3.6: Establishing Constant-Junction Temperature Condition…… 51
3.7: Constant Heat-sink Temperature Gain Measurement…… 52
3.7.1: Analysis and Discussion…… 53
3.8: Maintaining a Constant- junction Temperature…… 54
3.9: Constant-junction Temperature Gain Measurement…… 56
3.9.1: Analysis and Discussion…… 57
3.9.2: Internal Loss…… 58
3.10: Comparison Constant Heat-Sink and Constant-Junction Temperature Conditions…… 59
3.11: Empirical Fitting…… 60
Summary…… 64
3.12: Future Work…… 64
References…… 66

Chapter 4: Integrated Amplifier Method for 1.3µm Quantum Dot Laser Material…… 68
4.1: Introduction…… 68
4.2: Outline…… 69
4.3: Device Epitaxy and Fabrication…… 70
4.4: Device Characteristics…… 72
4.5: Device geometries…… 74
4.6: Apparatus…… 77
4.7: Results and discussion…… 78
4.7.1: Gain measurement…… 78
4.7.2: Results and Discussion…… 80
4.8: Summary…… 85
4.9: Future Work…… 85
References…… 86

Chapter 5: Lasing Spectral Analysis for O-band Optical Communication………… 87
5.1: Introduction………… 87
5.2: 3-dB Line width of Lasing Spectrum………… 89
5.3: Inhomogeneous Broadening………… 90
5.4: Homogeneous Broadening………… 91
5.5: Spectral Hole Burning………… 92
5.6: Out line………… 95
5.7: Material Characteristics………… 95
5.7.1: Inhomogeneous Line width Measurement………… 96
5.7.1.1: Significance and measurement methods………… 96
5.7.1.2: Experimental Results………… 96
5.7.2: Modal Gain Measurement………… 99
5.7.2.1: Measurement and significance………… 99
5.7.2.2: Experimental Results………… 99
5.7.2.3: Discussion………… 100
5.7.3: Device Length Selection………… 101
5.7.3.1: Significance of Device Length Selection………… 101
5.7.3.2: Length Selection………… 101
5.8: Device Characteristics………… 103
5.8.1: Significance of Single Mode Device………… 103
5.8.2: Modal behaviour of Innolume and Bi-layer Devices………… 103
5.9: 3-dB Line width Comparison………… 105
5.9.1: Light-Current Density Characteristics………… 105
5.9.1.1: Significance and Measurement of External Differential Efficiency………… 105
5.9.1.2: Results………… 106
5.9.1.3: Discussion………… 107
5.9.2: 3-dB Line Width Comparison………… 108
5.9.2.1: Experimental Conditions………… 108
5.9.2.2: Innolume Laser Device………… 108
5.9.2.2.1: Experimental Results 108
5.9.2.2.2: Homogeneous Line width of the Innolume Laser Device………… 109
5.9.2.2.2.1: Experimental Results and Discussion………… 110
5.9.2.3: Bi-layer Laser device………… 112
5.9.2.4: Comparison of 3-dB Lasing Spectral Line Width………… 114
5.9.2.5: Results and Discussion………… 114
5.10: Summary………… 116
5.11: Future Work………… 116
References………… 117

List of Publications

Journals

1. **H. Shahid,** D. T. D. Childs, B. J. Stevens and R. A. Hogg,"Negative Differential Gain Due to Many Body Effects in Self-Assembled Quantum Dot Lasers", Appl. Phys. Lett. Vol. 99, 6, 061104 (2011).

2. M. A. Majid, D.T.D Childs, **H. Shahid**, S.Chen, K. Kennedy, R. J. Airey, R. A. Hogg, E. Clarke, P. Howe, P. Spencer and R. Murray, "Towards 1550 µm GaAs-based Lasers Using InAs/GaAs Quantum Dot Bilayers", IEEE J. Sel. Top. in Quant. Elect. Vol. 17, 5, 1334 - 1342 (2011).

3. M.A. Majid, D.T.D. Childs, **H. Shahid**, R. Airey, K. Kennedy, R.A. Hogg, E. Clarke, P. Spencer and R. Murray,"1.52 µm electroluminescence from GaAs-based quantum dot bilayers", Elect. Lett. Vol. 47, 1, 44 - 46 (2011).

4. M. A. Majid, D.T.D Childs, **H. Shahid**, S.Chen, K. Kennedy, R. J. Airey, R. A. Hogg, E.Clarke, P. Spencer and R. Murray,"Excited State Bilayer Quantum Dot Lasers at 1.3 µm" ,Jpn. J. Appl. Phys. Vol. 50, 04DG10, April (2011).

5. Kristian M Groom, Benjamin J. Stevens, Purnima D. L. Greenwood, David T. D. Childs, John S.Roberts, Matthew Lomas, Maxime Hugues, **Hifsa Shahid** and Richard Hogg, "A Platform for GaAs Opto-electronic Integrated Circuits Based on GaAs/AlGaAs regrowth upon patterned InGaP", Proc. of SPIE, Vol. 7616, 76160A - 76160A-9 (2010).

6. B. J. Stevens, D. T. D. Childs, **H. Shahid**, and R. A. Hogg, "Direct modulation of excited state quantum dot lasers", App. Phys. Lett. Vol. 95, 6, 061101 (2009).

Conference Proceedings

1. **H. Shahid**, D. T. D. Childs, B. J. Stevens, and R. A. Hogg, "Negative differential gain in 1.3um quantum dot lasers: comparison of self-heating and free carrier effects", Proc. of SPIE, Vol. 8255, 82550B (2012).

2. **H. Shahid**, D. T. D. Childs, B. J. Stevens and R. A. Hogg. "Comparison of Gain Measurement Techniques for 1.3µm Quantum Dot Lasers". Novel In-Plane Semiconductor Lasers X, Proc. of SPIE, 79531W (2011).

3. M. A. Majid, **H. Shahid**, S.Chen, D. T. D. Childs, R. J. Airey, K. Kennedy, R. A. Hogg, E. Clarke, P. Spencer and R. Murray. "Gain and absorption characteristics of bilayer quantum dot lasers beyond 1.3 µm". Novel In-Plane Semiconductor Lasers X, Proc. of SPIE, Vol. 7953, 795303 (2011).

4. M. A. Majid, D.T.D. Childs, S. Chen, **H. Shahid**, K. M. Groom, K. Kennedy, R. A. Hogg, E. Clarke, P. Spencer, and R. Murray, "Gain Spectra Analysis of Bilayer Quantum Dot Lasers beyond 1.3µm". Proc. of IEEE, Vol. 5706039(2010).

Oral and Poster Presentations

1. 11th Expert Evaluation & Control of Compound Semiconductor Materials and Technologies (EXMATEC), France 2012: Oral Presentation

2. Solid State Devices and Materials (SSDM), Japan 2011: Oral Presentation

3. UK Semiconductors Conference, United Kingdom 2011: Oral Presentation

4. Semiconductor and Integrated Optoelectronics conference (SIOE), United Kingdom 2011: Oral Presentation

5. SPIE Photonics West San Francisco, United States 2011: Poster Presentation

6. UK Semiconductors Conference, United Kingdom 2010: Oral Presentation

7. Photonics Global Conference, Singapore 2010: Oral Presentation

Featured article

"Joining the Dots, UK researchers have extended the emission wavelength of quantum dots on GaAs to 1.52 μm using a bilayer growth technique".
http://kn.theiet.org/magazine/eletters/4701/joining-the-dots.cfm

Chapter 1
Historical Perspective of Semiconductor Quantum Dot Lasers

1.1: Introduction

In this chapter, firstly the evolution of the hetero-structure and the idea of carrier confinement in the active region is discussed. Then, the change in the density of states with respect to bulk, well, wire and quantum dot systems is shown. The molecular beam epitaxy method for the growth of quantum dots is then discussed. This is then followed by a historical overview of quantum dot lasers. The transition processes in a laser device, and their influence over gain is also detailed. Lastly the gain of a Fabry-Pérot laser device, its significance and the thesis summary is presented.

1.2: Evolution of Double Hetero-structures

The evolution of modern hetero-structures began with the concept of the semiconductor laser introduced by Bosov in 1961[1.1].The first GaAs based pn homo-structure was demonstrated by Dr R. N. Hall [1.2] in 1962. These lasers could operate only at cryogenic temperatures and had a high threshold current density due to low carrier and optical mode confinement. To improve upon this Kroemer *et al.* were the first to come up with the idea of using hetero-structures instead of homo-structures, to obtain high efficiency, [1.3] due to a higher degree of carrier confinement. On the same lines, further improvements were made by Alferov and Adreev in 1969 as they realized a double hetero-structure. These were comparatively low threshold, room temperature operating lasers [1.4].

1.2.1: Double Hetero-structures

A double hetero-structure is made up of more than one kind of semiconductor material. Usually a lower band gap material is sandwiched between higher band materials for efficient optical and electrical confinement in the growth direction.

In order to achieve an optical confinement in the lateral direction, mainly two types of hetero-structures are fabricated. In these the lateral variation of refractive index causes either gain-guiding or index-guiding. As an example, gain-guided edge emitting [1.5] and index-guided buried hetero-structure [1.6] lasers are shown in Figures 1.1, 1.2.

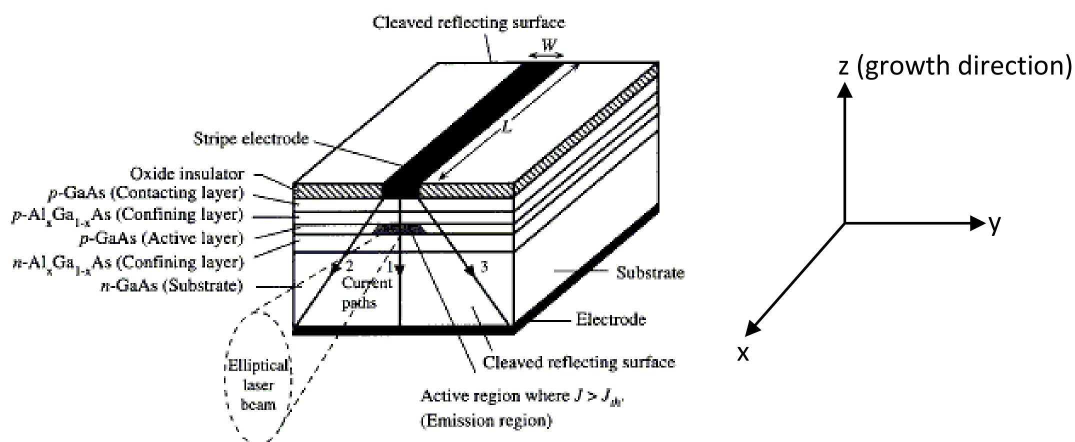

Figure 1.1: Gain guided edge emitting double hetero-structure[1.5].

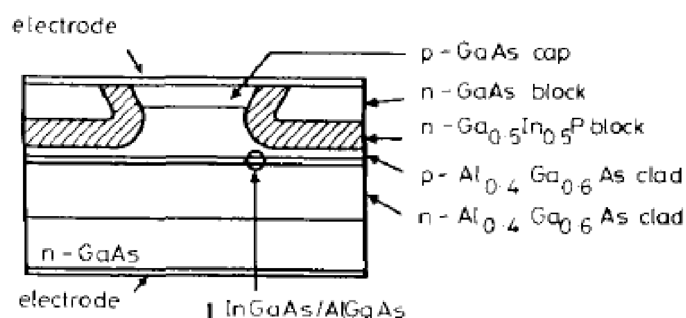

Figure 1.2: Index guided edge emitting double hetero-structure [1.6].

In this thesis the gain charcterisation of laser materials is performed via the fabrication of ridge lasers. These are a type of index-guided (weakly index-guided) [1.7] hetero-structures. The epitaxy and fabrication processes mainly involve a successive growth of the epitaxial layers which are then etched according to a required ridge width and depth. Figure 1.3 shows the schematic of an index-guided laser structure used for the analysis in this thesis. The fabrication details of the laser device are given in the later part of the thesis (chapter: 3). In this case a refractive index step between GaAs (~3.5) and the dielectric SiO_2 (~1.5) provided the lateral index guiding. This type of design (narrow ridge) is generally employed to achieve single lateral mode operation in addition to inhibiting lateral carrier spreading.

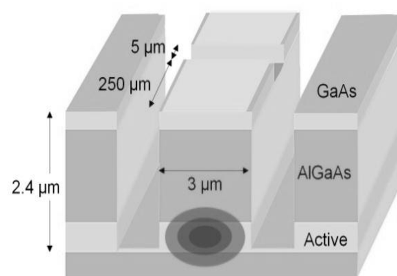

Figure 1.3: A narrow ridge (weakly index-guided) multi-section device, grown by Innolume GmBh (described in chapter: 3).

1.2.2: Active Region Engineering

In an attempt to improve the performance of hetero-structure lasers, it was proposed that carrier confinement in the active layer could be exploited further. This would result in the improvement of various important laser parameters such as threshold, gain, temperature insensitivity (characteristic temperature T_o), and wavelength tunability. The following section details how the application of the concept of carrier confinement in the active region in various spatial directions can lead to the achievement of these proposed advantages.

1.2.3: Density of States

Figure 1.4 is a schematic diagram which highlights the change in the density of states as a function of the degree of carrier confinement in the active layer. The density of states being the density of available energy states where the carriers can reside.

For a 3-D system (Bulk) a continuum of states is available in all three dimensions. At the band edge (E_g) the density of states is zero which then gradually increases as $(E)^{1/2}$. To achieve lasing threshold at a required energy level, high current densities would be required due to the carriers being used to fill the unused low energy states.

A 2-D quantum well system restricts the carrier movement in only one direction (z-direction Figure 1.1). Growing a very thin active layer (usually $\leq$ 10nm) leads to the quantisation of states in the direction of growth. The carriers are trapped (confined) in these states but are free to move in the plane of the well with the same probability of transition for each state. Therefore for the state being near to the band edge (lowest energy state), each of the injected carrier is available for inter band transition which leads to the possibility of achieving the same gain but with much lower current density in comparison to the bulk system The density of states is reduced compared to bulk and akin to a step like function. Therefore, the threshold condition is achieved at a lower current density in comparison to bulk semiconductors.

In the case of a 1-D quantum wire system (developed with the idea of lateral confinement in quantum well systems) the carrier movement is allowed only in one direction. The density of states is reduced compared to the quantum well system and varies as $(E)^{-1/2}$, which leads to an even lower threshold current density.

In the case of the 0-D quantum dot system (zero-dimensional system) the carrier movements are restricted in all three directions and the carriers within quantum dots are fully localised.

The density of states resembles a delta (δ) function and is the least of the other systems. Therefore the smallest comparative current density is required to achieve threshold.

It can be concluded from the above that by restricting carrier movement from 3-D to 0-D, the density of states is reduced. However, the carriers reside in a narrower energy range near the band gap edges (from 3-D to 0-D) which results in a correspondingly reduced threshold current density and hence gain is enhanced.

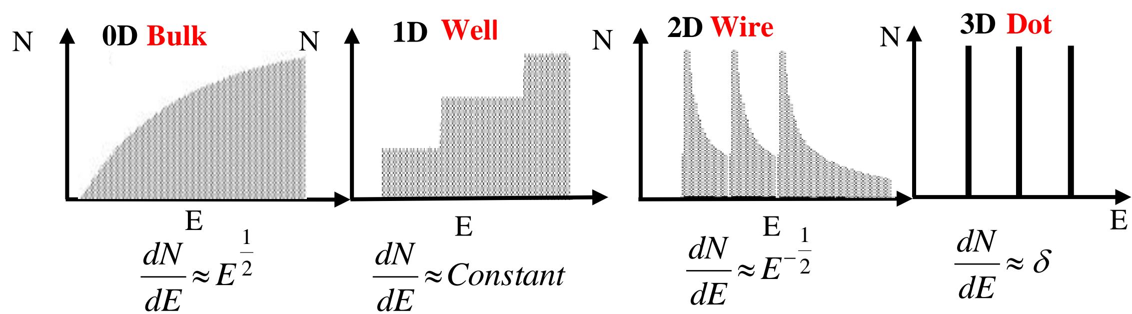

Figure 1.4: The density of states depending upon the degree of confinement in different systems.

Figure 1.5[1.8] plots the calculated modal gain as a function of current density for different systems depending on the carrier confinement. It can be clearly observed that the lowest threshold current density and highest material gain is possible in the quantum dot (Box) system. It is attributable to its highest degree of carrier confinement.

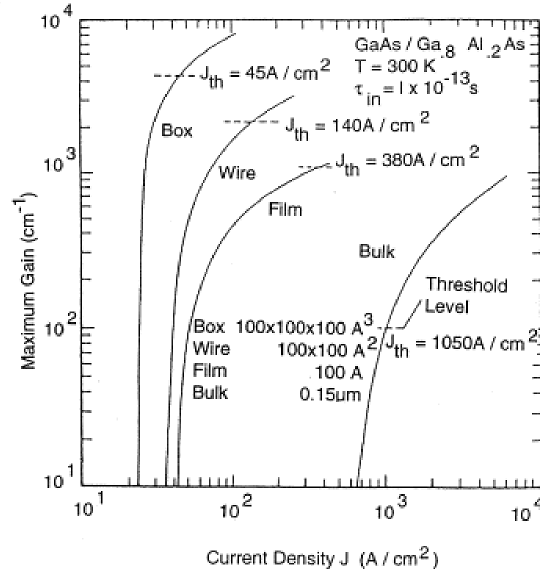

Figure 1.5: Calculated gain as a function of current density for different systems [1.8]. 100A° (10nm) is the quantum confinement dimension to observe the quantisation effects in each type of the system.

In this thesis, I shall only discuss the quantum dot system. The basic constituent of the system is a quantum dot/box which resembles an artificial atom with very small dimensions ($\leq$ ~10nm) to exhibit quantum confinement effects. High differential efficiency, high gain [1.8], lowest threshold current density and high temperature insensitivity [1.9] are theoretically predicted for the quantum dot system. However, practically due to the size variation among quantum dots we observe broad spectra. The dot densities are not very high ~ $10^{9\text{-}11}$/cm^2 and the confinement potentials are not infinite. All these issues tend to deteriorate the expected performance of the quantum dot laser system.

1.3: Molecular Beam Epitaxy

One of the main advancements towards the improvement of the optical properties of semiconductor devices is the possibility of device engineering via precise growth techniques. Molecular beam epitaxy (MBE) and metal organic vapour phase epitaxy (MOVPE) are the two major growth techniques by which complex compound semiconductor structures can be grown with precision and purity. For the growth of quantum dot nano-structures used for the characterisation in this thesis the MBE method is employed. It is usually preferred, as it has extensive in-situ monitoring tools. This technique was introduced by Alfred Y. Cho and J.R. Arthur in Bell Telephone Laboratories in the late 1960s [1.10].

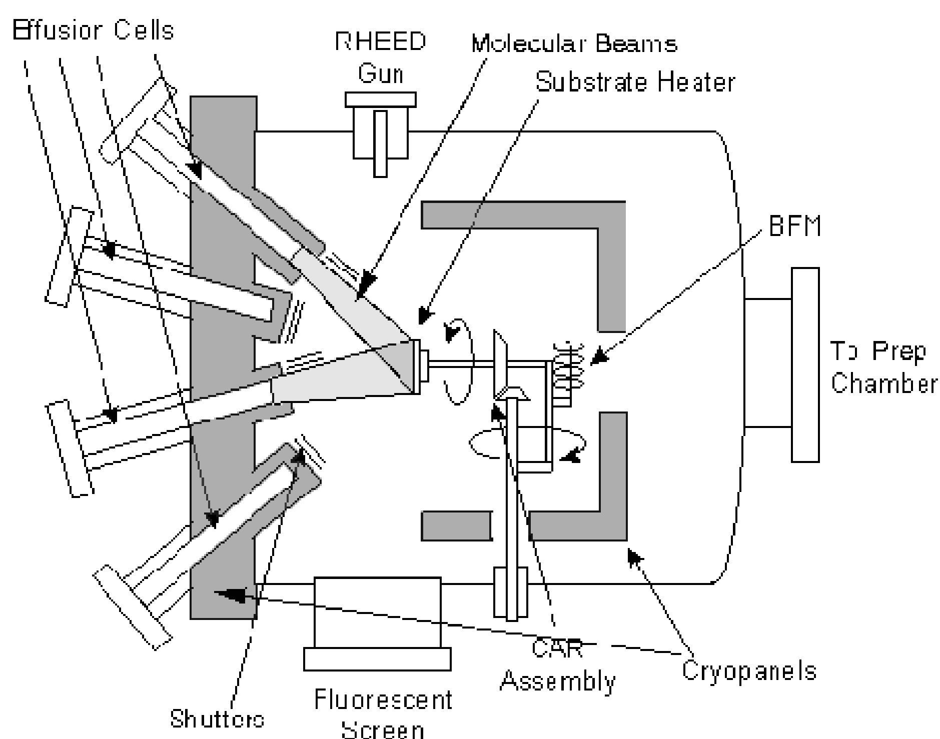

Figure 1.6: Schematic of molecular beam epitaxy (MBE) reactor [1.11].

The main chamber for molecular beam epitaxial growth with its essential constituent parts is shown schematically in Figure1.6 [1.11]. A high vacuum of ~10^{-8} Pascal is maintained inside the chamber to minimise any contamination. The effusion cells contain the metals: Al, Ga, In and As etc. and the dopants: Si and Be. By heating the desired materials to evaporate and letting the shutters open (speed:< 1 sec) of the corresponding effusion cells the atomic beams are directed towards a slowly rotating substrate (controlled via continuous azimuthal rotation (CAR)) assembly to ensure a uniform layer of atomic deposition. These beams of the corresponding elements do not interact. The substrate, usually GaAs, InP, Ge or Si is maintained at a high temperature, dependent upon the type of material to be deposited. The growth rate is usually around one monolayer per second. The opening and closing of the mechanical shutters before the effusion cells operates at a higher rate in comparison to the growth rate to ensure the exact deposition thickness. A Beam flux monitor (BFM) is used to monitor the atomic beam flux. Cryopanels are used to cool down the parts of MBE reactor other than the effusion cells. Reflection high energy electron diffraction (RHEED) assembly [1.12] is used to monitor the thickness of the deposition and the structure of the grown layer via electron beam diffraction pattern obtained on a screen. It is also used to maintain the substrate temperature at a constant value via feedback mechanism used for temperature calibration. All these features make MBE a preferable growth technique over MOVPE for the purpose of growing the dots with precision.

The quantum dots grown by MBE method are usually grown by the Stranski-Krastanov growth mode by which growth transforms from two dimensional to three dimensional (two dimensional wetting layer to quantum dots). The lattice constant for InAs is approximately 7% more than GaAs. In the case of growing InAs quantum dots on a GaAs substrate, a thin layer of InAs material is deposited upon the GaAs. Due to the lattice mismatch between the materials, a strain is developed in the InAs layer. However after the growth of the critical

thickness (usually ~1.5 mono-layers, known as a wetting layer) the InAs starts clustering together via a self assembly process in an attempt to relax the developed strain[1.13]. If the material is grown beyond the critical thickness then dislocations may be formed. However by achieving the critical thickness the 3-dimensional islands (quantum dots) are formed which can be pyramids, cones, or lenses. A quantum dot is usually made up of 10^4 to 10^5 atoms and exhibits atom like properties with its ground and excited state resembling s and p orbitals. The achievable densities up till now are ~$10^{9\text{-}11}$/cm^2. The energy spacing between the confined levels may be greater than 70meV, avoiding possible thermalisation, as at room temperature the thermal energy is 25meV(kT).

1.4: Historical Review of Quantum Dot Lasers

In1982 the theory of quantum dot lasers was described [1.8, 1.9] by which an improvement in overall characteristics such as material gain, differential gain, characteristic temperature and threshold current density of the laser was suggested. My work in this thesis is the gain characterisation of 1.3µm quantum dot laser devices. Therefore, the practical historical evolution of laser devices in terms of their threshold current density, beginning from homo-structure to quantum dot laser devices are shown in Figure 1.7 [1.14]. Kirstaedter *et al.* [1.15]in 1994, employed MBE to grow self-organized quantum dots and achieved room temperature lasing at a threshold current density of 950A/cm^2 from a single quantum dot layer. In 1996, Alferov *et al.* via 3 layer stacking managed to further reduce the threshold current density to 680A/cm^2 at room temperature and attempted to overcome the issue of gain saturation [1.16]. Ledentsov *et al.* in 1996 achieved a very low threshold current density of 90 A/cm^2 at room temperature via 10 layer vertical stacking [1.17]. Subsequently Iluaiig *et al.* [1.18] achieved a continuous wave room temperature threshold value of 24A/cm^2. A lower threshold current density of the order of 7A/cm^2 per quantum dot layer was achieved by

Bimberg *et al.* [1.19]. The 10.4A/cm^2, a further lower threshold current density has been reported for broad area laser with the cavity length of 1.6cm [1.20].

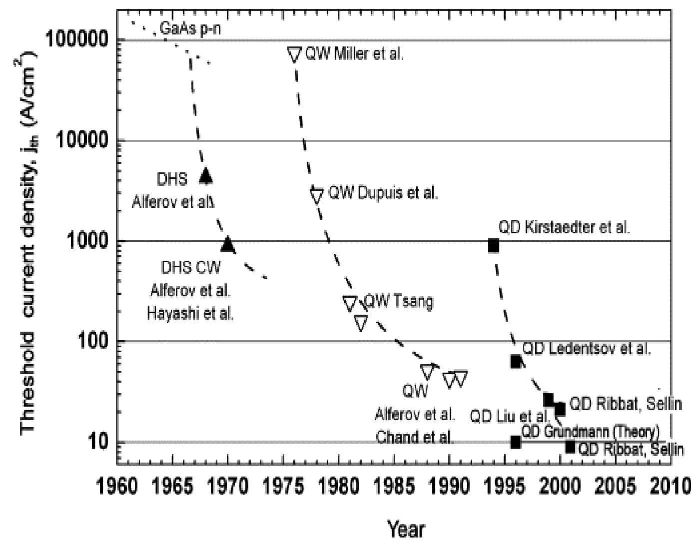

Figure 1.7: The improvement in threshold current density from homo-structure to quantum dot laser devices [1.14] (1960- 2010).

My work in this thesis is based on the empirical analysis of the static performance of 1.3µm AlInGaAs/GaAs quantum dot lasers via gain characterisation. The aim is to optimise the characterisation of quantum dot lasers for better understanding of the physical mechanisms behind their operation. This will enable the further evolution of quantum dots for FTTH telecommunications as transmitters where they are set to disrupt the dominance of InP quantum well lasers. Further applications are amplifiers [1.21] and in medical imaging for optical coherence tomography [1.22]. The gain characterisation of the laser devices performed in this thesis can not only be used in accessing the static, but also the dynamic performance of a laser device. It can be used for design optimisation and hence for device engineering purposes.

1.5: Transition Processes in Laser Device

In this section three main transition processes, common for all laser types are detailed:

1) Absorption

2) Spontaneous emission

3) Stimulated emission

Absorption: Figure 1.8 shows the process of absorption; an incoming photon is annihilated and its energy is transferred to an electron in the valence band. In this case, two situations may occur i.e. $E_{ph} \geq E_g$ or $E_{ph} < E_g$, where E_{ph} is the incoming photon energy and E_g is the band gap energy.

In the first situation if the energy of the photon is equal or greater than the band gap energy then upon annihilation the electron is promoted to the conduction band, leaving a hole behind. If the energy of the photon is more than the band gap energy then not only would it promote the electron but also impart to it some kinetic energy.

In the second case, if the photon energy is less than the band gap energy then ideally it would pass through the material without interaction in the absence of non-linear effects (e.g. two photon absorption). The rate of the absorption process essentially depends upon the number of empty conduction band states, the number of filled valence band states and the incoming photon density. If f_c and f_v are the occupation probabilities in the conduction and valence bands respectively, then the condition of absorption can be expressed in the form of eq. 1.1:

$$Rate\ of\ absorption = A_{vc} \times photon\ density \times f_v\left(1-f_c\right) \qquad (1.1)$$

A_{vc} is the Einstien's coeffiecient for absorption.

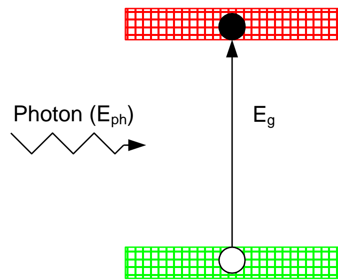

Figure 1.8: A schematic of the absorption process.

Spontaneous Emission: As shown in Figure 1.9 a free electron from the conduction band may combine with a hole in the valence band producing a photon, released with a random phase in a random direction. From the recombination of many electron–hole pairs incoherent light is generated. The condition of spontaneous emission is given in eq. 1.2:

$$Rate\ of\ spontaneous\ emission = B_{cv} \times f_c (1 - f_v) \qquad (1.2)$$

B_{cv} is the Einstein's coefficient of spontaneous emission.

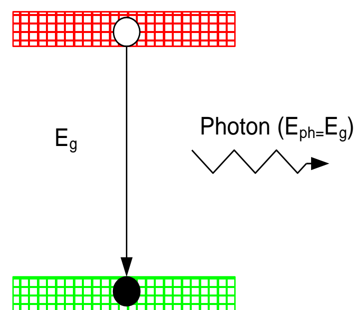

Figure 1.9: The schematic of the spontaneous emission process.

Stimulated Emission: During this process a photon interacts with an electron and hole, stimulating recombination. After recombination as shown in Figure 1.10 a second photon is

generated. It has exactly the same energy, phase and momentum as of the stimulating photon. The process depends upon the number of full conduction band states, number of empty valence band states and the incoming photon density. The condition of stimulated emission is given in eq. 1.3:

$$Rate\ of\ stimulated\ emission = A_{cv} \times Photon\ density \times f_c(1 - f_v) \qquad (1.3)$$

A_{cv} is the Einstein's coefficient for stimulated emission.

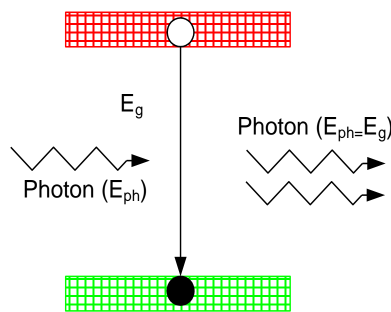

Figure 1.10: The schematic of the stimulated emission process.

1.5.1: Gain of a Fabry-Pérot Laser

Until now we have discussed hetero-structures which allowed us to understand how carrier and optical mode confinement is achieved in these structures. Combined with the understanding of transition processes occurring in a laser device, in the following section I shall discuss how population inversion is achieved in a Fabry-Pérot laser device.

1.5.2: Population Inversion

In a laser device at low injection levels photons are emitted through radiative recombination. However due to the low carrier concentration the rate of photon absorption is greater than that for stimulated recombination. Resultantly, absorption dominates and gain is not observed. In

the absence of any cavity loss, by increasing the current density transparency is achieved when the number of electrons in the conduction band equals the electron population in the valence band. Then by a further increase in the current density, the electron density in the conduction band exceeds that of the valence band's and population inversion is achieved. Under this condition, as the photons travel through the waveguide stimulated emission dominates and we obtain gain. However, taking into consideration the optical loss (α_i), the device needs to be operated at a higher level of inversion (electron densities) to achieve a net modal gain. The condition of net modal gain can be given by eq. 1.4:

$$Net\ Modal\ Gain = Stimulated\ \ Emission - absorption \qquad (1.4)$$

Therefore by eqs. 1.1 and 1.3:

$$Net\ ModalGain = f_c - f_v \qquad (1.5)$$

With f_c-f_v= 1, the highest net modal gain is achieved. For f_c=f_v the material is transparent and in case of f_c-f_v < 1 the material would be absorbing.

1.5.3: Threshold Gain

A Fabry-Pérot laser device (an optical resonator) can be thought of as involving a medium of length (L) which provides gain. It is cleaved along its crystallographic axis to provide two parallel facets on either of its sides to achieve the necessary optical feedback. The ~3.5 times higher refractive index of GaAs (the semiconductor material used to fabricate the laser in this thesis) than air, provides ~ 30% reflectivity. To achieve threshold, the modal gain: G (increase in photon density (cm^{-1})) must equal the losses which occurs due to absorption (e.g. free carrier), scattering due to defects and roughness (side walls), and mirror loss: α_m

(due to the laser facets) during a round trip. All losses except mirror loss are referred as optical loss.

The round-trip gain (cm^{-1}) is given by eq. 1.6. It can be further used to calculate the incremental gain as the optical mode travels through the waveguide.

$$Round-trip\ gain = \exp(2GL) \qquad (1.6)$$

Where 'G' is the material gain and 'L' is the length of the laser device. The factor of 2 accounts for the round trip between both facets.

The round-trip optical loss/photon loss (cm^{-1}) due to the laser cavity material and facets is given as:

$$Round-trip\ loss = R_1 R_2 \exp(-2\alpha_i L) \qquad (1.7)$$

Where 'α_i' is internal loss, $R_1$and R_2 are the mirror reflectivities.

According to the condition of threshold:

$$(Round-trip\ loss)(Round-trip\ gain) = 1$$

At threshold G = G_{th}. Then by eqs. (1.6, 1.7) at threshold:

$$R_1 R_2 \exp(2G_{th}L)\exp(-2\alpha_i L) = 1 \qquad (1.8)$$

$$R_1 R_2 \exp 2L(G_{th} - \alpha_i) = 1 \qquad (1.9)$$

By rearranging the eq. 1.9 the threshold modal gain is given by eq. 1.10:

$$G_{th} = \alpha_i + \frac{1}{2L}\ln\left(\frac{1}{R_1 R_2}\right) = \alpha_i + \alpha_m \qquad (1.10)$$

Where $\alpha_m = \frac{1}{2L}\ln\left(\frac{1}{R_1 R_2}\right)$

1.6: Significance of Gain Measurement

Gain measurement is of vital importance to assist in the understanding of the underlying physical behaviour of materials and hetero-structures. The spectral gain measurement is usually performed as a function of current density or as a function of the temperature to assist in the determination of various static (g (J,T)) and dynamic characteristics(dg/dJ (J, T)) of a laser device, dictating its performance. The analysis can be performed under two modes of operation either pulsed or continuous wave. To avoid self heating effects (thermal effects) as they usually mask the actual physical properties of the laser material, the devices are operated in pulsed mode. However, during pulsed mode operation the gating time is inversely proportional to the integration time so very long data acquisition times are expected. As a result, continuous wave operation may be used under the condition that a constant junction temperature is maintained. In the later part of this thesis, (Chapter: 3) a method to fix the junction temperature is discussed in detail.

1.7: Thesis Outline

Chapter 2: Presents a historical review of gain measurement techniques broadly subdivided into two types: high resolution spectroscopy and variable injection/stripe length. Then a technical review is presented. The theory, device requirements, resolution fidelity, experimental set ups and low power limitations of Hakki and Paoli [1.23], segmented contact [1.24] and integrated mode filter [1.25] techniques are analysed and compared for the first time. Self heating issues are also discussed. The suitability and comparison of the said

techniques for high current density measurement (with/without constant-junction temperature) and low current density analysis is also presented.

Chapter 3: This chapter explores the origin of negative differential gain in the case of 1.3μm ground state quantum dot laser devices. For this purpose an empirical analysis of the net modal gain spectra of quantum dot laser material at high carrier densities (~ 8 e-h) is presented. The spectral analysis was performed under constant heat-sink and constant-junction temperature conditions. The junction temperature was kept fixed by using a Fabry-Pérot mode as a temperature gauge. Therefore, by eliminating the self-heating effects entirely, the observation of free carrier effects was made possible. At excitation levels of up to ~8 e-h pairs per quantum dot for both constant heat-sink and constant-junction temperature conditions a very similar reduction in peak ground-state gain was observed. The results are attributed to free carrier effects, where increasing dephasing effects combined with saturated gain resulted in spectral broadening and hence a reduction in the peak gain.

Chapter 4: Quantum dot lasers exhibit a broad band emission, low threshold current density and lower transparency current density accompanied by a lower net modal gain. Therefore, the techniques which can be used at lower current densities to measure a wider spectral range are important to the characterisation of quantum dot devices. In this chapter the segmented contact method due to its better signal to noise ratio has been selected to perform low current density measurements (~0.04 e-h pairs/dot). A modified gain measurement technique, the integrated amplifier method is employed for the analysis by using the output sections of a multi-section device as an integrated optical amplifier and mode filter. The resultant enhancement to the spectral range over which the gain can be determined is discussed in detail. This technique is shown to be particularly advantageous for the

measurement of the absorption/gain spectrum at low carrier densities where the waveguide is operating in loss.

Chapter 5: The lasing line width of a laser transmitter is one of the key factors which determine the dispersion limit of an optical communication system. QD lasers are currently being commercialized for fibre-to-the-home (FTTH) optical communication systems. In this chapter the effect of inhomogeneous linewidth on the lasing linewidth of QD lasers is studied. Two samples, with different inhomogeneous linewidth are compared under conditions where it is hoped that the effects of homogeneous linewidth and spectral hole burning are maintained at a constant level, allowing the effects of inhomogeneous linewidth alone to be studied.

References

[1.1] W. W. Chow, S. W. Koch, "Semiconductor laser fundamentals", Springer-Verlag Berlin Heidelberg, New York, (1999).

[1.2] R. N. Hall, G. E. Fenner, J. D. Kingsley, "Coherent light emission from GaAs junctions", Phy. Rev. Lett. Vol. 9, 366(1962).

[1.3] H. Kroemer, "Theory of a wide-gap emitter for transistors", Proc. IRE Vol. 45, 11, 1535 (1957).

[1.4] Z. I. Alferov, V. M. Andreev, E. L. Portnoy, and M. K. Trukan, "AlAs–GaAs heterojunction injection lasers with a low room-temperature threshold", Fiz. Tekh. Poluprovodn. Vol. 3, 1328 – 1332(1969).

[1.5] S. O. Kasap, "Optoelectronics and Photonics: Principles and Practices", Prentice Hall, Ch.4, (2006).

[1.6] S. Ishikawa, K. Fukagi *et al.*, "0.98-1.02 μm Strained InGaAs/AlGaAs double quantum-well high power lasers with GaInP buried waveguides", IEEE J. Sel. Top. In Quant. Elect. Vol. 29, 6, 1936(1993).

[1.7] G. P. Agrawal, N. K. Dutta, "Semiconductor lasers", Van Nostrand Reinhold, Ch.5, (1993).

[1.8] M. Asada, Y. Miyamoto, "Gain and the threshold of three-dimensional quantum-box lasers", IEEE J. Quant. Elect. Vol. 22, 1915 – 1921(1986).

[1.9] Y. Arakawa and H. Sakaki, "Multidimensional quantum well laser and temperature dependence of its threshold current", Appl. Phys. Lett. Vol. 40, 939(1982).

[1.10] A. Y. Cho, J. R. Arthur, "Molecular beam epitaxy", Prog. Solid State Chem.Vol.10, 157 – 192 (1975).

[1.11] G. Biasiol and L. Sorba, "Crystal growth of materials for energy production and energy-saving applications", Edizioni ETS, Pisa, (2001).

[1.12] J. H. Neave, B. A. Joyce and P. J. Dobson, "Dynamic RHEED observations of the MBE growth of GaAs", Appl. Phys. A Vol. 34, 3, 179 - 184(1984).

[1.13] D. Bimberg, M. Grundmann and N. N. Ledentsov, "Growth, spectroscopy, and laser applications of self-ordered III-V quantum dots", MRS Bulletin Vol. 23, 2, 31(1998).

[1.14] M. Henini, M. Bugajski, "Advances in self-assembled semiconductor quantum dot lasers", Microelectronics Journal Vol. 36, 11, 950 – 956 (2005).

[1.15] N. Kirstaedter, N. N. Ledentsov, M. Grundmann, D. Bimberg, V. M. Ustinov, S. S. Ruvimov, M. V. Maximov, P. S. Kop'ev, Zh. I. Alferov, U. Richter, P. Werner, U. Gosele and J. Heydenreich, "Low threshold, large T_o injection laser emission from (InGa)As quantum dots", Elect. Lett. Vol. 30, 17, 1416 - 1417 (1994).

[1.16] M. Grundmann, N. N. Ledentsov, R. Heitz, D. Bimberg, V. M. Ustinov, A. Yu. Egorov, M. V. Maximov, P. S. Kop'ev, Zh.I. Alferov, "Growth, characterizations, theory and lasing of vertically stacked quantum dots", Proc. IPRM , 738 - 741 (1996).

[1.17] N. N. Ledentsov *et. al*, "Direct formation of vertically coupled quantum dots in Stranski-Krastanow growth", Phy. Rev.B, Vol. 54, 12, 8743 - 8750(1996).

[1.18] X. Iluaiig, A. Stinlz, C. P. Hains, G.T. Liu, J. Cheng and K. J Malloy, "Efficient high-temperature CW lasing operation of oxide-confined long-wavelength lnAs quantum dot lasers", Elect. Lett. Vol. 36, 1, 41 - 42(2000).

[1.19] D. Bimberg, N. N. Ledentsov and J. A. Lott, "Quantum-Dot Vertical-Cavity Surface - Emitting Lasers", MRS Bulletin Vol. 27, 7, 531 - 537(2002).

[1.20] D. G. Deppe, K. Shavritranuruk, G. Ozgur, H. Chen, S. Freisem, "Quantum dot laser diode with low threshold and low internal loss", Elect. Lett. Vol. 45,1, 54 - 55(2009).

[1.21] T. Akiyama, M. Sugawara, and Y. Arakawa, "Quantum-Dot Semiconductor Optical Amplifiers", Proc. IEEE Vol. 95, 9, 1757 - 1766(2007).

[1.22] P. D. L Greenwood *et al.*, "Quantum Dot Superluminescent Diodes for Optical Coherence Tomography: Device Engineering", IEEE J. sel. Top. In Quant. Elect. Vol. 16, 1015 - 1022(2010).

[1.23] B. W. Hakki and T. L. Paoli, "CW degradation at 300K of GaAs double heterostructure junction lasers. II. Electronic gain", J. Appl. Phys. Vol. 44, 9, 4113 - 4119 (1973).

[1.24] P. Blood, G. M. Lewis, P. M. Smowton,"Characterization of semiconductor laser gain media by the segmented contact method", IEEE J. sel. Top. In Quant. Elect. Vol. 9, 1275 - 1282(2003).

[1.25] Y. C. Xin *et al.*, "Determination of optical gain and absorption of quantum dots with an improved segmented contact method", Proc. of SPIE Vol. 5722, 49 - 59(2005).

CHAPTER 2
Review of Gain Measurement Techniques

2.1: Introduction

GaAs based quantum dot (QD) devices are an area of interest owing to their low cost and applications in laser displays, pointers, telecommunication and medical fields. In the telecommunication sector some of the important features include mode-locking [2.1], direct modulation for optical communications [2.2], temperature insensitive threshold current density [2.3], [2.4] and small line width enhancement factor [2.5]. In terms of their mode locking application in telecommunications, due to their inherent broad band and ultrafast carrier dynamics QD lasers are capable of producing ultra short pulses at high repetition rates (more than 1 THz) [2.1]. The line width enhancement factor being a ratio of real and imaginary parts of the refractive index as a function of carrier density has a very small value in case of QD [2.5] laser devices due to the symmetric shape of the gain spectra at high current densities. Therefore a lower chirp and correspondingly higher bit rates are expected. In medicine, due to their inherent broad spectral bandwidth they find application for biomedical imaging purposes (optical coherence tomography) to provide high resolution imaging [2.6]

Due to the applications discussed earlier, in addition to new emerging fields, there is a need for the analysing the static and dynamic performance of QD devices to improve and optimize their efficiency and to obtain required characteristics through careful device engineering. To this end, an understanding of the spectral gain-current relationship is required which can be obtained via gain spectral analysis as a function of increased current. A number of techniques for spectral gain measurement are available, but are rarely compared as they often require bespoke fabricated device structures to allow the analysis.

2.2: Chapter Outline

This chapter presents a historical review of gain measurement techniques. Particularly, technical reviews are presented for high resolution spectroscopy (Hakki and Paoli method) [2.7], [2.8], variable stripe length methods (segmented contact method) [2.9], and integrated mode filter method [2.10], [2.15]. A direct comparison of device requirements, experimental setups and issues regarding high/low current density measurements via high resolution spectroscopy (Hakki and Paoli method) [2.7],[2.8] and variable stripe length methods (segmented contact method [2.9] and Integrated mode filter method [2.10]) are discussed. A method to achieve a constant-junction temperature for the Hakki-Paoli technique is introduced and its advantage at high current density is discussed.

2.3: History of Gain Measurement Techniques

Gain measurement is of vital importance to assist in the understanding of the physical behaviour of the materials and hetero-structures. Various static and dynamic /modulation characteristics (differential gain, linewidth enhancement factor) can be analysed via gain spectral measurements. The available techniques can be broadly categorised into two types:

1) High Resolution Spectroscopy

- Hakki and Paoli [2.7], [2.8]

- Cassidy and modified Cassidy methods [2.11, 2.12]

2) Variable Stripe Length Techniques

- Shaklee and Leheney [2.13]

- Variable stripe length [2.14]

- Segmented contact method [2.9]

- Integrated mode filter method [2.10], [2.15]

These methods are rarely compared as some require bespoke devices to be fabricated and may require different drive techniques as well. Here, a brief introduction of each of the above techniques is presented, along with experimental data, comparing Hakki-Paoli, segmented contact and integrated mode filter methods. To the best of my knowledge, this is the first comparative analysis of these different gain spectrum measurement techniques.

2.4: High Resolution Spectroscopy

2.4.1: Hakki and Paoli Method

This method was introduced by Hakki and Paoli in 1975 [2.7] and as of the time of writing this paper has been cited 555 times. It is usually preferred as a special fabrication run is not required, as long as a single-mode laser is already made. It is a round trip method and is usually applied to single mode, short length Fabry-Pérot devices. This method is based on high resolution spectroscopy which requires the length of the cavity to be small enough to allow the full resolution of the electroluminescence spectrum in terms of individual Fabry-Pérot modes. It calculates net modal gain below threshold depending on the modulation depth of the resolved peaks and valleys of an electroluminescence spectrum. The difference in electroluminescence between the peaks and the troughs, where gain is constructive and destructive, allows gain and spontaneous emission to be determined. In Figure 2.1 an example electroluminescence spectrum is shown.

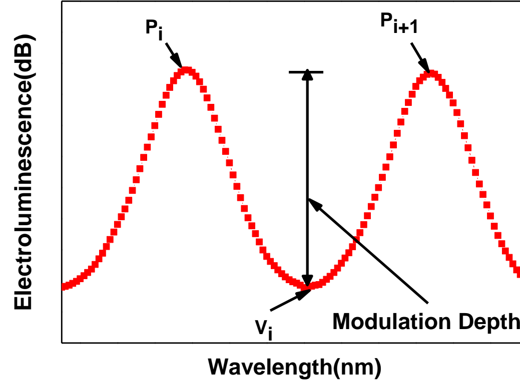

Figure 2.1: Febry–Pérot resonances of an electroluminescence spectrum indicating the peaks, valley and modulation depth.

The modulation depth is given by eq. 2.1:

$$Modulation\ depth = \gamma_i = \frac{P_i + P_{i+1}}{2V_i} \tag{2.1}$$

Where P_i , P_{i+1} are the intensities of the two consecutive peaks and V_i is the intensity of the valley in between them. The net modal gain is calculated in the case of the Hakki and Paoli method by eq.2.2:

$$Net\ modal\ gain = \frac{1}{L}\ln\left(\frac{\sqrt{\gamma_i}+1}{\sqrt{\gamma_i}-1}\right) + \frac{1}{2L}\ln\left(\frac{1}{R_1R_2}\right) \tag{2.2}$$

Facet reflectivities (R_1, R_2), modulation depth (γ_i) and the length of the device (L) are the main factors, required in determining the net modal gain value. This method also allows the calculation of the spontaneous emission by eq. 2.3. In this case the same electroluminescence spectrum is used as is for the net modal gain evaluation [2.8].

$$Spontaneous\ emission = \frac{4P_iV_i}{\left(\sqrt{P_i}+\sqrt{V_i}\right)^2} \tag{2.3}$$

2.4.2: Cassidy and Improved Cassidy Methods

The Cassidy method [2.10] was introduced as an improvement to the Hakki and Paoli method in 1984 and has been cited 91 times. It is used for the case when low S/N ratio is a major issue. In this case it was claimed that the gain could be determined via the contrast of the average mode intensity of a Fabry-Pérot mode instead of its maxima to its minima. The measurement would therefore be less sensitive to noise. It was further proposed that if additional averaging is performed over a spectral range around the minima of each mode then the measurements becomes even less sensitive to noise.

V. Jordan in 1994 proposed a method known as the “Modified Cassidy method” [2.12] which is cited 16 times, is an additional averaging method. The author analysed the Cassidy method and proposed that if additional averaging is not done around the minima of the mode then the Cassidy method becomes *more* sensitive to noise than the Hakki and Paoli method. In this case averaging is to be done over an additional wavelength interval which would give some percentage error in gain measurement.

2.4.3: Modal Spacing & Resolution

The separation between resolved longitudinal modes, $\Delta\lambda$, in an electroluminescence spectrum is determined by eq. 2.4 [2.16]:

$$\Delta\lambda = \frac{\lambda^2}{2nL} \qquad (2.4)$$

Where λ is emission wavelength, n is modal refractive index and L is the length of the device cavity. Device length determines the modal spacing which must be fully resolved to allow the correct determination of the net modal gain. A short cavity length is desirable as wider mode separation is obtained, making the resolution of modes easier. Furthermore, the threshold gain

increases, allowing the measurement of the gain spectrum to higher current densities (higher gain). Eq.2. 4 can, also be used to identify any additional modes other than the fundamental mode, if present in the cavity. It is not always recommended to go for the highest spectral resolution adjustment as with the increase in resolution of the optical spectrum analyser the signal to noise ratio of the optical signal is reduced.

The presence of additional lateral modes would render the gain measurements incorrect. It is theoretically possible to consider ultra-high resolution spectroscopy and the deduction of the gain spectrum by careful selection of the correct peaks and valleys. However, a practical method to avoid additional lateral modes is to spatially adjust the fibre used for light collection, or use a spatial filter (lens and the pinhole arrangement) to collect only the fundamental mode.

2.4.4: Device Requirements

As discussed previously, single mode Fabry-Pérot devices of a short length are preferable. To ensure a single mode device the selection of a narrow ridge device is more promising as the side walls of the device cavity provide a lossy medium for higher order lateral modes and high current densities may be accessed.

I do not consider the 'Modified Cassidy method' in my thesis. The high resolution spectroscopy gain measurements are performed by Hakki and Paoli method. In this chapter a detailed analysis of Hakki-Paoli method is presented regarding its power limitation, experimental apparatus and resolution requirements to perform the gain measurements.

2.4.1.1: Technical Review: Hakki and Paoli Method

Here, a single mode, 1300nm quantum dot Innolume laser device with the dimensions of 450µm x 3µm, fabricated by B.J.Stevens was selected. Light-current density and

electroluminescence vs. wavelength characteristics are shown in Figure 2.2 and in the inset, respectively. The device exhibited lasing after 1.8kAcm^{-2}.

Hakki and Paoli analysis could be made up to the lasing threshold. Whilst it would be very interesting to measure the gain spectrum above threshold, to investigate non-ideal gain clamping, it was found that this was not practical. Stray, scattered lasing light within the optical spectrum analyser modulates the measured Fabry-Pérot spectrum resulting in erroneous gain measurements. Inspection of the mode structure (as shown in the inset) is performed over a wide range of wavelengths to check for modulations on a wider range than the Fabry-Pérot mode-spacing to confirm there are no additional lateral modes.

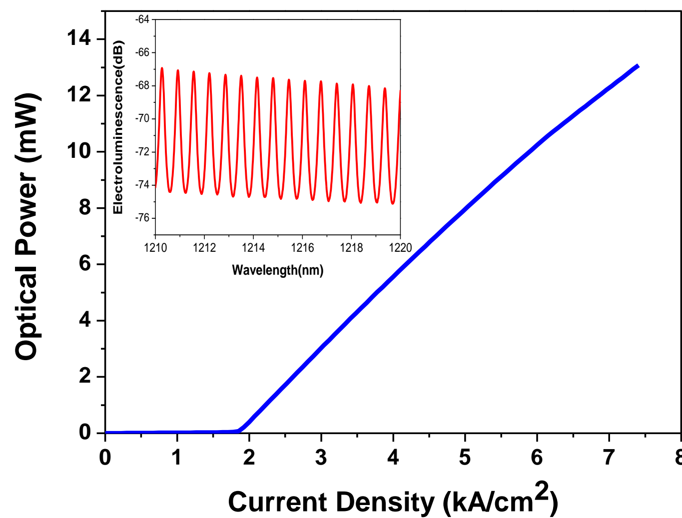

Figure 2.2(a): Light-Current density characteristics of 450x3µm, Innolume laser device used for Hakki and Paoli analysis, **(Inset)** Electroluminescence as a function of wavelength for 1.1kAcm^{-2} exhibiting the single mode characteristics for the device.

2.4.1.2: Apparatus

The experimental set up used for the Hakki and Paoli technique is shown in Figure 2.3.To fulfil the high resolution measurement requirement, an optical spectrum analyser with spectral resolution of 10pm was used (Advantest Q8384). In order to maintain constant, and high

coupling efficiencies, a set up consisting of optical splitter and piezoelectric actuator was used. The optical splitter was used to split the output optical power from the device in the ratio of 99:1. 99% percent of the optical power is coupled to the optical spectrum analyser and the remaining 1% is fed to a power meter. This allows positional feedback to the piezoelectric actuator to maintain highly stable experimental conditions which allowed a lensed fibre to be positioned dynamically, for maximum coupling.

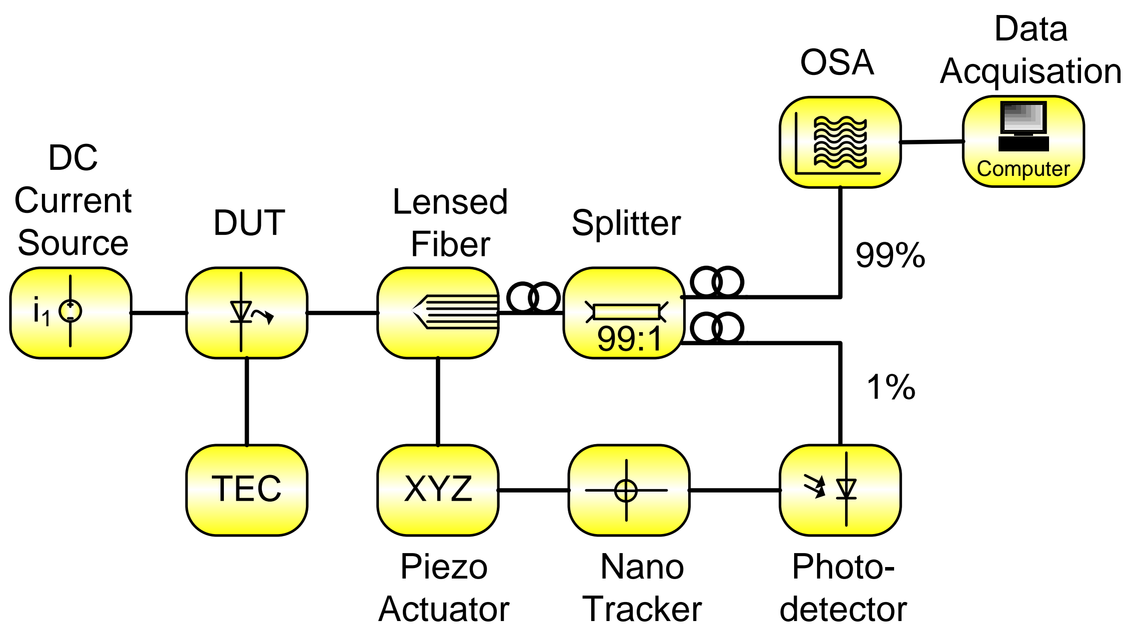

Figure 2.3: Experimental set up for Hakki and Paoli gain measurement.

2.4.1.3: Experimental Issues: Trade-offs with Resolution

The selection of a suitable spectroscopic resolution is vital. In order to fully resolve the Fabry-Pérot peaks and valleys a reduced throughput reduces the signal to noise of the data. As a consequence, the spectral resolution should not be over-specified. In order to optimize this, a series of spectra were obtained at different resolution settings for the same Innolume device as described in section 2.4.1.1. The gain was then calculated using eq.2.2. It was observed that the effect of insufficient resolution was an underestimation of the valley depth,

leading to an underestimation of the gain. As a result, the optimum spectroscopic resolution was determined at the point just before the onset of this reduction in calculated gain, corresponding to the maximum in light throughput and hence the maximum signal to noise ratio.

2.4.1.4: Experimental Issues: Fidelity of Gain Spectrum for Low Signals

Here, I describe an investigation into the effects of small signal powers on the gain spectra obtained via the Hakki and Paoli technique. In this case, the same Innolume device, as described in section 2.4.1.1 was used. While maintaining a constant current density the lensed fibre is misaligned (drawn back along the same axis of the device). This allows us to observe how the electroluminescence spectra would look at both limiting values of highest and lowest coupled optical powers, to explore how the Hakki and Paoli method fails. In an ideal case, calculation of the gain should result in identical results. However S/N ratio reduction will manifest itself in changes to the calculated spectrum. Figure 2.4 plots the electroluminescence spectra with the highest (722nW) and lowest coupled power (20nW), respectively. The noise floor of the measurement system is retrieved by not allowing any light to enter the optical spectrum analyser. From the spectra as shown in the Figure 2.4 it is possible to predict the spectral ranges over which gain can be deduced. Inspection of their corresponding valleys touching the noise floor indicates where gain measurement fidelity is lost.

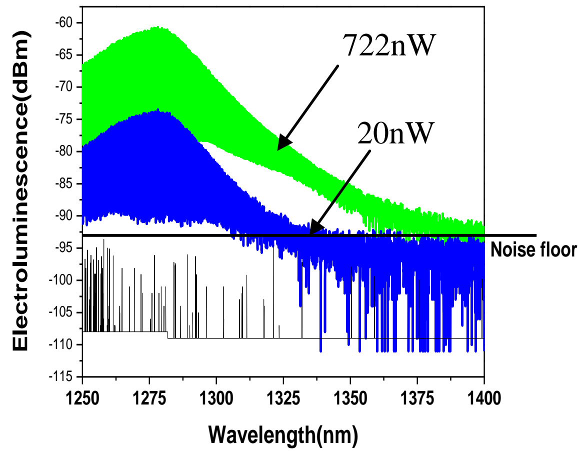

Figure 2.4: Electroluminescence as a function of wavelength for maximum and minimum power being coupled via lensed single mode fibre having 5µm core diameter to explore power limits of Hakki and Paoli method.

Figure 2.5 plots the net modal gain spectra calculated from eq.2.2 using spectral data similar to that shown in Figure 2.4 for a range of coupled powers. It can be observed that with a reduction in coupled power random noise is added to the calculated gain spectrum. Also some parts of the spectrum (at longer wavelengths) are elevated due to the valleys of the electroluminescence approaching the system noise floor. As a result the gain may be significantly over-estimated. Due to this the spectral range over which gain can be measured is reduced. However, the peak net modal gain as function of coupled power shows the variation within the limits of ±1 cm^{-1}, even at the lowest coupled power used here.

The increase in calculated gain at the edges of the spectrum is a tell-tale sign that the measurement is failing. As the gain calculations are based upon the measurement of the modulation depth, which in this case would be wrong due to valleys being over estimated. Referring back to the Figure 2.4, the signal approaches the noise floor at ~1300nm, in good agreement with the wavelength at which the gain spectrum calculation fails in Figure 2.5.

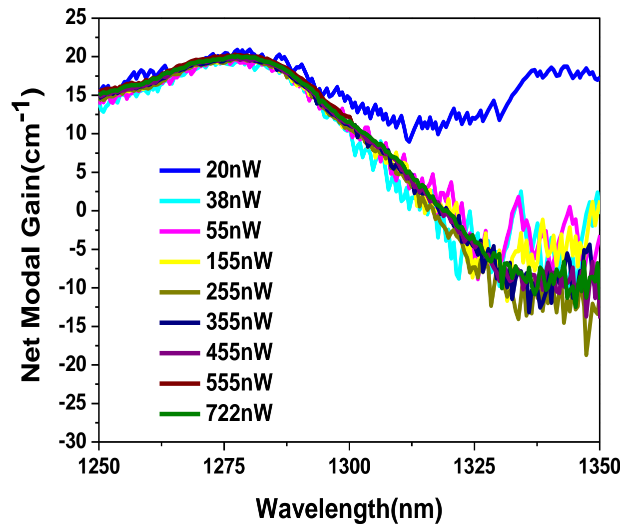

Figure 2.5: Hakki and Paoli net modal gain spectra for the Innolume device (section :2.4.1.1)as a function of wavelength for the increase in distance between the fibre and the device showing a corresponding decrease in coupled power and its effect on overall gain spectra.

2.4.1.5: Maintaining a Constant Junction Temperature

In later chapter (Chapter 3) I present data which shows that the shift of Fabry-Pérot modes as a function of current density is predominantly due to self heating. By utilizing the wavelength shift of a single Fabry-Pérot mode it is therefore possible to maintain a constant junction temperature. This is shown to be a significant advantage of the Hakki and Paoli method.

2.5: Variable Stripe Length Techniques

These techniques employ single pass measurement schemes for gain measurement and optical feed back is avoided.

2.5.1: Shaklee and Leheney Method

This method [2.13] was introduced by Shaklee and Leheney in 1971. It is a photoluminescence measurement technique to determine the gain spectrum of the material. In

this case, before fabrication, different lengths of the crystal are optically excited using a cylindrical lens and a spatial filter. The single pass amplified spontaneous emission is measured from the edge of the wafer, allowing the gain spectrum to be calculated. Whilst this method provides a rapid feed back to epitaxy on the *potential* of the material to make a laser, the carrier/current density within the laser is unknown. It is therefore of less use in the engineering of practical devices.

2.5.2: Variable Stripe Length Method

This method [2.14] of electrical excitation of laser material was given by A. Oster, G. Erbert and H. Wenzel in 1997. For the sake of current confinement, the cladding layer is etched as shown in Figure 2.6 and metal stripes are deposited. It is ensured via long passive lengths, and anti reflection coatings on both facets that feedback is avoided. This then allows single pass gain measurements by measuring the amplified spontaneous emission in a similar manner to the Shaklee-Leheney method. In this case though, the current density is a well-defined quantity.

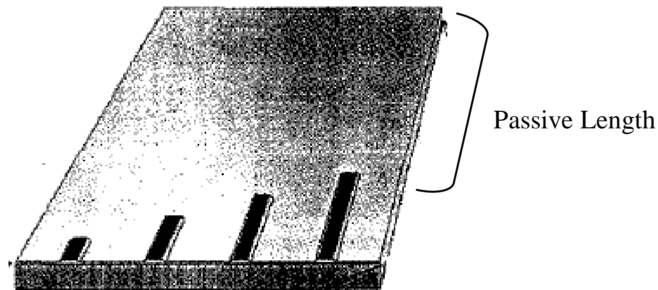

Figure 2.6: Electrically excited variable stripe length method [2.14]

2.5.3: Segmented Contact Method

The segmented contact method [2.9] (cited 80 times), regarded as an improvement to the "Oster" method of variable metal stripe lengths, the modal gain can be obtained by a single multi-section device. The advantage mainly is; the same proportion of the light is collected for

each of the lengths and no realignment is required. A further advantage is the choice of driven and passive lengths. However, this method requires bespoke devices to be fabricated in order to avoid reflections from the device facets, to inhibit lasing, and to ensure single pass gain measurement. Therefore for gain measurement, long multi-section devices with an absorber [2.17] at one end and a tilted facet on the other end are generally used [2.18]. To suppress round trip amplification the rear sections are often reverse biased [2.19] and single pass gain can be successfully achieved.

The segmented contact method can be used to determine net modal gain for both multimode as well as single mode devices. The unguided spontaneous emission and higher order modes can be eliminated either by using an external spatial filter [2.9] or by leaving the waveguide at the front of the device unpumped [2.10]. A multimode fibre having a ~ 62.5μm diameter is generally used to couple light from the device to an optical spectrum analyser.This method allows the length of an electrically driven multi-section device to be varied in order to perform the measurement of gain at each wavelength. The device geometry used is shown schematically in Figure 2.7.

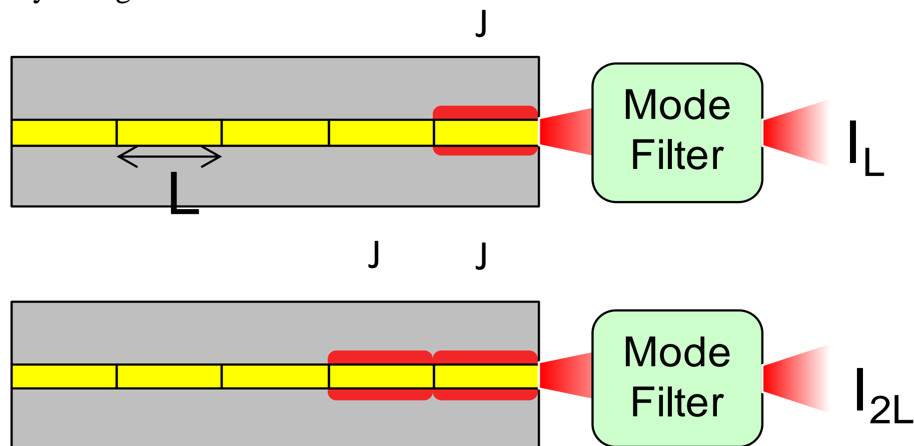

Figure: 2.7: The device geometry used for segmented contact method.

The first section of length L is pumped with a desired current density and then the section of length 2L is pumped with the same current density. The corresponding amplified spontaneous

emission $I_{measured\ L}$ and $I_{measured\ 2L}$ is then recorded in each case by an optical spectrum analyser. Then a ratio of the two allows for the derivation of net modal gain for the device under test given by eq.2.5.

$$Net\,modal\,gain = \frac{1}{L}\ln\left(\frac{I_{measured2L}}{I_{measuredL}} - 1\right) \tag{2.5}$$

Where, L is the length of a single section of the multi-section device, $I_{measured\ L}$ and $I_{measured\ 2L}$ are the amplified spontaneous emissions from section lengths L and 2L respectively driven at same current density. Longer individual sections provide the means to improve the signal to noise ratio in this case.

The spontaneous emission spectrum can also be derived using eq.2.6 [2.8]. The spectra obtained can also be used to estimate the radiative efficiency of the material under test by measuring the integrated power.

$$Spontaneous\,emission = \left(\frac{1}{L}\ln\left(\frac{I_{measured2L}}{I_{measuredL}}\right)\right) x \left(\frac{\left(I_{measiredL}\right)^2}{I_{measured2L} - 2I_{measuredL}}\right) \tag{2.6}$$

This technique usually requires a special fabrication run to fabricate the devices but the major advantage of this technique is that it allows a high S/N ratio to be achieved due to longer section lengths and low resolution requirements. The measurement cannot be performed in two cases; either when the electroluminescence signal approaches the noise floor of the measurement system, or signals from the two section lengths L and 2L are so noisy that they become indistinguishable from each other.

2.5.3.1: Technical Review: Segmented Contact Method

For the gain measurement via the segmented contact method, a 10mm long multi-section Innolume device was used. Individual section lengths were fabricated as 250 or 500µm in

length. The device was fabricated into a 3μm wide ridge with electrically isolated contacts 5μm apart. The device operated via a single lateral mode. The schematic of the device is shown in Figure 2.8. For the analysis, each section length was selected to be 500μm.

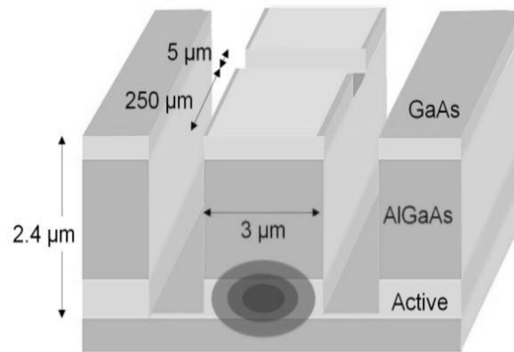

Figure 2.8(1.3): The schematic of the multisection device.

The gain measurement for this technique is based upon the selection of the device with two front sections for the same turn on and voltage-current (differential resistance) characteristics. An identical voltage-current characteristic is assumed to result in identical optical power-current characteristics. The voltage-current characteristics for individual sections are shown in Figures 2.9 (a). As these are essentially identical (differential resistance ~ 4Ω), it is assumed that amplified spontaneous emission from both sections is the same. The optical power-current density (L-J) characteristics for 1st section and 2nd section are shown in Figure 2.9(b) which shows the reduction in power for the 2nd section is due to absorption in the 1st section. A constant attenuation (same ratio of optical powers i.e. P_1/P_2 ~ 2 at each current density) is observed which suggests that the individual sections have the same response at each current density, given a constant attenuation in the front section.

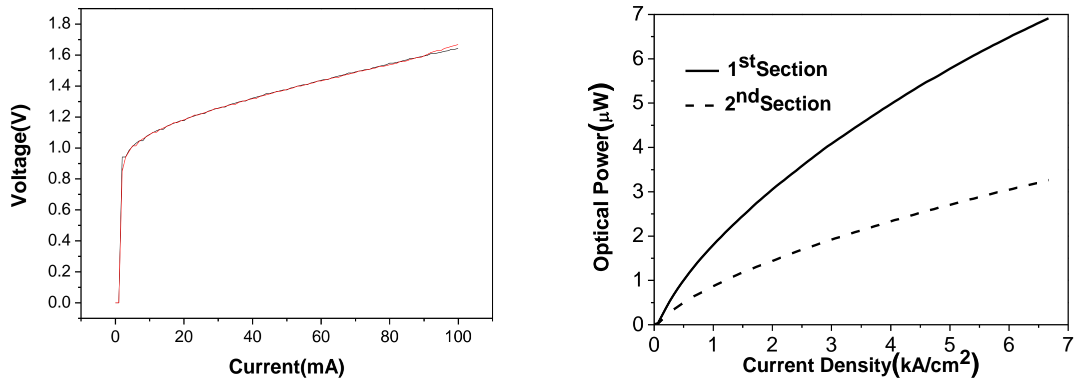

Figure 2.9: (a) Voltage - current characteristics, **(b)** Optical power - current density characteristics of 1st and the 2nd section (each section length: 500µm) of a multi section Innolume device.

2.5.3.2: Apparatus

The experimental set up for the segmented contact measurement is shown in the Figure 2.10. Spatial fibre alignment is necessary to avoid any reflections due to the air and glass (fiber) interface modulating the amplified spontaneous emission.

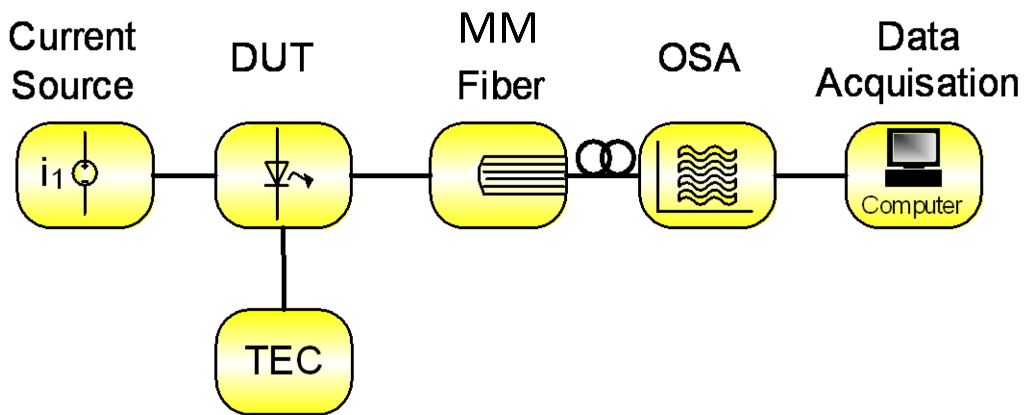

Figure 2.10: Experimental set up for segmented contact measurement method.

In order to ensure the maximum coupling efficiency and to avoid the use of piezo-electric actuators, a multimode fibre is used.

2.5.3.3: Experimental Issues: Trade-offs with Resolution

The optical spectrum analyser plays the main role in retrieving the electroluminescence spectrum from the device under test to perform various analyses to understand the behavior of the laser material. Therefore, the accuracy of the measurement depends upon precise adjustment of its parameters for the acquisition of the electroluminescence spectra.

In the case of the segmented contact method a comparatively low spectral resolution is required. Typically, spectral features in the gain spectrum require a ~ 5 to 10 nm resolution. Long device section lengths may be used and the coupling efficiency is generally high due to the use of a multimode fibre.

2.5.3.4: Experimental Issues: Fidelity of Gain Spectrum for Low Signals

To explore the minimum power limits of this measurement method, the distance between the device (Innolume multi section: section 2.5.3.1) and the fibre is increased, reducing the coupling efficiency and so the collected signal. The net modal gain is evaluated for each of the corresponding spectra to explore how the failure of the measurement manifests itself. Figure 2.11 plots the calculated net modal gain as a function of wavelength by moving the fibre back along the axis of the device until the optical signal becomes close enough to the noise floor to render the gain measurement erroneous. It is observed that the spectral shape does not change significantly, but that the noise level increases in the calculated gain spectrum as the collected signal power reduces. It can be observed (e.g. Pink trace in Figure 2.11) that the noise is lower in the spectral regions of high intensity, such as at the peak gain.

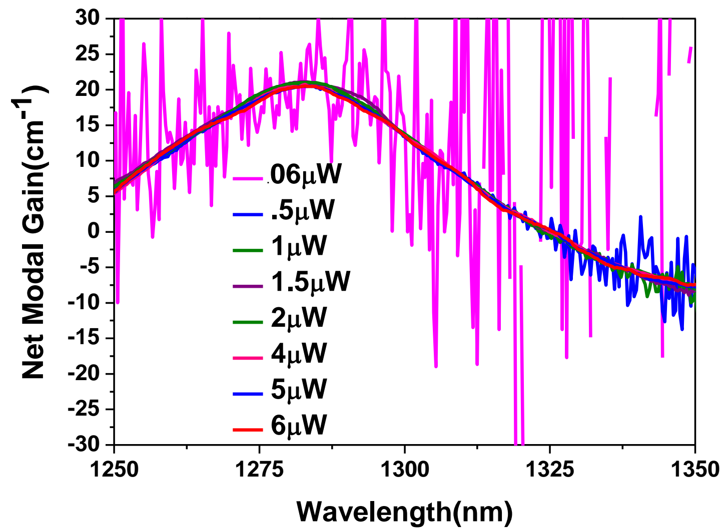

Figure 2.11: Net modal gain spectra as function of wavelength for a range of coupled power corresponding to change in distance between fibre and the device (Innolume multi section: 2.5.3.1).

The amplified spontaneous emission spectra from sections L and 2L are plotted as a function of wavelength for a current density of 1.1kA/cm^2 in the Figure 2.12. In this case the regions where gain cannot be measured can be identified as being <1225nm and >1400nm as electroluminescence spectra either approach the noise floor or become indistinguishable from each other.

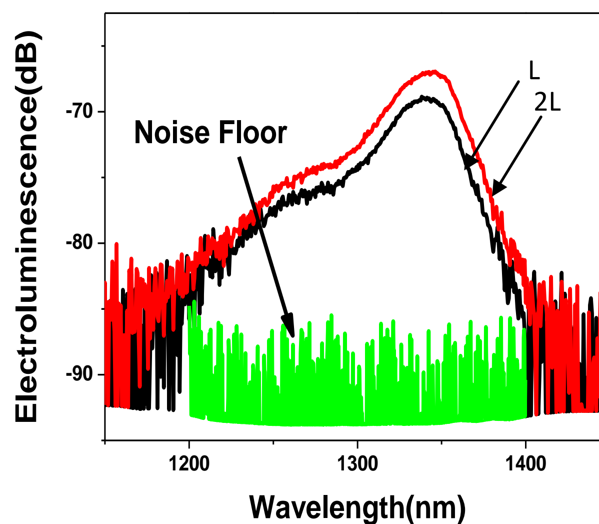

Figure 2.12: Electroluminescence spectra as a function of wavelength for same value of current density from sections L and 2L (Innolume multi section: section 2.5.3.1). The noise floor (green) of the measurement system is also shown.

2.5.4: Integrated Mode Filter Technique

This method by Xin *et al.* [2.10], [2.15] was introduced to overcome the need for an external spatial mode filter to eliminate unguided spontaneous emission in the segmented contact method. It was suggested that the front section of a multi-section device could be used as a spatial mode filter (biasing at 0V).

2.5.4.1: Technical Review

The device geometry used for the integrated mode filter method is schematically as shown in Figure 2.13. This measurement uses the front three section of a multi-section device. For the analysis purpose, a bi-layer multi section device was used which will be discussed in detail in the forthcoming chapters (chapter 4, section: 4.3, chapter 5, section 5.8). In this case each section length is 1mm and electrical contacts are 5μm apart. The first section of length L is driven with a current density J_A, then the other the two sections are pumped with the same current density J, which is varied. It is noted that J_A and hence I_A may be zero, and in previous work [2.15] J_A has not been sufficient to give gain in the front section.

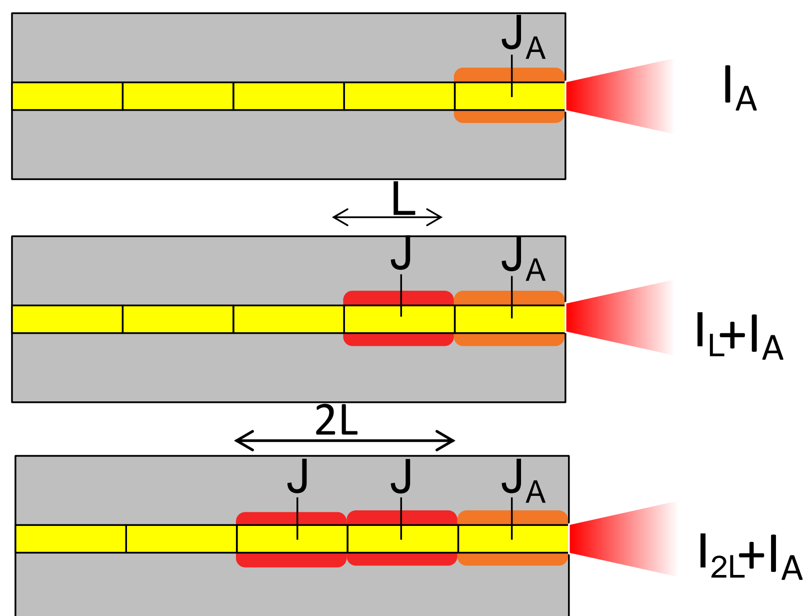

Figure 2.13: Device geometry used for integrated mode filter method using multi section bi-layer device.

The corresponding amplified spontaneous emission I_A, $I_L + I_A$ and $I_{2L} + I_A$ are then recorded as shown in Figure 2.14, by the optical spectrum analyser and with the same experimental set up as used for the segmented contact method..The intensity from the mode filter section is then subtracted from the other intensities.

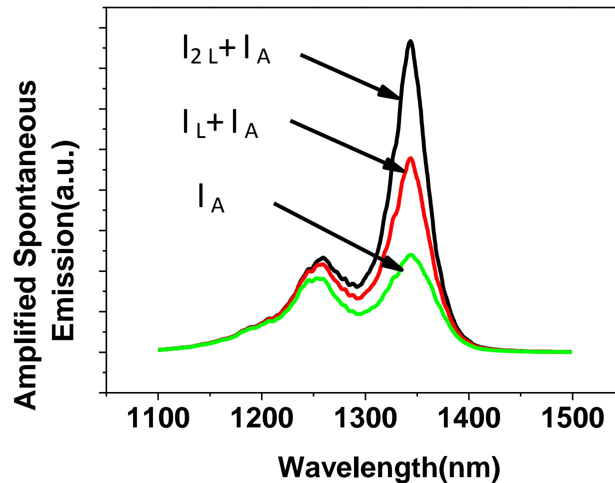

Figure 2.14: Amplified spontaneous emission spectra as a function of wavelength by driving mode filter section, L & 2L with same current density for multisection bi-layer device with each section length: 1mm.

Then the net modal gain for the device under test is given by eq.2.7 [2.9].

$$Net\,modal\,gain = \frac{1}{L}\ln\left(\frac{(I_{2L}+I_A)-I_A}{(I_L+I_A)-I_A}-1\right) \qquad (2.7)$$

Here I_A, I_L+ I_A and I_{2L}+I_A are amplified spontaneous emissions from amplifier section (length L), the section lengths L, and 2L and amplifier section respectively.

Here, the waveguide of the first section is used as a mode filter, eliminating unguided amplified spontaneous emission generated in sections 2 and 3. Therefore this method has the advantage of simplifying the experimental setup in terms of optics, compared to the standard segmented contact technique.

2.6: Self Heating Issues

At high current densities it is a usual observation that the net modal gain spectrum obtained under continuous wave conditions exhibits a red shift caused mainly by device self heating (Joule heating). In the case of variable stripe length methods it is not possible to easily avoid or mitigate these effects.

2.7: Comparison of Gain Measurement Methods

I now compare the key features of the gain measurement techniques discussed earlier in this chapter. In the case of the Hakki and Paoli method, narrow ridge single mode devices of short length are required. The presence of additional lateral modes would result in erroneous gain measurements. The first requirement of data acquisition is high resolution spectroscopy to resolve the electroluminescence spectrum which leads to a reduced signal to noise ratio of the optical signal. An anti reflection (AR) coated single-mode lensed fibre is used to couple the optical signal from the device to the optical spectrum analyser. Its diameter is usually comparable with the ridge width of the device. Therefore a complex experimental set up with piezoelectric stages is required through which the fibre continuously spatially self aligns to the device under test to dynamically couple the maximum power. All these data acquisition requirements lead to long measurement times, complex experimental set up requirements, and a low S/N ratio of the gain spectra.

However, the ability to maintain a constant junction temperature for the Hakki and Paoli method is explained in chapter 3. The advantage is two fold. Firstly, the device does not need to be operated in pulsed mode. This would require a complex setup for impedance matching and requires time gated signal detection, resulting in long data acquisition times. Secondly, the constant junction temperature gain measurements by the Hakki and Paoli method can be

used in the characterization of a device where self heating effects are removed. In this case free carrier effects alone can be analyzed in detail. Therefore, the Hakki and Paoli method can used to compare the behaviour and physics of laser material at both constant heat sink and constant junction temperature conditions, allowing a comparison of free carrier and thermal effects.

For the case of the segmented contact/integrated mode filter methods the devices can be narrow ridge or broad area i.e. these methods are applicable to single mode as well as multimode devices. To avoid higher order modes a spatial mode filter or the device's own waveguide can be used as a filter. A multimode fibre is used to channel the optical signal from the device to the optical spectrum analyser. Therefore, the coupling efficiency is high and dynamic adjustment of the coupling is not a requirement. The electroluminescence spectrum does not require high resolution spectroscopy. The optical signal measurement requirements are less stringent due to a reduced complexity of the measurement setup, lower resolution, and lower sensitivity requirements. These factors lead to reduced data acquisition times and higher S/N ratio, compared to the Hakki and Paoli method. Due to a high signal to noise ratio lower current densities can be readily accessed. However, self heating is a critical issue for variable stripe length techniques under continuous wave measurement conditions which cannot be easily avoided.

Based on this analysis, the segmented contact techniques lend themselves to low current density measurements, whilst the Hakki and Paoli technique is better suited to high current densities. The Hakki and Paoli technique may therefore allow a comparative study of thermal effects and free carrier effects.

2.8: Summary

In this chapter firstly a review of high resolution spectroscopy and variable stripe length gain measurement techniques was presented. Then the theory, device requirements, resolution fidelity, experimental apparatus and low optical power limitations of the Hakki and Paoli and segmented contact were explored. A method to maintain a constant junction temperature for the Hakki and Paoli method was mentioned (see chapter 3). An improvement to the segmented contact method: the integrated mode filter method was discussed. Self heating issues related to variable stripe length methods were mentioned. The suitability of the said techniques for high current density measurement (with/ without constant junction temperature) and low current density analysis was presented.

References

[2.1] E. U. Rafailov, M. A. Cataluna & W. Sibbett "Mode-locked quantum-dot lasers", Nature Photonics 1, 395 - 401(2007).

[2.2] S. Fathpour, Z. Mi and P. Bhattacharya, "High-speed quantum dot lasers", J. Phys. D: Appl. Phys., Vol. 38, 2103(2005).

[2.3] K. Otsubo, N. Hatori, M. Ishida, S. Okumura, T. Akiyama, Y. Nakata, H. Ebe, M. Sugawara and Y. Arakawa, "Temperature-insensitive eye-opening under 10-Gb/s modulation of 1.3-µm P-doped quantum-dot lasers without current adjustments", Jpn. J. Appl. Phys. Vol. 43, 1124 - 1126(2004).

[2.4] S. Fathpour, Z. Mi, P. Bhattacharya, A. R. Kovsh, S. S. Mikhrin, I. L. Krestnikov, A. V. Kozhukhov, and N. N. Ledentsov, "The role of Auger recombination in the temperature-dependent output characteristics ($T0 = \infty$) of p-doped 1.3µm quantum dot lasers", Appl. Phys. Lett. Vol. 85, 5164 - 5166(2004).

[2.5] R. R. Alexander, D. Childs, H. Agarwal, K. M. Groom, H. Liu, M. Hopkinson, R. A. Hogg, "Zero and controllable linewidth enhancement factor in p-doped 1.3µm QD lasers", Jpn. J. Appl. Phy. Vol. 46 (2007).

[2.6] P.D.L Greenwood *et al.* "Quantum dot superluminescent diodes for optical coherence tomography: Device engineering", IEEE J. of sel. Top. In Quant. Elect. Vol. 16, 1015 - 1022(2010).

[2.7] B. W. Hakki and T. L. Paoli, "Gain spectra in GaAs double−heterostructure injection lasers", J. Appl. Phys. Vol. 46, 1299(1975).

[2.8] B. W. Hakki and T. L. Paoli, "CW degradation at 300K of Ga-As double heterostructure junction lasers. II. Electronic gain", J. Appl. Phys. Vol. 44, no.9, 4113 - 4119(1973).

[2.9] P. Blood, G. M. Lewis, P. M. Smowton, "Characterization of semiconductor laser gain media by the segmented contact method", IEEE Journal of selected Topics in Quant. Elect. Vol. 9, 1275 - 1282(2003).

[2.10] Xin *et al.* "Determination of optical gain and absorption of quantum dots with an improved segmented contact method", Proc. of SPIE Vol. 5722, 49 - 59(2005).

[2.11] D. T. Cassidy, "Technique for measurement of the gain spectra of semiconductor diode lasers", J. Appl. Phys. Vol. 56, 3096 (1984).

[2.12] V. Jordan,"Gain measurement of semiconductor laser diodes: Requirements for the wavelength resolution and sensitivity to noise", Proc. Inst. Elect. Eng. Vol. 141, 13-15 (1994).

[2.13] K. L.Shaklee and R. F. Leheny, "Direct determination of optical gain in semiconductor crystals", Appl. Phys. Lett. Vol. 46, 11, 475 - 477(1971).

[2.14] A. Oster, G. Erbert, H. Wenzel, "Gain spectra measurements by a variable stripe length method with current injection", Elect. Lett. Vol. 33, 10, 864-866(1997).

[2.15] Y.C. Xin, Yan Li, Anthony Martinez, Thomas J. Rotter, Hui Su, Lei Zhang, Allen L. Gray, S. Luong, K. Sun, Z. Zou, John Zilko, Petros M. Varangis, and Luke F. Lester, "Optical gain and absorption of quantum dots measured using an alternative segmented contact method", IEEE J. Quant. Elect. Vol. 42 (2006).

[2.16] T. S. Yu Francis, Y. Xiangyang, "Introduction to optical Engineering", Cambridge University Press, Chapter 6, (1997).

[2.17] Z. Y. Zhang,a_ I. J. Luxmoore, C. Y. Jin, H. Y. Liu, Q. Jiang, K. M. Groom, D. T. Childs,M. Hopkinson, A. G. Cullis, and R. A. Hogg, "Effect of facet angle on effective facet reflectivity and operating characteristics of quantum dot edge emitting lasers and superluminescent light-emitting diodes", Appl. Phys. Lett. Vol. 91, 081112(2007).

[2.18] J. D. Thomson, H. D. Summers, P. J. Hulyer, P. M. Smowton, and P. Blood, "Determination of single-pass optical gain and internal loss using a multisection device ", Appl. Phys. Lett. Vol. 75, 2527 (1999).

[2.19] D. J. Derickson, R. J. Helkey, A. Mar, J. R. Karin, J. E. Bowers, and R. L. Thornton, "Suppression of multiple pulse formation in external-cavity mode-locked semiconductor lasers using intrawaveguide saturable absorbers", IEEE Photonics Tech. Lett. Vol. 4, 4, April (1992).

Chapter3
Free Carrier Effects in 1.3μm Quantum Dot Lasers

3.1: Introduction

The measurement and prediction of the evolution of the gain spectrum with temperature and current density is key to describing the operation of a semiconductor laser. The free carrier theory assumes that the inter carrier interactions are more dominant than the carrier field interactions which allow them to settle into their respective bands according to respective quasi-fermi levels. The many body effects however, are due to the interaction between the carriers which result in coulomb enhancement (increased inter band transitions) and band gap renormalization. As a consequence of the coulomb enhancement the peak gain increases, blue shifts and reshaping the gain spectra is observed. The band gap renormalisation occurs due to the screening effects at high current densities which causes the inter carrier distance to get reduced and increased collision between them results in reduction of carrier life time. Due to that the band edge experiences a red shift and reshaping of gain spectra takes place. Band-gap renormalization, broadening due to intra-band scattering, and Coulomb enhancement of the optical transition brought about at high carrier densities make many body effects [3.1], an important factor in laser engineering. Of late, quantum dot (QD) lasers have been commercialized, due in part to the prediction [3.2], and demonstration of temperature insensitive operation at 1300 nm [3.3- 3.4]. However, there are few reports on many body effects in such devices.

Modelling of an ensemble of quantum dots at room temperature using screened Hartree-Fock theory to describe Coulomb interactions between carriers localized in quantum dots and the wetting layer predicted up to 20 meV red shifts of the quantum dot gain peak with ~15 e-h

pairs per quantum dot [3.5]. Modelling of the low temperature photoluminescence (PL) spectra of single quantum dots predicts similar band-gap renormalization shifts and highlighted the possibility for significant broadening of the optical transitions at high quantum dot occupancy due to intra-band Auger scattering [3.6]. Low temperature PL of a quantum dot ensemble as a function of excitation intensity showed a broadening of the optical transitions and band-gap renormalization induced shifts of the quantum dot ground-state [3.7]. In addition, a reduction in luminescence efficiency with significant excited state population was noted by the same group [3.7]. Photoluminescence of single quantum dots as a function of excitation density at room temperature has shown that the onset of both broadening and band-gap renormalization occur simultaneously [3.8]. Intra-quantum dot Auger scattering via Coulomb scattering was highlighted as the probable source of the broadening. Dephasing has been recognized as an important factor in the description of gain and lasing spectra of quantum dot lasers [3.9]. Of particular interest is the recent prediction of negative differential gain in quantum dot lasers at excitation levels beyond ground-state gain saturation [3.10]. This is expected due to gain saturation, yet a non-saturable increase in dephasing due to increased carrier density in higher lying states (excited states of quantum dots and 2D states). Most recently, many body effects on the gain spectrum were studied experimentally up to dot occupancy levels of ~2 e-h pairs per quantum dot and a red-shift of the peak gain from its modelled position of up to 8 meV was observed [3.11]. Significantly this report studied the quantum dot ensemble below ground-state gain saturation.

3.2: Outline

In this chapter the Hakki and Paoli method [3.12] is used to perform high current density analysis of the gain spectrum of 1300nm quantum dot laser material under continuous wave conditions. The device is characterised with and without self-heating effects. The elimination of self-heating effects is achieved by using a longitudinal mode as a junction temperature

monitor to keep the junction temperature constant. This allows an unambiguous study of the continuous wave gain spectrum at average dot occupancy levels up to ~8 e-h pairs per quantum dot. A negative differential gain is observed in both cases. This is shown to be predominantly due to the free carrier effects. As a result, free-carrier related negative differential gain is observed for the first time [3.13].

3.3: Device Epitaxy & Fabrication

The quantum dot laser structure studied [3.14] was grown by Innolume GmbH by molecular beam epitaxy (chapter 1: section 1.6). The epitaxial and device structures are shown in Figures 3.1 and 3.2 respectively. Initially a 1.5 µm $Al_{0.35}Ga_{0.65}As$ n-cladding was grown, on top of which 10 repeats of 33nm GaAs, InAs quantum dots and 5 nm. $In_{0.15}Ga_{0.85}As$ strain reducing layer were grown on each quantum dot layer. A 1.5 µm $Al_{0.35}Ga_{0.65}As$ p-cladding was then grown and finished by a 200 nm heavily doped p+ GaAs contact layer. The wafer was processed into 3 µm wide deep etched (2.2µm) ridge lasers (By Dr. B. J. Stevens) to achieve strong electrical and optical confinement and to eliminate high order lateral modes. The laser ridge had 250µm long contacts which were electrically isolated by a 5µm wide gap in the metal contact, and n^+ GaAs contact-layer etch. Bars of 450 um and 300 um cavity length were cleaved and mounted on aluminium oxide tiles, subsequently mounted on copper heat-sinks for testing.

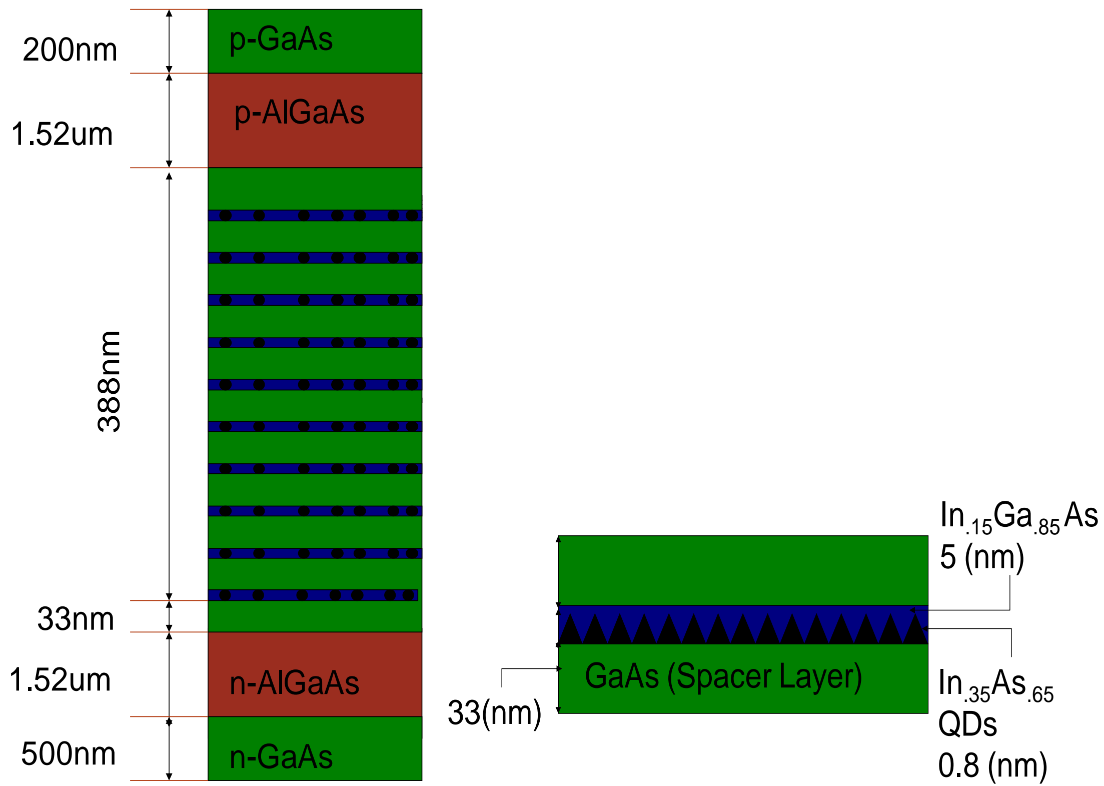

Figure 3.1: Schematic of the device.

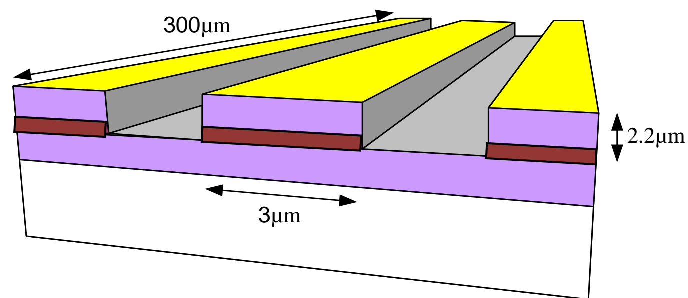

Figure 3.2: Schematic of laser device structure.

3.4: Apparatus

The experimental set up used for Hakki and Paoli method is already described in detail in Chapter 2**(section: 2.4.1)**. In order to resolve the individual Fabry- Pérot modes an optical spectrum analyser (Advantest 8384) with spectral resolution of 10 pm was used. The heat-sink temperature was regulated and monitored via a thermoelectric cooler and thermistor. The analysis was performed under continuous wave operation. Initially the device was characterised at a constant heat-sink temperature (17°C) and then at a fixed-junction temperature (30°C) by using the shift of individual Fabry-Pérot mode as a measure of the change in temperature due to the Joule (I^2R) heating which was subsequently compensated for by adjusting the heat-sink temperature.

3.5: Device Characteristics

Light-current density (L-J) characteristics of the 300µmx3µm and 450µmx3µm devices are shown in Figure 3.3(a) and (b) respectively. For the 450µmx3µm device lasing characteristics are observed at ~ 2Acm^{-2} (with external differential efficiency of 20%). The lasing is observed from the excited state of the quantum dot ensemble at around 1190nm. However, the 300µmx3µm laser device exhibits non lasing characteristics. This is further confirmed by their electroluminescence spectrum at 5kAcm^{-2} as shown in the Figure 3.4 (a), (b). The offset in electroluminescence spectra for both devices at ~ 1250nm is a stitching error. This produces a single erroneous data point in the calculation of gain which is removed. A peak in the electroluminescence spectrum of the 450µmx3µm is quite obvious around 1250µm. It is attributed to reflection of the light inside the optical spectrum analyser after lasing introducing 'ghost' images in the electroluminescence spectrum. Due to this the gain measurement were not performed after lasing.

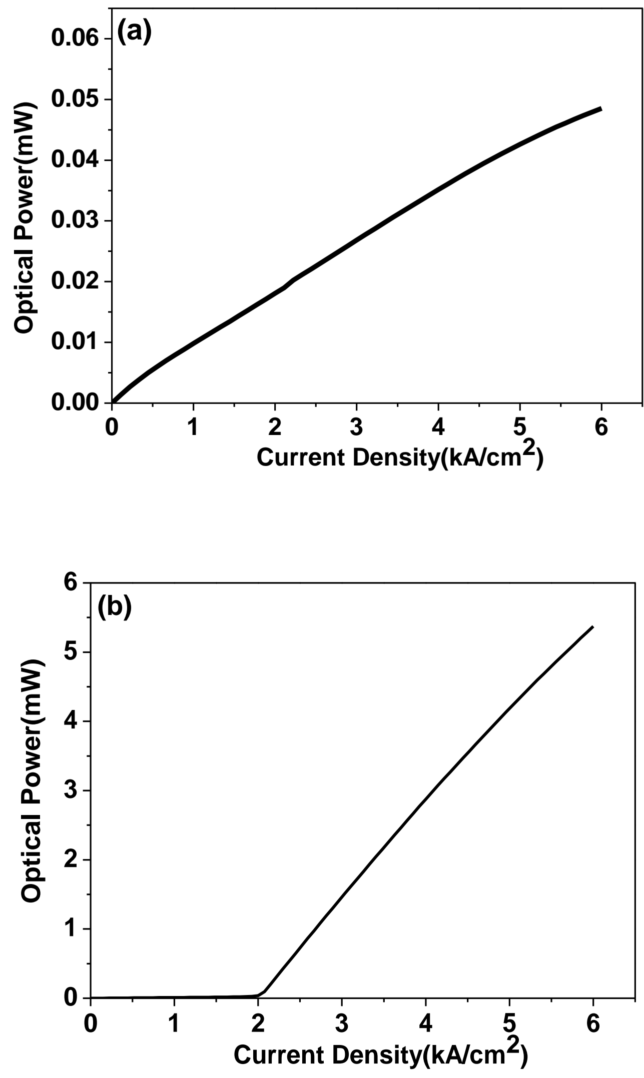

Figure 3.3: (a) Light- Current density characteristics (a) 300µm x 3µm (b) 450µm x 3µm laser devices.

The inset to Figure 3.4 confirms the single mode behaviour of the laser devices. Here, I have used the spectral peaks in the region of the quantum dot ground state to predict the Fabry-Pérot mode positions at ~1160nm. These predicted Fabry- Pérot mode positions are plotted as dots in the inset spectra. These are in excellent agreement with measurement. The non-lasing characteristics (due to the short cavity length) of the 300µmx3µm device allowed it to be used for high current/carrier density analysis whilst 450µmx3µm device could be used only up to 2kAcm^{-2}. This allows the quantum dot ground state to be studied under strong gain saturation conditions

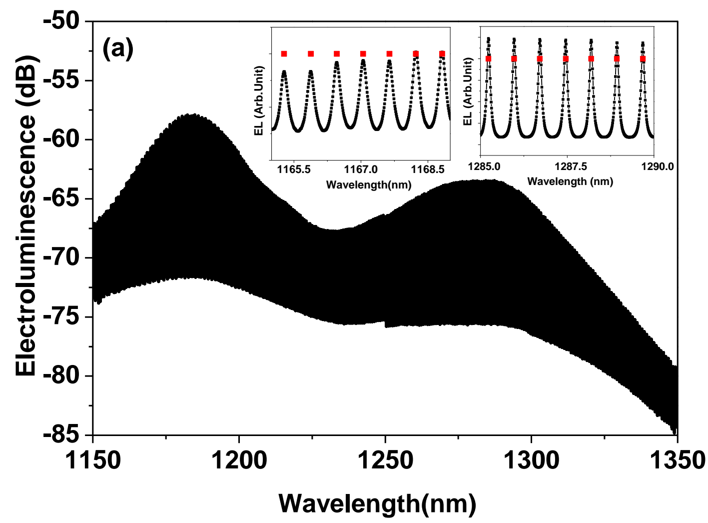

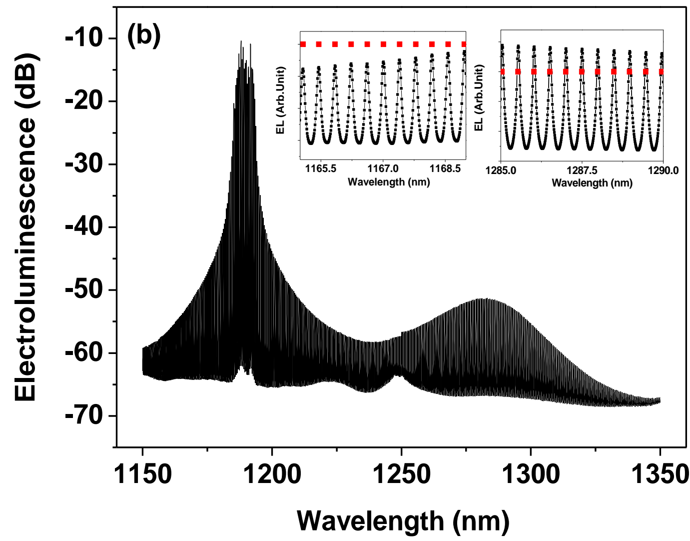

Figure 3.4: (a) The electroluminescence spectrum as a function of wavelength for (a) 300µm x 3µm (b) 450µm x 3µm laser devices at 5kAcm^{-2}.

3.6: Establishing a Constant-Junction Temperature

Figure 3.5 shows the wavelength of an individual Fabry- Pérot mode as a function of current density in the region of the peak in ground state gain at a constant heat-sink temperature of 30°C. The devices were as-cleaved with cavities of length 450μm and 300μm. For the device with 300 μm cavity length, laser oscillation was not observed over these current densities, and a quadratic shift of Fabry-Pérot modes is observed with increasing current density. For the 450 μm cavity length lasing occurred at ~2 $kAcm^{-2}$ and the Fabry-Pérot peak position of the mode is plotted as a function of current density above lasing threshold.

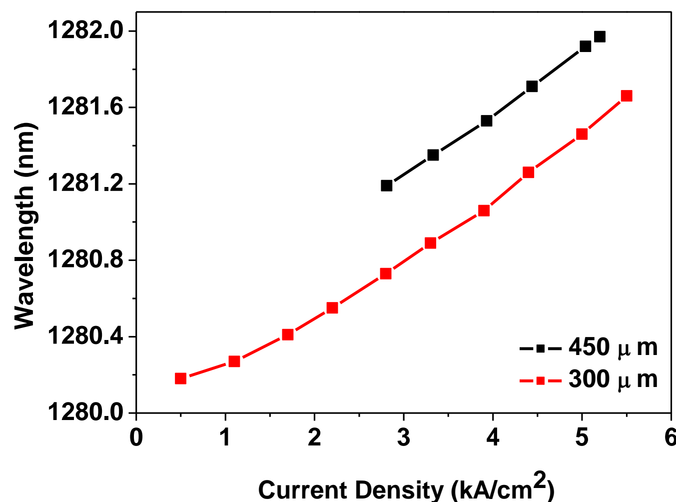

Figure 3.5: Wavelength of individual Fabry-Pérot mode in the region of the peak in ground state gain as a function of carrier density at a constant heat-sink temperature of 30° C for 300μm x 3μm and 450μm x 3μm laser devices.

The essentially identical shifts for both lasing and non-lasing cases (where carrier densities can be expected to be very different) indicate that the shift in lasing wavelength is dominated by thermal expansion of the cavity and thermal change in refractive index, rather than a change in refractive index due to free carriers. This observation allows the wavelength of an individual Fabry-Pérot mode in the case of the 300μm x 3μm device to be used as a measure

of junction- temperature. This allows the effects of Joule heating (self–heating) to be removed by reducing the heat-sink temperature during the course of continuous wave operation, to maintain a constant Fabry-Pérot mode wavelength (hence constant junction temperature).

3.7: Constant Heat-sink Temperature Gain Measurement

The net modal gain spectra were obtained via the Hakki and Paoli technique at a constant heat- sink temperature (17°C) in the current density range of 0.5kAcm^{-2} to 5.5kAcm^{-2}. This allowed the analysis of the spectral evolution of the net modal gain due to the combined effects of free carriers and self heating. The results are shown in Figure 3.6.

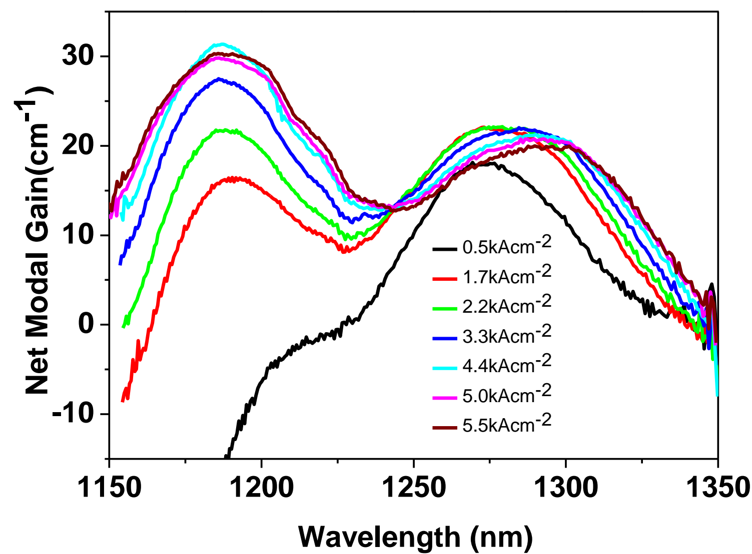

Figure 3.6: Net modal gain spectra for as a function of wavelength for 300μm x 3μm, for a current density range of 0.5kAcm^{-2} to 5.5kAcm^{-2} at constant heat-sink temperature of 17°C.

3.7.1: Analysis and Discussion

Over these current densities the quantum dot ground state shows a red shift which continues with increasing current density. The peak ground state gain saturates at 2.2kAcm^{-2}. The measured saturated net modal gain value was ~ 22cm^{-1}. Towards higher current densities, in addition to this red shift, an asymmetric broadening and decrease in peak net modal gain i.e. negative differential gain is observed. This behaviour is attributable to the combined effects of increasing self heating and free carrier effects.

The excited state peak experiences a blue shift up to 2.2kAcm^{-2} attributed to state filling effects. However from current densities of ~2.2kAcm^{-2} to 4.4kAcm^{-2} the excited-state peak wavelength remains almost static. The double degeneracy of the excited state is suggestive of ~ 46cm^{-1} excited state net modal gain [3.14] but the experimental results show a value close to 32cm^{-1}. The difference in the predicted and experimental value may be due to self heating effects at high current densities at constant heat-sink temperature leading to the thermalisation of carriers out of the dot and lost via non radiative recombination.

The internal loss may be determined from the net modal gain measurement at long wavelengths. For a constant heat-sink temperature of 17°C at various current densities i.e. below, at, and after ground state saturation in this case is measured to be ~ 1.5cm^{-1}.

The reduction in ground state gain at high current densities which leads to negative differential gain may be thermally generated. So in order to determine whether the dominant effect is Joule heating, the junction temperature is fixed so as to allow the observation of free carrier effects on their own.

3.8: Maintaining a Constant-Junction Temperature

The method to fix the junction temperature for the 300µm x 3µm device is detailed in the following section. In Figure 3.8 (a) the wavelength of a Fabry-Pérot mode as a function of heat- sink temperature from 17.5^{o}C to 22°C at a constant current density of 1.1kAcm^{-2} is plotted. The inset shows a plot of the Fabry-Pérot peak position as a function of heat- sink temperature. It is observed that there exists a linear relationship between temperature increase and Fabry-Pérot peak wavelength and this shift is attributed to crystal expansion and the change in refractive index of the cavity material [3.15] due to thermal effects. The slope of the linear fit, $\frac{\Delta\lambda}{\Delta T}$ is measured to be 0.1nm/^{o}C.

Figure 3.8 (b) plots the Fabry-Pérot mode wavelength as a function of current density for a heat- sink temperature of 17°C. A quadratic shift in Fabry-Pérot mode peak position is observed indicating that the dominant effect is Joule heating of the device (being proportional to I^2). With this assumption this modal shift is converted to an increase in cavity temperature (inset Figure 3.8 (b)).It is then possible to adjust the heat- sink temperature for any increase in current through the device to negate the effects of self-heating in the chip, maintaining a constant junction temperature.

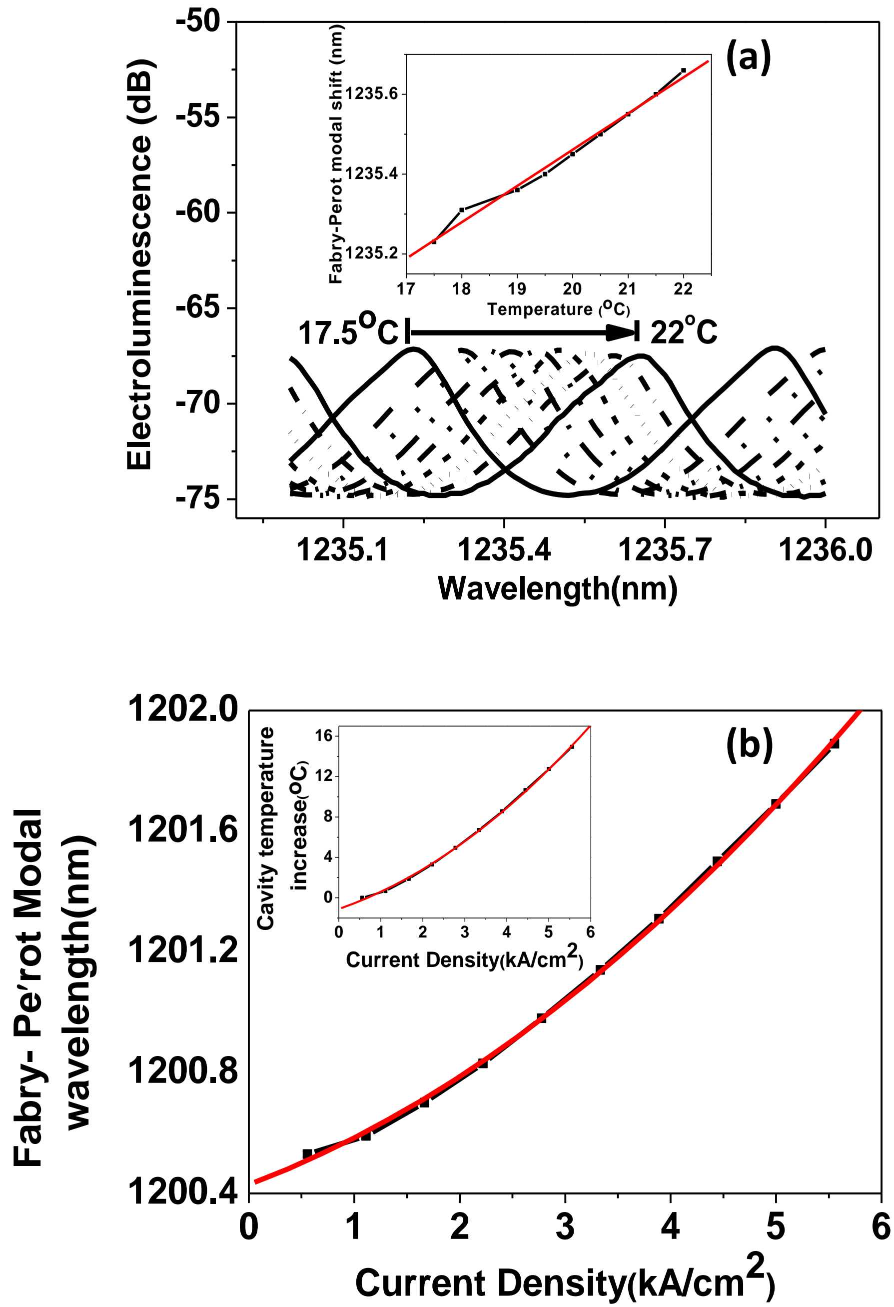

Figure 3.8: **(a)** A Fabry-Pérot modal shift with temperature. Inset plots Fabry-Pérot peak position shift as a function of temperature. (b) Fabry- Pérot modal shift with carrier density at 17°C constant heat- sink temperature. Inset shows cavity temperature rise as a function of carrier density.

3.9: Constant-Junction Temperature Gain Measurement

Figure 3.9(a) shows gain spectra obtained via the Hakki and Paoli technique at a constant-junction temperature of 30° C as a function of current density. It is carried out over the same current densities and spectral range as was selected for the constant heat-sink condition. Figure 3.9(b) plots the same data for the ensemble of quantum dot ground states alone, over the spectral range 1250 nm to 1350 nm. Being at a fixed junction temperature, the free carrier effects alone can be determined up to an injection level of ~8 e-h pairs per quantum dot.

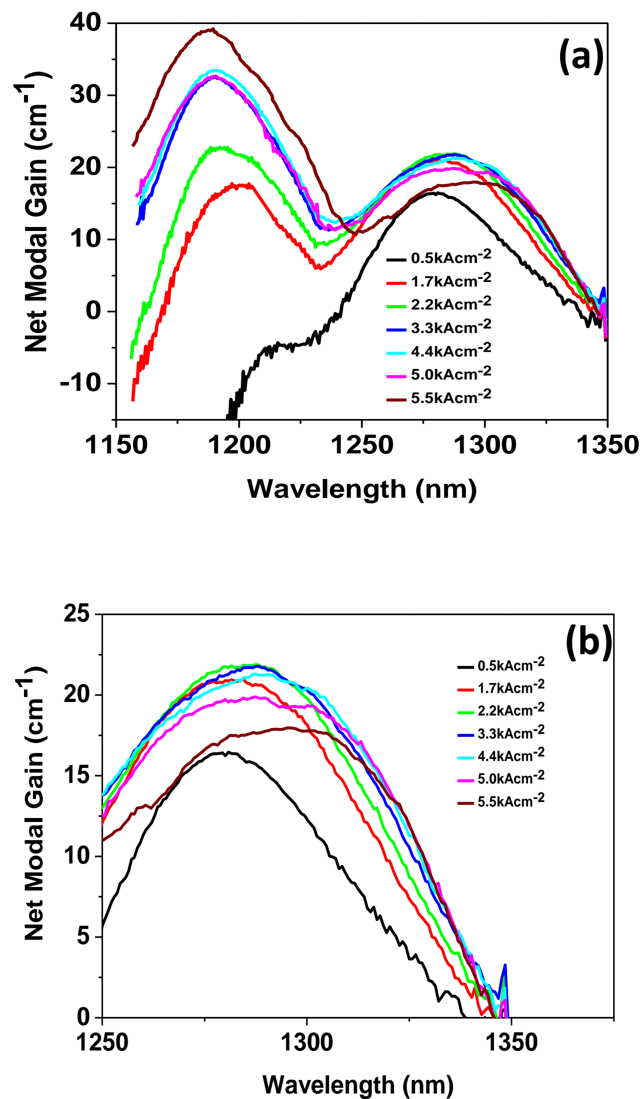

Figure 3.9: (a) Net modal gain spectra as a function of wavelength obtained for 300 µm x 3µm laser device at a constant-junction temperature of 30°C. (b) Net modal gain as a function of wavelength for the same device in the region of the ensemble of quantum dot ground states.

3.9.1: Analysis and Discussion

For this analysis the junction temperature was maintained at 30°C. This particular temperature was selected as at ~ 5kAcm^{-2} the self heating effects in Figure 3.9(a) gave a junction temperature of 30°C. For the ground state in the case of a constant-junction temperature, very similar trends are observed as for the constant heat-sink temperature case i.e. a continuous red shift, asymmetric broadening and a reduction in net modal gain (negative differential gain) after saturation. The net modal gain spectra show approximately the same red shift after saturation as before. A slightly more asymmetric broadening towards longer wavelengths is observed in comparison to the constant heat-sink temperature condition. The broadening of the ground-state gain peak at high current densities in this case is attributed to increasing dephasing effects due to free carriers in the quantum dots causing an increase in homogeneous linewidth.

In Figure 3.9(b) the excited state exhibits a similar blue shift up to 2.2kAcm^{-2} as was the case for a constant heat-sink temperature. By contrast to the case for a constant heat-sink temperature, the excited state continues to increase in gain up to the highest current density of 5.5kAcm^{-2}. A higher value of net modal gain (~ 38cm^{-1}), closer to that expected, considering the increased degeneracy (i.e. 2x ground state G_{sat}) is observed. All these observations point towards self-heating effects playing a strong role in the behaviour of the excited state gain in the case of a constant heat-sink temperature.

3.9.2: Internal Loss

The Figure 3.10 plots the net modal gain in the spectral region 1300 nm to 1360 nm below, at and above ground state saturation. At long wavelengths (beyond 1340nm) all traces converge on the same internal loss of ~1.5±0.5cm^{-1} as was in the case of constant heat-sink temperature condition. Measurements do not show any indication of a significant increase in internal loss (i.e. within the 0.5cm^{-1} error) with increase in drive current density in the case of a constant-junction temperature.

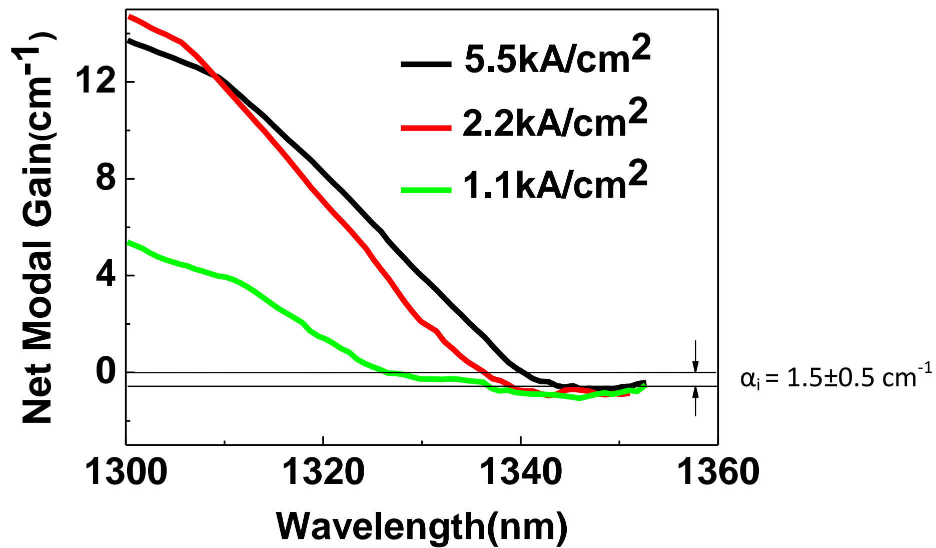

Figure 3.10: The net modal gain spectra at various current densities at long wavelengths where the internal loss can be deduced.

3.10: Comparison Constant Heat-sink and Constant-Junction Temperature Conditions

The peak gain wavelength as a function of current density for the quantum dot ground state and excited state is shown in Figure 3.11(a) at constant heat-sink (RT = 17°C) and constant junction temperature (30°C). The peak gain is similarly plotted in Figure 3.11(b). As has been noted, self heating at ~ 4.5kAcm^{-2} results in the same junction temperature in the two cases. As expected, the peak wavelength and gain values are very similar at this point.

For the QD ground-state, the peak gain is essentially identical for the two cases, indicating that the origin of the observed negative differential gain is free-carrier related, rather than being related to self-heating effects. Interestingly, a difference in peak gain between the two temperature regimes is observed for the excited state. Here, higher values of excited state gain are observed. This is consistent with an increased carrier lifetime at higher temperatures, due to a reduction in Auger recombination [3.16]. The differences in peak wavelength at low J (~8nm) are in line with a difference in temperature of ~13°C.

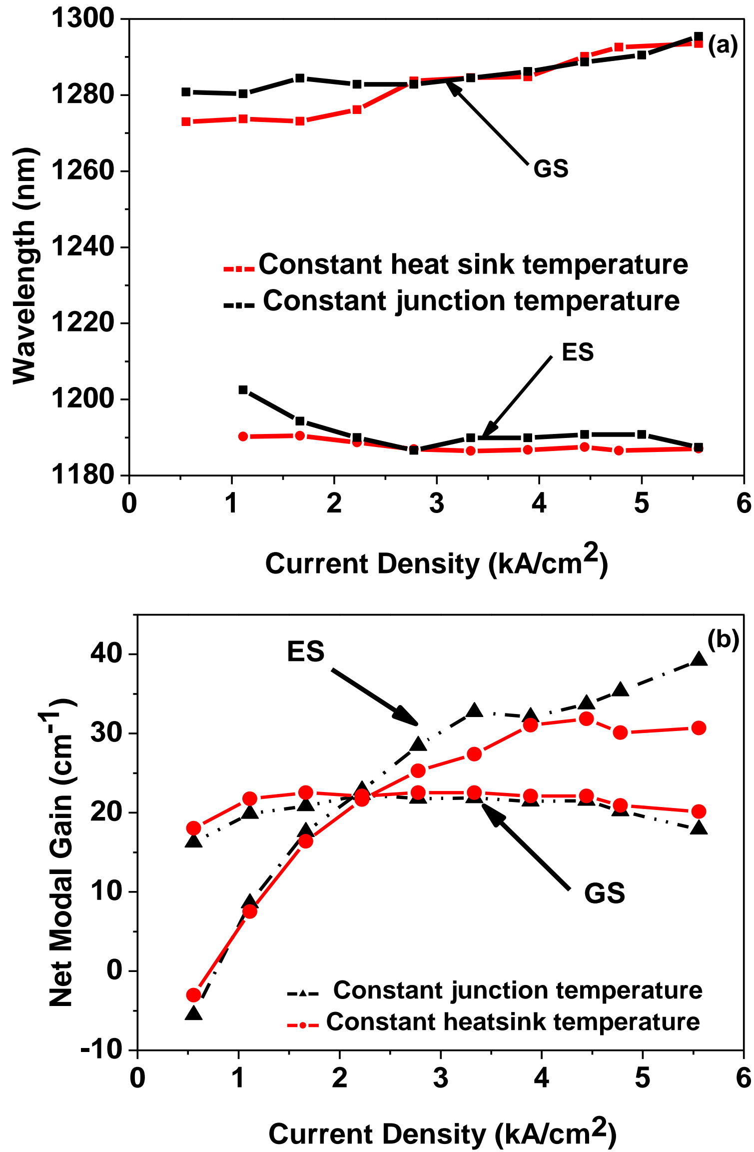

Figure 3.11: (a) Peak wavelength for ground state and excited state at constant heat- sink (17°) and constant-junction temperature (30°). (b) Peak net modal gain for ground state and excited state at constant heat- sink (17°) and constant-junction temperature (30°),

3.11: Empirical Fitting

A full model of to account for the free carrier effects in QD gain is outside the scope of my PhD. However, an empirical model can be built up using various elements of the literature.

Key elements in our model are the shift of band-gap energy with increasing carrier occupancy [3.6, 3.5] with in the dot and we did not take into account the shift due to the carriers dynamics in the wetting layer (2-D states) , QD emission broadening with increasing carrier occupancy [3.8], and the Poisson distribution of carriers in the QDs [3.17].

Figure 3.12 plots two reports in the literature which highlight the predicted band-gap shift with increasing QD carrier occupancy. Both reports use different calculation techniques and are focussed on slightly different experiments and temperatures. However, a reduction of emission energy of ~1meV per e-h pair is predicted in both cases.

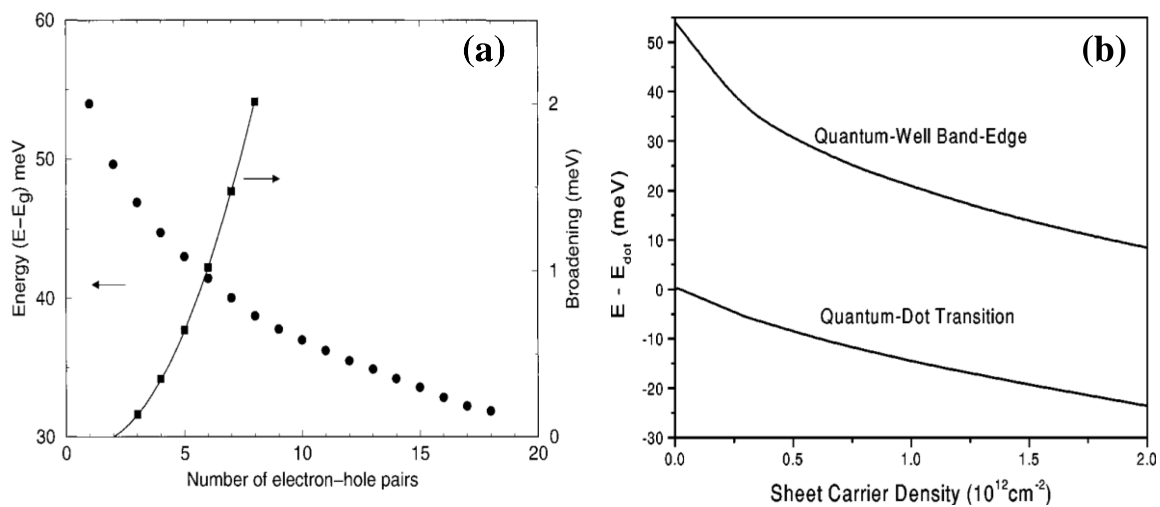

Figure 3.12 Plots of band-gap reduction for QDs from theoretical calculations in the literature. (a) Single QD PL at low temperature [3.6], (b) room temperature gain [3.5].

Figure 3.13 plots data from a paper by Matsuda et al. [3.8] where single QD micro PL was studied as a function of excitation density at room temperature. They observed a homogeneous linewidth of the QDs of 7-10 meV, which broadened as carrier occupancy was increased. Analysis of their results suggests shifts of ~1meV per carrier (in agreement with theory), and broadening of ~2meV per carrier.

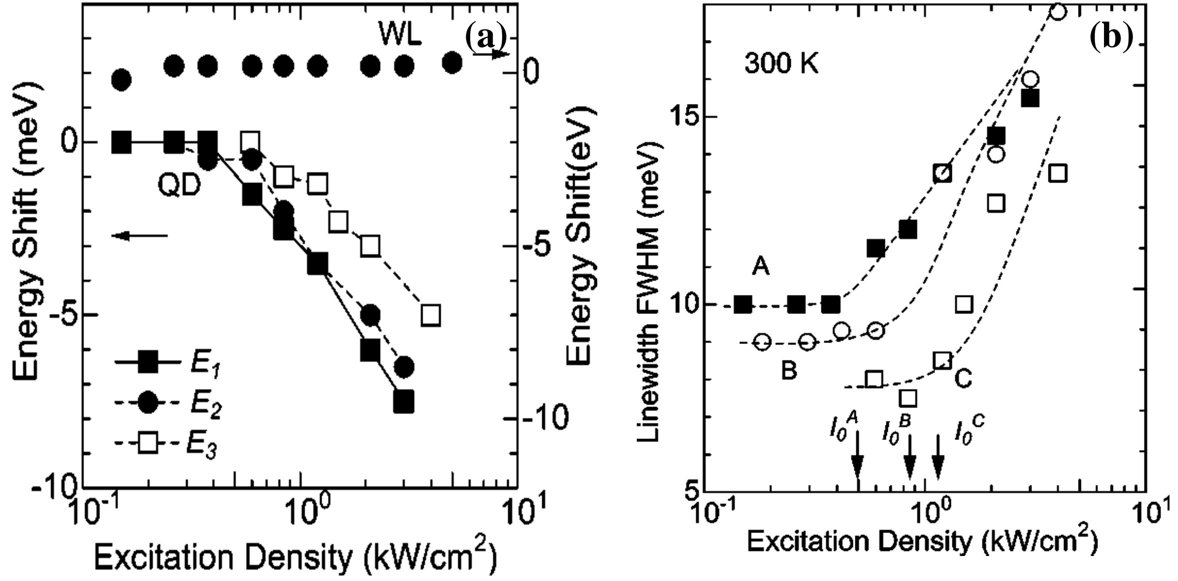

Figure 3.13: (a) Energy shift as function of excitation density for the three electronic transitions, (b) homogeneous line width of the dots of three different sizes(10-40nm) as a function of excitation density [3.8].

The random population of QDs plays a significant role in the evolution of QD gain and spontaneous, and the presence or absence of this at room temperature is currently being discussed in the literature. My results are suggestive of a random population with free carrier effects playing a strong role in modifying the gain spectrum (this chapter and chapter 4). Figure 3.14 plots the probability of a given QD occupancy, given a particular average dot occupancy. If we now consider a ~1meV/e-h pair shift in emission, and ~2 meV/e-h pair broadening as higher occupancies are obtained, we can begin to see the origin of the negative differential gain.

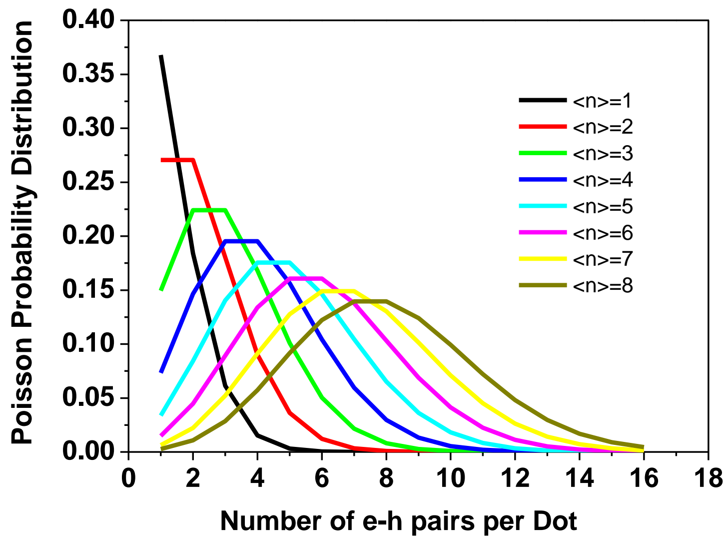

Figure 3.14: Poisson carrier distribution as a function of mean dot occupancy

Figure 3.15 plots the gain spectra obtained by applying all these elements. Here a Gaussian gain profile is assumed for both ground-state and excited state. To this, a Lorentzian broadening and shift are applied, in line with the work of Matsuda *et al*. A Poisson carrier distribution is assumed, which determines the gain spectrum. A reasonable qualitative fit to our experiment is obtained, with the blueshift of gain at low current density, broadening, shift and reduction in peak gain of the excited state at high current density. The broadening of spontaneous emission and gain due to the time-averaging of QD occupancies is termed Poisson broadening).

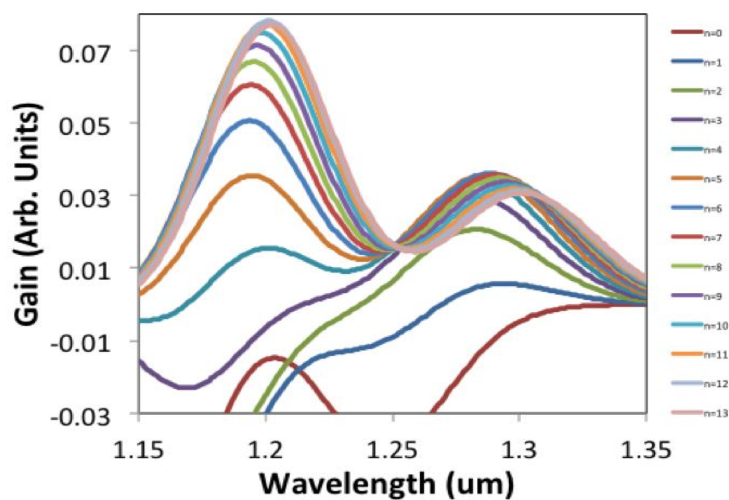

Figure 3.15: Gain spectra calculated using an empirical model as described in the text (Courtesy RA Hogg).

3.12: Summary

This chapter detailed the analysis of net modal gain spectra of quantum dot laser materials at high carrier densities. The analysis was performed at constant heat-sink temperature and constant-junction temperature obtained by using a Fabry-Pérot mode as a temperature gauge. Then, self-heating effects were entirely removed to allow the observation of many-body effects alone. At excitation levels up to 8 e-h pairs per quantum dot a reduction in peak ground-state gain was observed. We find that the negative differential gain we observed for the ensemble of quantum dot ground-states was mainly due to free carrier effects, where increasing dephasing effects, combined with saturated gain result in spectral broadening and a reduction in the peak gain. However at higher current densities the excited state gain was significantly lower in the case of a constant heat-sink temperature. This suggested that self-heating effects were more significant than free carrier effects in the case of excited state. Finally, the origin of the negative differential gain is briefly discussed in terms of an empirical model.

3.13: Future Work

To the best of my knowledge, a negative differential gain has not been observed in any other semiconductor laser. An initial step is in a more thorough and systematic fitting of theoretical models.

This observation opens up new considerations which must be made in how the ground-state lasing is quenched in dual state lasing [3.18], the operation of SLDs [3.19] and amplifiers [3.20]. In the case of dual-state lasers, the prospect that gain reduces from the saturated gain value has not been made. Experiments which combine the observation of dual state lasing and careful measurements of gain may assist in understanding here. Furthermore, as free carrier effects are fast, new modulation schemes can be imagined [3.21]. The shift of gain to longer wavelength also opens new prospects for low current density lasing in highly

homogeneous QD laser materials. Here, one can imagine that due to the Poisson distribution high dot occupancy QDs will exist even at low current densities. If the free carrier shift is sufficiently large compared to the inhomogeneous linewidth, this gain may appear where there is no absorption due to unpopulated QDs. Further work in this area requires significant advances in QD epitaxy.

The magnitude of the differential gain (and the sign) is of importance in determining the modulation properties and line-width enhancement factor of a laser. A negative differential gain therefore gives the prospect of a negatively chirped laser. It is possible to imagine a DFB laser operating in the negative differential gain region with tuneable negative chirp. GaAs based DFBs are now emerging, and such devices may be realised. The need for these in optical communications systems is not yet evident though.

References

[3.1] H. Haugh and S. W. Koch, "Semiconductor laser theory with many-body effects", Phys. Rev. A. Vol. 39, 1887(1989).

[3.2] Y. Arakawa and H. Sakaki, "Multidimensional quantum well laser and temperature dependence of its threshold current",Appl. Phys. Lett. Vol. 40, 939(1982).

[3.3] S. Fathpour, Z. Mi, P. Bhattacharya, A. R. Kovsh, S. S. Mikhrin, I. L.,Krestnikov, A. V. Kozhukhov, and N. N. Ledentsov, "The role of Auger recombination in the temperature-dependent output characteristics ($T0=\infty$) of *p*-doped 1.3 μm quantum dot lasers", Appl. Phys. Lett. Vol. 85, 5164(2004).

[3.4] K. Otsubo, N. Hatori, M. Ishida, S. Okumura, T. Akiyama, Y. Nakata, H.Ebe, M. Sugawara, and Y. Arakawa, "Temperature-insensitive eye-opening under 10-Gb/s modulation of 1.3-μm P-doped quantum-dot lasers without current adjustments", Jpn. J. Appl. Phys. 43, L1124(2004).

[3.5] H. C. Schneider and W. W. Chow, "Many-body effects in the gain spectra of highly excited quantum-dot lasers",Phys. Rev. B 64, 115315(2001).

[3.6] S. V. Nair and Y. Masumoto, "Multi-Exciton States in Semiconductor Quantum Dots", Phys. Stat. Sol. (A) Vol. 178, 303(2000).

[3.7] R. Heitz, F. Guffarth, I. Mukhametzhanov, M. Grundmann, A. Madhukar, and D. Bimberg,"Many-body effects on the optical spectra of InAs/GaAs quantum dots", Phys. Rev. B Vol. 62,16881(2000).

[3.8] K. Matsuda, K. Ikeda, and T. Saiki, "Carrier–carrier interaction in single $In_{0.5}Ga_{0.5}As$ quantum dots at room temperature investigated by near-field scanning optical microscope", Appl. Phys. Lett. 83, 2250(2003).

[3.9] M. Sugawara, K. Mukai, Y. Nakata, and H. Ishikawa, "Effect of homogeneous broadening of optical gain on lasing spectra in self-assembled InxGa1-xAs/GaAs quantum dot lasers", Phys. Rev. B Vol. 61, 7595(2000).

[3.10] M. Lorke, W. W. Chow, T. R. Nielsen, J. Seebeck, P. Gartner, and F. Jahnke, "Anomaly in the excitation dependence of the optical gain of semiconductor quantum dots",Phys. Rev. B Vol. 74, 035334(2006).

[3.11] I. O'Driscoll, M. Hutchings, P. M. Smowton, and P. Blood, "Many-body effects in InAs/GaAs quantum dot laser structures", Appl. Phys.Lett. Vol. 97, 141102 (2010).

[3.12] B. W. Hakki and T. L. Paoli, "Gain spectra in GaAs double−heterostructure injection lasers", J. Appl. Phys. Vol. 46, 1299 (1975).

[3.13] H. Shahid, D. T. D. Childs, B. J. Stevens, and R. A. Hogg, "Negative differential gain due to many body effects in self-assembled quantum dot lasers", Appl. Phys. Lett. Vol. 99, 6, 061104, (2011).

[3.14] B. J. Stevens, D. T. D. Childs, H. Shahid, and R. A. Hogg, "Direct modulation of excited state quantum dot lasers", Appl. Phys. Lett. Vol. 95, 061101, (2009).

[3.15] G. P Agarwal and N. K. Dutta, Semiconductor Lasers 2nd Edition,Van nostrand Reinhold, New York, Chapter 2,(1993).

[3.16] Kejia Zhou, Siming Chen, David T. D. Childs, Richard A. Hogg, "Effect of modulation p-doping on the differential carrier lifetime of quantum dot lasers", Proc. SPIE Vol. 8277, DOI: 10.1117/12.909705(2012).

[3.17] M. Grundmann and D. Bimberg, "Theory of random population for quantum dots", Phys. Rev. B Vol.55, 15, 9740–9745 (1997).

[3.18] A. Markus, J. X. Chen, C. Paranthoe¨n, and A. Fiore, "Simultaneous two-state lasing in quantum-dot lasers", Appl. Phys. Lett. Vol. 82, 1224(2003).

[3.19] P. Resneau, A. Enard, Y. Robert, M. Calligaro, M. Krakowski, M. Hopkinson, P. Bardella, M. Gioannini, M. Rossetti, I. Montrosset, M. Blazek, W. Elsaesser, "High power performances of broad bandwidths superluminescent diodes (SLDs) based on chirped-quantum-dot structures operating at 1100 and 1200 nm for optical coherence tomography (OCT) applications", CLEO EUROPE/EQEC DOI : 10.1109/CLEOE-EQEC.2009.5192762 (2009).

[3.20] Tomoyuki Akiyama, Mitsuru Sugawara, M. Ekawa, K. Kawaguchi, Haruhiko Kuwatsuka,H. Sudo, Hiroji Ebe, A. Kuramata, Yausuhiko Arakawa, "Recent progress of quantum-dot semiconductor optical amplifiers", Proc. SPIE Vol. 5594, DOI: 10.1117/12.579889(2004).

[3.21] R. A. Hogg, D. T. D Childs, B. J. Stevens, K. M. Groom, "Methods of Modulating a Quantum Dot Laser and a Multisection Quantum Dot Laser" GB Patent : GB2472361(2009).

Chapter 4
Integrated Amplifier Method for the Measurement of Spectral Gain of 1.3µm Quantum Dot Laser Material

4.1: Introduction

The accurate determination of gain of a material is a key requirement to obtain an understanding of lasers and amplifiers. The peak gain as a function of current density and temperature is used to determine static performance such as the threshold of the laser devices. The rate at which the peak gain evolves with current and temperature is used to determine its various dynamic and non-linear performances; the modulation characteristics of the laser, etc. The form of the gain spectrum allows the determination of the line width enhancement factor and is influenced by the carrier distribution, and configuration of higher energy states. Understanding how the peak in gain evolves is best understood by observing the gain spectrum. Quantum dot lasers exhibit a broad band emission, low threshold current density and lower transparency current density accompanied by a lower net modal gain as compared with their quantum well counterparts. At these low current densities the spontaneous emission power is also low. Furthermore, the broad spectral bandwidth of some quantum dot devices makes the measurement of the spontaneous emission and amplified spontaneous emission signal, required to one degree or another for all spectral techniques, a challenging task. Therefore, techniques which can be used at low current densities to measure the net modal gain correctly with a wide spectral range are vital to characterise quantum dot devices and hence be used to improve their performance.

Laser engineering and design optimization often requires the exact determination of transparency current density, transparency point, internal loss and evolution of states due to

free carrier effects. The determination of the change in transparency energy and carrier distributions among dots as a function of increase in excitation levels is vital to understand the physics of dots and material behavior. All these require the access of wider spectral ranges and the lowest possible current densities.

4.2: Outline

A conventional technique for spectral gain measurement at room temperature is the segmented contact method [4.1] where different lengths of a waveguide are driven to determine the single pass gain. This is the electrically driven equivalent of the variable optical stripe excitation method [4.2]. By this method, unguided spontaneous emission is eliminated through the use of external spatial mode filters. A modification of this method was demonstrated by Xin *et al.* where the device's own waveguide was used as a mode filter [4.3] eradicating the requirement of an external filter. However, one drawback of this technique is the signal attenuation in the unpumped mode filter section. This is discussed later in this chapter.

Another method, the integrated amplifier method, a modification proposed by Xin *et al.* [4.4] as an enhancement to their integrated mode filter method [4.3] is demonstrated for the first time, and analysed in detail in this chapter. It is shown that the waveguide material may act as a combined integrated amplifier *and* mode filter. By driving the amplifier section, it is possible to achieve 3-dB signal amplification. As a result, the gain spectrum may be deduced over a broader spectral range. The measurement of the gain/absorption spectrum is obtained under identical data acquisition conditions as for the integrated mode filter and segmented contact methods. Further, it is shown that the integrated amplifier method enables gain measurements at lower current densities, as compared to the standard technique [4.1], [4.3].

The relative advantages and disadvantages of conventional techniques [4.1], [4.3] and the integrated amplifier method are discussed in detail.

4.3: Device Epitaxy & Fabrication

A bi-layer InAs/GaAs quantum dot laser device was used for the gain comparison grown by Dr. E. Clark. The schematic is shown in Figure 4.1. The structure comprises five pairs of closely-stacked quantum dot layers. The small separation (10 nm GaAs) between the paired layers results in preferential nucleation of quantum dots in the second layer above quantum dots in the first (seed) layer, so that the seed layer acts as a template for quantum dot growth in the second layer, fixing the quantum dot density [4.5]. This allows suitable growth conditions for the second quantum dot layer to be chosen to achieve emission wavelengths at room temperature from the quantum dot ground state beyond 1300 nm while maintaining a reasonable QD density i.e. ~2.7×10^{10} cm^{-2}. The device epitaxial details are described elsewhere [4.6].

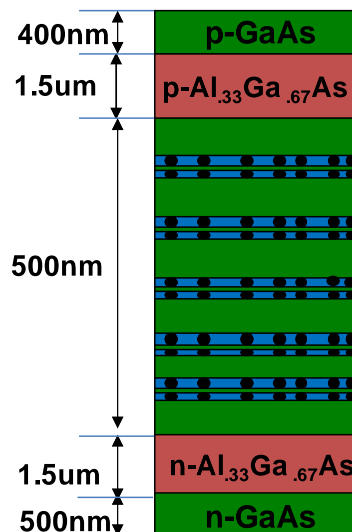

Figure 4.1: Schematic of InAs/GaAs bi-layer device.

The small separation between the paired layers allows efficient electronic coupling between the layers so that emission occurs from the second, long-wavelength quantum dot layer [4.6]. The TEM image of the bi-layer sample is shown in Figure 4.2[4.7].

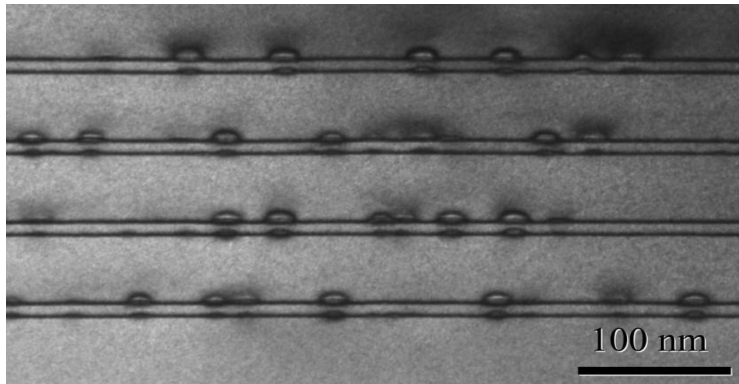

Figure 4.2: TEM of 5 bi-layer sample showing the coupled seed layer and emission layer for each composite layer known as bi-layer [4.7].(courtesy: Richard Beoland, Integrity Scientific),

The wafer was fabricated into 10mm long devices with 1mm isolated contacts and 300nm, the etch depth as shown in Figure 4.3 by Dr. K. Kennedy and Dr. Kristian Groom. This etch depth ensured the individual segments were electrically isolated, however an optical wave guiding was successfully achieved. The waveguides were 7 microns wide. A v-etched absorber was fabricated and cleaved to avoid reflections to allow the single pass measurement.

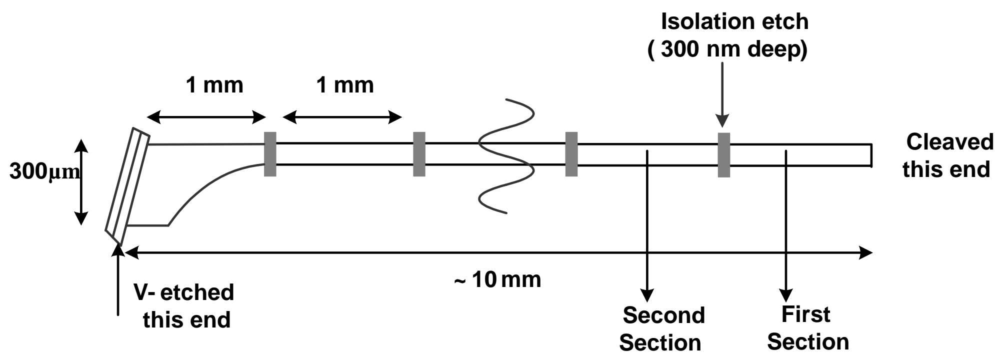

Figure 4.3: Bi-layer device fabrication details.

4.4: Device Characteristics

For the integrated amplifier method the front two sections of the multi-section device are used to act both as mode filter and amplifier and the 3rd and 4th sections are electrically driven in the same way as for the segmented contact method. Therefore the front four sections of the device under test are required to be identical. The optical power vs. current characteristics cannot be measured for each section for direct comparison without cleaving up the device. As a consequence, I assume that identical voltage vs. current characteristics will correspond to identical optical power vs. current characteristics. The device geometries to obtain voltage vs. current and optical power vs. current characteristics from the front four individual sections of bi-layer multi-section device are shown in Figure 4.4.

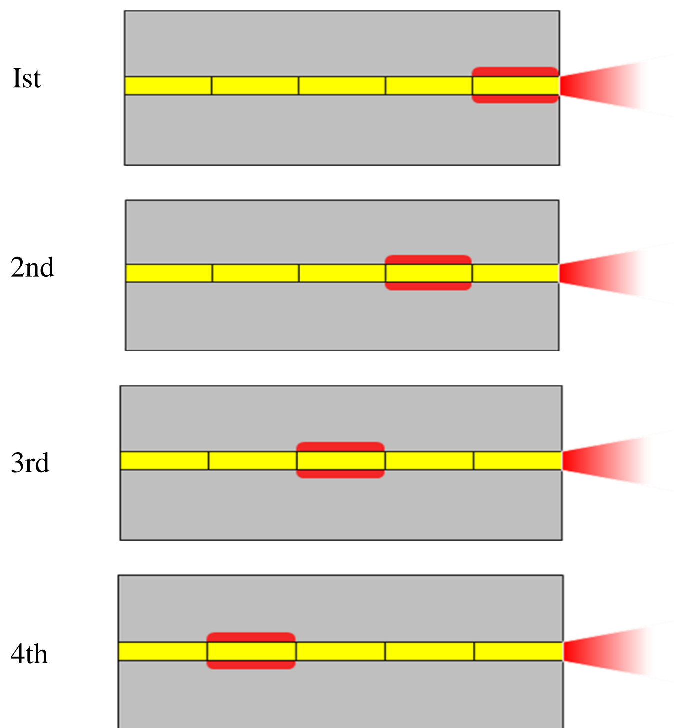

Figure 4.4: Device geometries to obtain voltage vs. current and optical power vs. current of multi-section bi-layer device.

The voltage vs. current characteristics of the first four individual sections is shown in Figure 4.5(a). It can be observed that 1mm section lengths of the multi-section device showed essentially identical differential resistance (~ 4 Ohms) and turn on voltage confirming that all the four sections were electrically identical. The optical power vs. current (L-I) characteristics of the individual sections are shown in Figure 4.5(b).

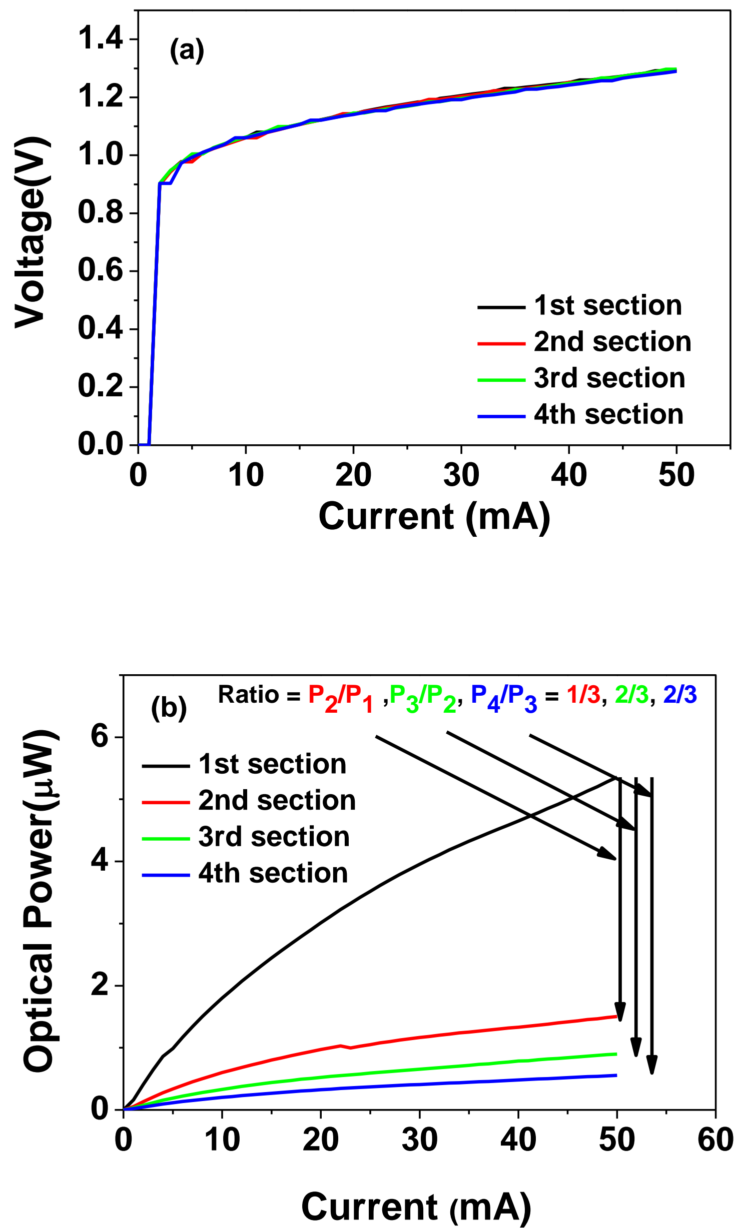

Figure 4.5: (a) Voltage-current characteristics of first four sections of bi-layer device under test. (b) Optical power-current characteristics of the same four sections individually.

A constant attenuation (a constant ratio between the optical power of the corresponding sections) is observed suggesting the individual sections have similar L-I responses. The attenuation ratios are in good agreement with expectation. As absorption is proportional to $e^{-\alpha L}$ then the ratio should be ~3 (e). The higher values of the ratios of the light from the other three sections i.e. 2/3 instead of 1/3 are attributable to the unguided spontaneous emission being added due to the front section.

4.5: Device Geometries

Different multi-section device current injection schemes usually employed for the three different gain measurement methods i.e. segmented contact method, integrated mode filter method, and integrated amplifier method are schematically shown in Figure 4.6.

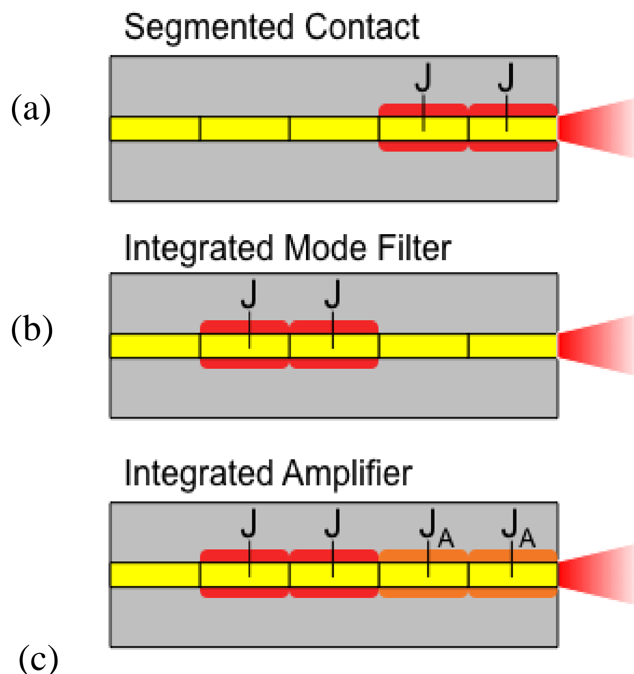

Figure 4.6: Schematic of the different device drive geometries employed.

Using the segmented contact method (Geometry a, Figure 4.6(a)) without the use of an external mode filter the length of the electrically driven device was varied in order to allow the measurement of gain and absorption at each wavelength.

In this case the amplified spontaneous emission spectra are measured for the bi-layer sample at 17°C with driven section lengths of L and 2L at a given current density as shown in Figure 4.7. The comparison of the spectra at each wavelength indicates the presence of gain (or loss) at that particular wavelength which can be calculated [4.1] using eq. 4.1(eq.2.5):

$$Net\ Modal\ Gain = \frac{1}{L}\ln\left(\frac{I_{2L}}{I_L} - 1\right) \tag{4.1}$$

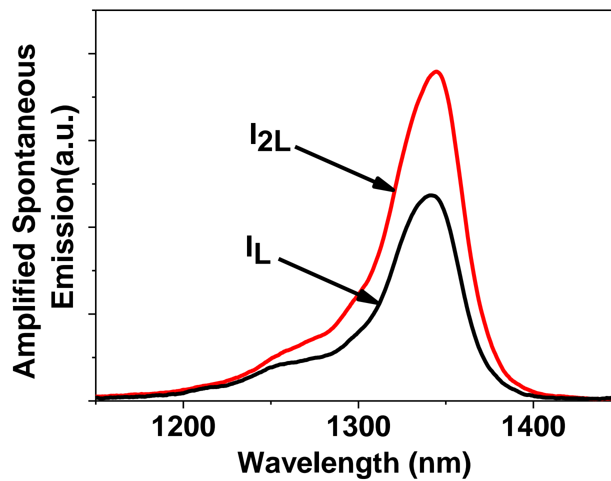

Figure 4.7: Amplified spontaneous emissions from section lengths L and 2L by geometry (A), for a 10mm long (each section length: 1mm) bi-layer device at 17°C.

The integration of a mode filter may be achieved through the introduction of un-pumped sections of the waveguide at the output of the device (Figure 4.6(b)). The electrically driven sections are operated in exactly the same manner as in the segmented contact method (Geometry a). This method has the advantage of simplifying the experimental setup in terms

of optics and improvement in gain measurement as mentioned by Xin *et.al* [4.3]. However, it is identified that as the front section is typically in loss, the signal is significantly attenuated. The net modal gain in this case can be determined by the same relationship as given by eq.4.1.

An integrated amplifier *and* mode filter is obtained by driving the front sections of the device into gain over the spectral region of interest by pumping it with an optimum current density. The device geometry for the integrated amplifier method is as shown schematically by Geometry 'c' in Figure 4.6, where the front sections act as a combined amplifier and mode filter. In order to deduce the gain spectrum through the integrated mode filter method, initially the emission spectrum from only the amplifier/mode filter is measured, i.e. with the front two sections driven at a current density of J_A in our case. This intensity, I_A, is subtracted from the intensities I_L (driving a single contact at a given current density) and I_{2L} (driving two contacts at the same current density as is for I_L). The amplified spontaneous emissions obtained are shown in Figure 4.8. The net modal gain in this case can be deduced using [4.4] the eq. 4.2 (eq.2.7):

$$Net\,Modal\,Gain = \frac{1}{L}\ln\left(\left(\frac{(I_A + I_{2L}) - I_A}{(I_A + I_L) - I_A}\right) - 1\right) \qquad (4.2)$$

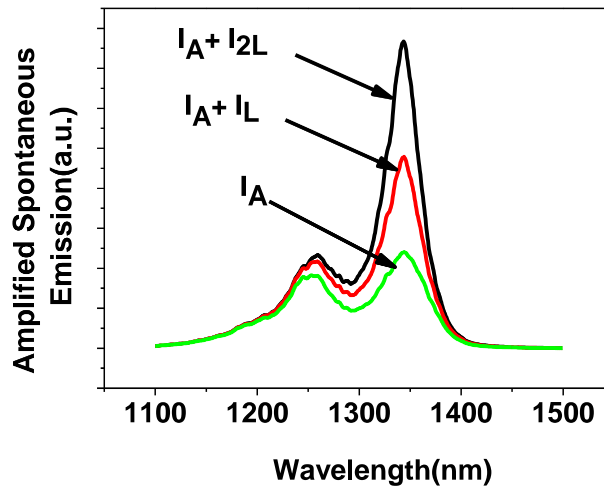

Figure 4.8(2.14): Amplified spontaneous emissions from amplifier section (I_A) and sections of lengths L and 2L (I_L and I_{2L}) for geometry C.

4.6: Apparatus

The measurement system is shown schematically in Figure 4.9. It is important to note that for a fair comparison of the different methods an external mode filter was not employed for any of the methods. This is a key requirement for the segmented contact method, however, this ensured that the light collection efficiency was constant for all the three cases. All other acquisition parameters (resolution, sensitivity and integration times) were kept constant. The experimental apparatus is quite simple (compared to the apparatus for Hakki and Paoli described in the previous chapter). The continuous wave output, from the chip is fed directly into an optical spectrum analyser via a multimode mode fibre. Finally, the data acquisition is performed via computer.

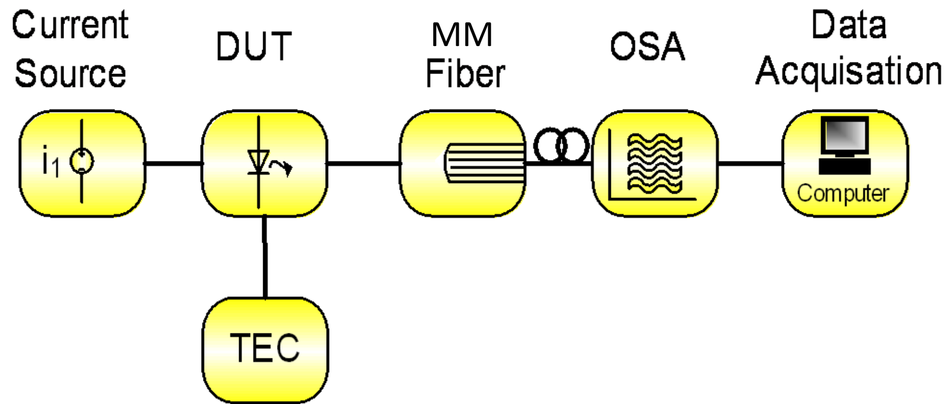

Figure 4.9. Experimental setup for the three gain measurement schemes.

4.7: Results and Discussion

4.7.1: Gain Measurement

Generally with these methods, the gain spectrum can only be determined for wavelengths at which spontaneous emission occurs and the optical signal intensity is above the noise floor. Figure 4.10(a) plots the spontaneous emission spectrum at $14Acm^{-2}$ at which the material is operating in loss for the whole spectral region. So, depending upon the details of spectral acquisition and the magnitude of the absorption, the spectral region over which the gain can be deduced will be significantly smaller than the region of spontaneous emission. Therefore, the gain spectrum may not be obtained over shorter wavelengths than say < ~ 1275nm where spontaneous emission is weak and signals are lost in the noise floor. Figure 4.10(b) plots the gain spectrum determined using, the segmented contact method of Figure 4.6(a) at a current density of $1.42kAcm^{-2}$, where positive net modal gain is obtained in the spectral region 1150 - 1300nm. The amplifier section may therefore be expected to increase the spectral range over which the gain/loss can be deduced.

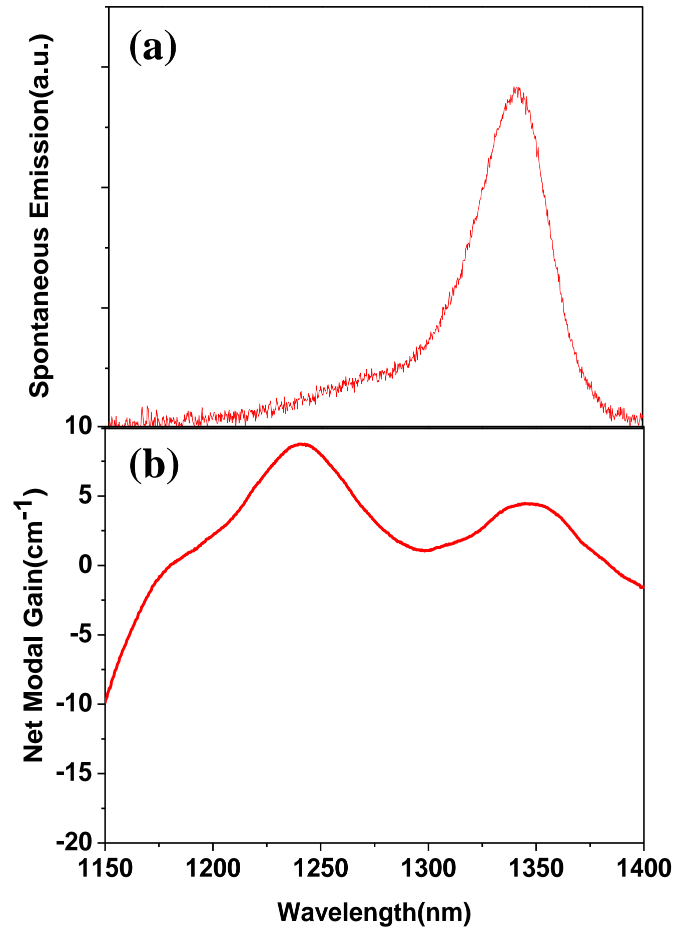

Figure 4.10: (a) Spontaneous emission spectrum at $14Acm^{-2}$ by pumping a section of length L. (b) Net modal gain spectrum at $1.42kAcm^{-2}$ obtained from the amplifier section as a function of wavelength measured by the segmented contact method.

4.7.2: Results and Discussion

Comparison of the gain spectra deduced using the three measurement schemes is shown in Figure 4.11 at a current density of 350 Acm^{-2} with an amplifier current density (J_A) of 350 Acm^{-2}.

Towards longer wavelengths all three techniques show essentially identical results in terms of the spectral shape and magnitude of the peak gain for the ground state. At shorter wavelengths the methods utilizing the integrated mode filter (Geometry (b)) and integrated amplifier (Geometry (c)) are coincident. For shorter wavelengths the gain spectrum may not be obtained with these data acquisition parameters utilizing the integrated mode filter method (Geometry (b)), due to attenuation of the emission (mode filter operated in loss) and the signal being indistinguishable from the noise floor.

For the two techniques (Geometry (b)) and Geometry (c)) that utilize a mode filter a slightly different gain spectrum is obtained in comparison with the segmented contact method (Geometry (a)) towards shorter wavelengths. The difference suggests either the presence of unguided spontaneous emission in configuration 'a' or spatial inhomogeneity of the sample. However, similar measurements for different materials where the length of the contact was varied showed similar results, suggesting that this difference is due to the absence of external mode filtering in Geometry (a). Furthermore, the observation of a change in the excited state gain but not in ground state gain between the different spectra in Figure 4.11 is unlikely to be due to spatial inhomogeneity of the QDs. However, a spatial variation in carrier life time could produce such an effect.

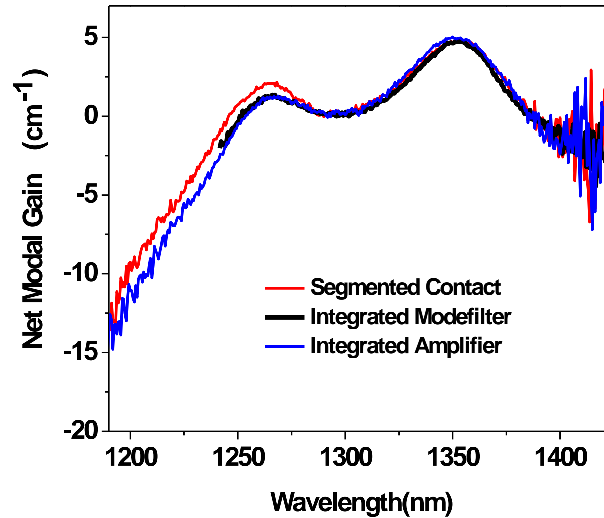

Figure 4.11: Net modal gain spectra as a function of wavelength for J=350Acm^{-2} and J_A=350Acm^{-2} utilizing schemes a, b, and c.

Figure 4.12 plots the gain spectra as a function of current density for (a) segmented contact (Geometry (a)) and (b) integrated amplifier (Geometry (c)) with an amplifier current density of J_A=1.42kAcm^{-2}. For these plots, the data is manually inspected and only where the signal can be distinguished from the noise floor is it plotted. Wider ranges of the gain spectrum are measured using the integrated amplifier method (Geometry (c)) with identical data acquisition conditions. These differences become smaller as the current density in the sections being measured is increased, where the sections under test are no longer in loss but are in gain. For low current densities however, the difference is clearer; in terms of enhanced spectral range and with some current densities only being accessed through the use of the integrated amplifier. The gain spectra are noisier in the case of the integrated amplifier method as it is expected that the signal experiences both attenuation and amplification while passing through the amplifier section of the waveguide. This is clearer towards the shorter wavelengths and at lower current densities where the waveguide material operates in loss.

It should be noted that for the segmented contact method (Geometry (a)) the external mode filter was omitted. The introduction of this lossy component is expected to enhance the observed benefits of the integrated amplifier.

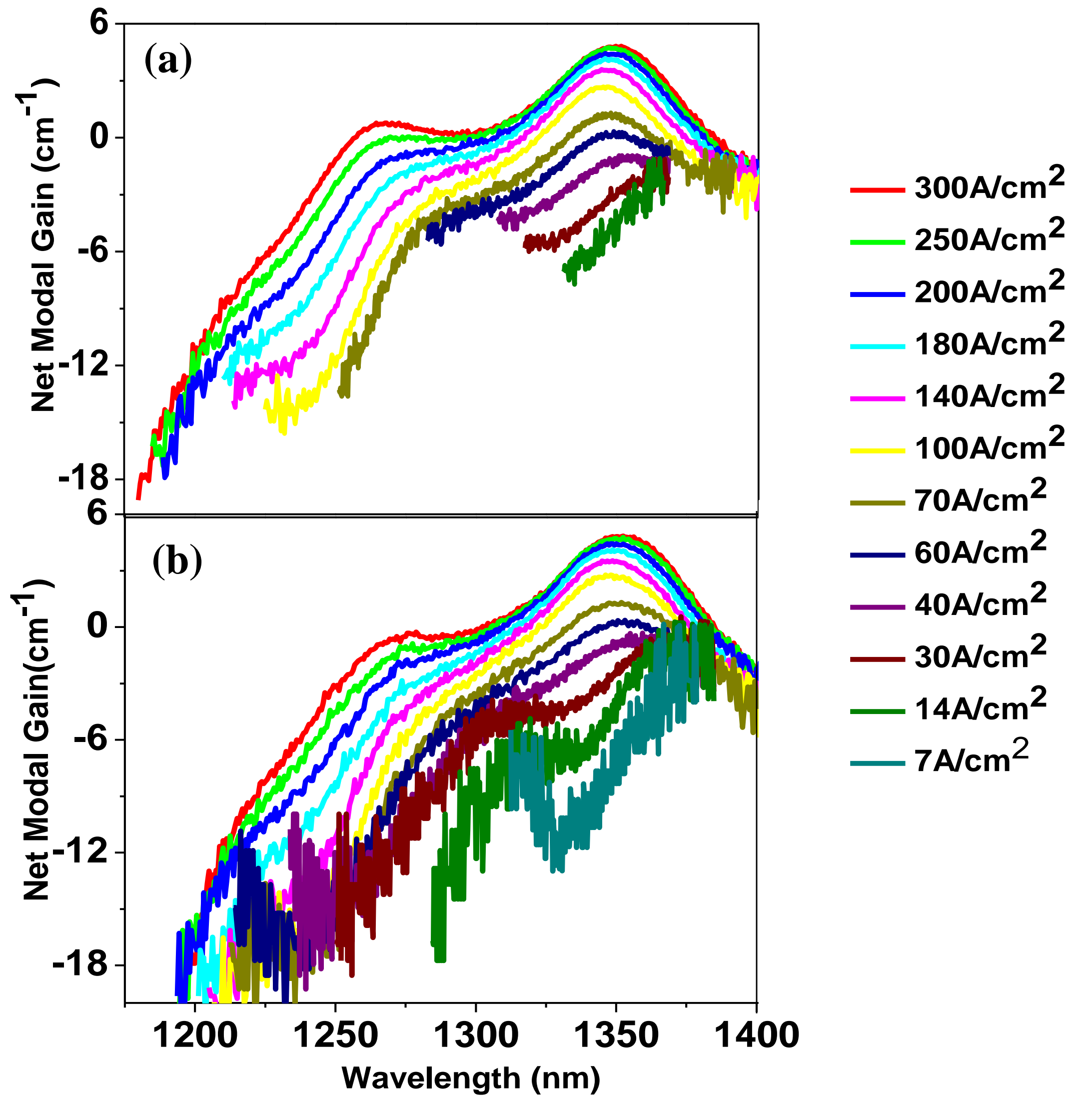

Figure 4.12: Net modal gain spectra as a function of wavelength for (a) a current density range $14Acm^{-2}$ – $300Acm^{-2}$ utilizing the segmented contact method and (b) $7Acm^{-2}$ – $300Acm^{-2}$ utilizing the integrated amplifier method.

This method allows the measurement of the gain/absorption spectrum at low forward current density. The lowest current density shown corresponds to average dot occupancy of ~ 0.04 e-h /QD, deduced from the peak intensity of spontaneous emission at this current density, compared to the saturated spontaneous emission.

Figure 4.13 plots the modal gain derived from Figure 4.12 including α_i (~ 2cm^{-1}) and spontaneous emission as a function of wavelength. In Figure 4.13 (a) at 7Acm^{-2} (~ 0.04 e-h /QD), where the dots are essentially empty, modal absorption of 9 ±1 cm^{-1} is measured for the ground state. The saturated modal gain of the ground state (at ~300 A cm^{-2}) is 7±1 cm^{-1}. These values are very similar, with the difference in these two values attributed to the different possible carrier occupancies of the filled quantum dot leading to an additional broadening mechanism (due to different magnitudes of the free carrier shift of the band-gap) which reduces the peak gain, as compared to the peak absorption at these biases. This contrasts previous reports where absorption spectra and gain spectra were compared under different bias conditions [4.1, 4.8], where very different values for absorption and saturated gain were deduced.

Figure 4.13 (b) shows that at low current density, i.e. at 7Acm^{-2} (~ 0.04 e-h /QD), the spontaneous emission and absorption peak (Figure 4.13 (a)) are observed to be coincident (1338nm/0.93 eV). However, at high current density the spontaneous emission and peak in gain do not coincide, with the gain peak being ~4meV smaller in energy. As self-heating effects are identical in both cases [4.1, 4.3], this shift is attributed to free carrier effects, where the free carrier shifted gain spectra is superimposed upon the absorption spectra. The observation that the spontaneous emission does not significantly shift in peak position (certainly no blue shift) from low occupancies (0.04 e-h pairs per QD) to ground state saturation appears at odds with the blue shift of the gain peak with increasing current density. This is once more attributed to the free-carrier shift of the gain as compared to the absorption

spectrum. It is tentatively suggested that the red-shift of QDs in gain, superimposed upon the absorption shows self heating effects and that the free carrier effects where carrier population is more random-like in nature.

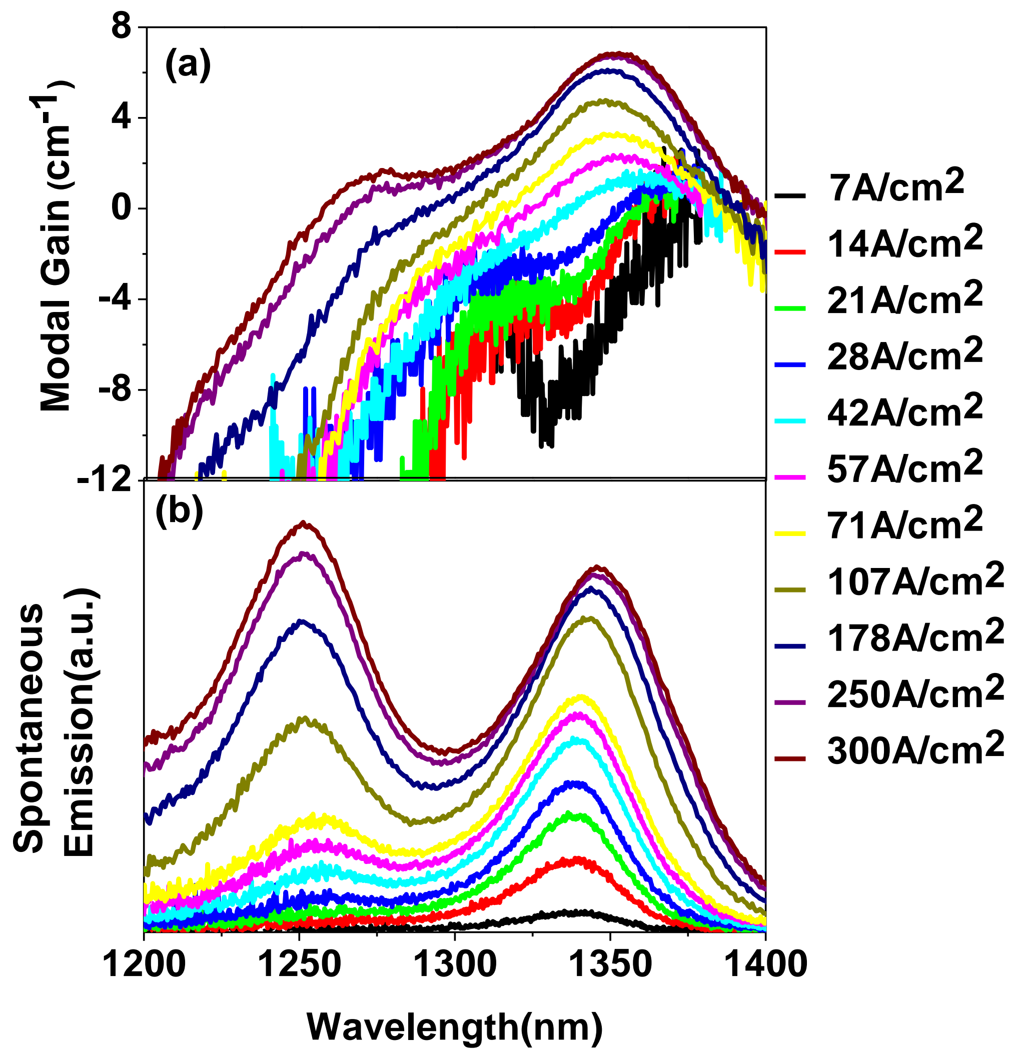

Figure 4.13: (a) Modal gain and (b) spontaneous emission spectra obtained by integrated amplifier method.

4.8: Summary

In this chapter a comparison of gain spectrum measurement techniques utilizing a multi-section bi-layer InAs/GaAs quantum dot laser device to access low current densities was presented. A modified measurement technique, the integrated amplifier method was employed for the analysis by using the output sections of a multi-section device as an integrated optical amplifier and mode filter. The resultant enhancement to the spectral range over which the gain can be determined was discussed in detail. This technique was shown to be particularly advantageous for the measurement of the absorption/gain spectrum at low carrier densities where the waveguide is operating in loss. A brief comparison of gain spectra and spontaneous emission spectra is presented, highlighting the use of integrated amplifier method in analysing the quantum dots at low injection levels.

4.9: Future work

The integrated amplifier method has demonstrated that more gain spectrum information can be obtained. This has been carried out on-chip, with a modest amplification (~3dB). It would be interesting to try this technique on high gain material where the amplification could be higher and therefore benefits would be greater. Significant insight into the carrier distributions in QD lasers at low current densities may be made. Another possible experiment is to try using an external fibre coupled amplifier. Whilst this is less convenient, costly, and suffers from a possible spectral mis-match between the device under test and the amplifier, large levels of amplification (e.g. 20-25dB) may be possible.

References

[4.1] P. Blood, G. M. Lewis, P. M. Smowton,"Characterization of semiconductor laser gain media by the segmented contact method", IEEE J. sel. Top. In Quant. Elect. Vol. 9, 1275 - 1282(2003).

[4.2] K. L. Shaklee and R. F. Leheny, "Direct Determination of Optical Gain in Semiconductor Crystals"**,** Appl. Phys. Lett. Vol. 18(1971).

[4.3] Xin *et al.*, "Determination of optical gain and absorption of quantum dots with an improved segmented contact method", Proc. SPIE Vol. 572, 49 - 59 DOI: 10.1117/12.591241(2005).

[4.4] Y.C. Xin, Yan Li, Anthony Martinez, Thomas J. Rotter, Hui Su, Lei Zhang, Allen L. Gray, S. Luong, K. Sun, Z. Zou, John Zilko, Petros M. Varangis, and Luke F. Lester, "Optical gain and absorption of quantum dots measured using an alternative segmented contact method", IEEE J. Quant. Elect. Vol. 42 (2006).

[4.5] P. Howe, E. C. Le Ru, E. Clarke, B. Abbey, R. Murray, T. S. Jones, "Quantification of segregation and strain effects in InAs/GaAs quantum dot growth",J. Appl. Phys. Vol. 95 (2004).

[4.6] M. A. Majid, D. T. D. Childs, H. Shahid, S. C. Chen, K. Kennedy, R. J. Airey, R. A. Hogg, E. Clarke, P. Spencer, and R. Murray, "Excited state bilayer quantum dot lasers at 1.3μm", Jpn. J. Appl. Phys. 50 (2011).

[4.7] E. Clarke, P. Howe, M. Taylor, P. Spencer, E. Harbord, R. Murray, S. Kadkhodazadeh, D. W. McComb, B. J. Stevens, and R. A. Hogg, "Persistent template effect in InAs/GaAs quantum dot bilayers", J. Appl. Phys. Vol. 107, 113502 (2010).

[4.8] I. C. Sandall, C. L. Walker, P. M. Smowton, D. J. Mowbray, H. Y. Liu, "Measurement of modal absorption, gain and recombination in p-doped and intrinsic quantum dot structures", Optoelectronics, IEE Proceedings, 153 , 6, 316 - 320, (2006).

Chapter 5: Lasing Spectral Analysis for O-band Optical Communication

5.1: Introduction

For a fibre optic optical communications system, there are two limits in order to successfully maintain a given bit error ratio for the transmitted signal. Firstly, attenuation of the signal may result in the signal being indistinguishable from noise. Secondly, dispersion of the optical pulses may result in inter-symbol interference, overlapping the train of optical pulses. A figure of merit for determining the dispersion limit of an optical system is ε (epsilon); eq.5.1:

$$\varepsilon = \mathrm{BL}\Delta\lambda D(\lambda) \qquad (5.1)$$

where B is the bit rate, L is the transmission length, $\Delta\lambda$ is the spectral linewidth of the transmitter, and $D(\lambda)$ is the fibre dispersion coefficient. Depending on the specifics of the particular system $\varepsilon \leq 0.5$. Whilst the launch power of the transmitter, power budget, and sensitivity of the receiver, determines the attenuation limit, the linewidth of the transmitter is key in determining the dispersion limit.

QD lasers are currently being commercialized for fibre-to-the-home (FTTH). Figure 5.1 plots the spectral line-width of commercial 10GHz, QD laser devices as a function of temperature along with spectral width requirements of a PX10 optical transmitter to achieve the IEEE P802.3av 10G-EPON standard [5.1] (data provided by Dr M. Sugawara, QD Laser Inc.) for O-band telecommunication. The linewidth requirement to achieve $\varepsilon = 0.123$ by PX10 optical transmitter are also shown in Figure 5.1.The empirically obtained data corresponds to 1905 samples, showing the difficulty in meeting this specification using quantum dot lasers.

In this chapter the effect of inhomogeneous linewidth on the lasing linewidth of QD lasers is studied. Two samples, with different inhomogeneous linewidth are compared under conditions where it is hoped that the effects of homogeneous linewidth and spectral hole burning are maintained at a constant level, allowing the effects of inhomogeneous linewidth alone to be studied.

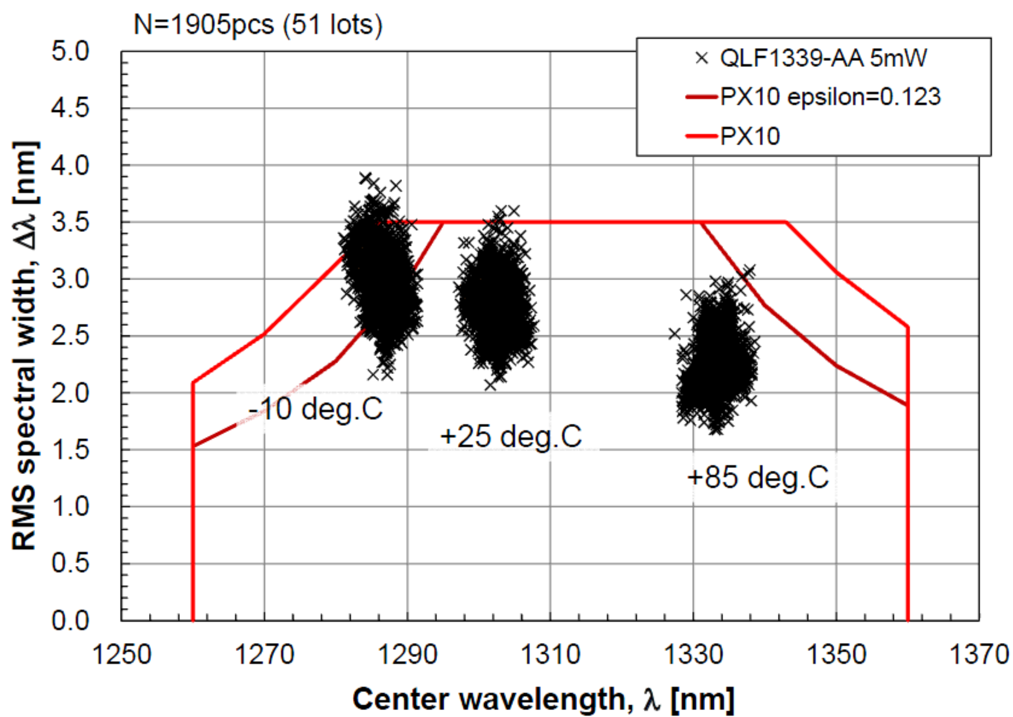

Figure 5.1: black crosses: The measured RMS spectral width of 1905 samples of the material: QLF1339-AA at 5mW, as a function of central wavelength at -10°C, 25°C and 85°C (courtesy: Dr M. Sugawara, QD Laser Inc.), (light red) RMS spectral width for the standard PX10 transmitter for o-band (1260nm-1360nm), (dark red) Required RMS spectral width to achieve $\varepsilon = 0.123$ for PX10 optical transmitter.

5.2: 3-dB Line Width of Lasing Spectrum

By increasing the drive current, the gain and hence the corresponding intensity of the individual longitudinal modes (where round-trip phase matching is satisfied) of a Fabry-Pérot laser device increases. As soon as the net modal gain equals the mirror loss, the device starts lasing. With any further increase in injection current the gain spectrum should not change. However, increasing the drive current above threshold often manifests itself as an increase in the intensity of (neighbouring) modes in addition to the main mode which initially met the threshold gain condition. The processes by which this occurs are described in the subsequent sections. Resultantly, a number of lasing modes may be observed at a given drive current, with the lasing line width increasing (an increase in the number of lasing modes) with increasing injection current [5.2]. Figure 5.2 plots the, electroluminescence spectrum above threshold for a 1.3µm InAs/GaAs Innolume quantum dot (QD) laser device (1mm long, 3µm wide as described in (section: 5.5)), with 3mW output power at 30°C, constant heat-sink temperature, under continuous wave operation. The, 3-dB lasing spectral line width of a lasing spectrum is shown, which is ~ 6.5nm (4.5meV).

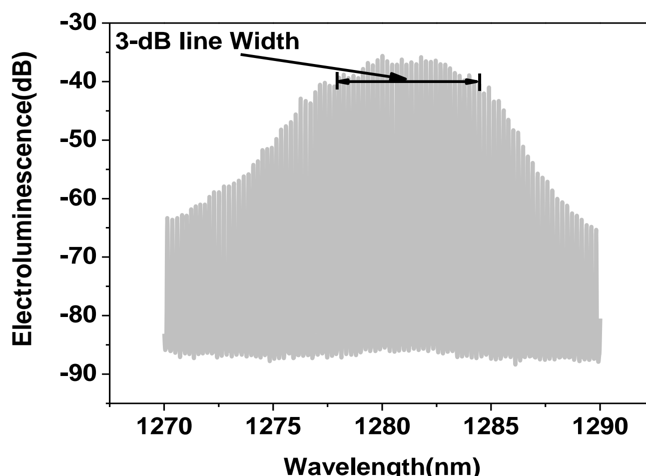

Figure 5.2: The lasing, electroluminescence spectrum, for 1.3µm Innolume laser device as a function of power (optical power: 3mW, heat-sink temperature: 30°C), showing 3-dB lasing spectral line width measurement.

5.3: Inhomogeneous Broadening

Ideally in the case of QDs of identical size and composition the individual energy transitions of each would perfectly overlap. Resultantly, as shown in Figure 5.3(a) the ensemble of identical electronic states would appear as delta like function.

However, the Stranski-Krastanov (self-assembled) QDs grown by molecular beam epitaxy are not of the same size, with the QD size distribution being approximated as Gaussian [5.3]. The broadened, resulting emission spectrum of the ensemble is due to many dissimilar electronic states. In the case of this inhomogeneous broadening being small compared to the separation between states, an emission spectrum similar to that in Figure 5.3(b) is obtained.

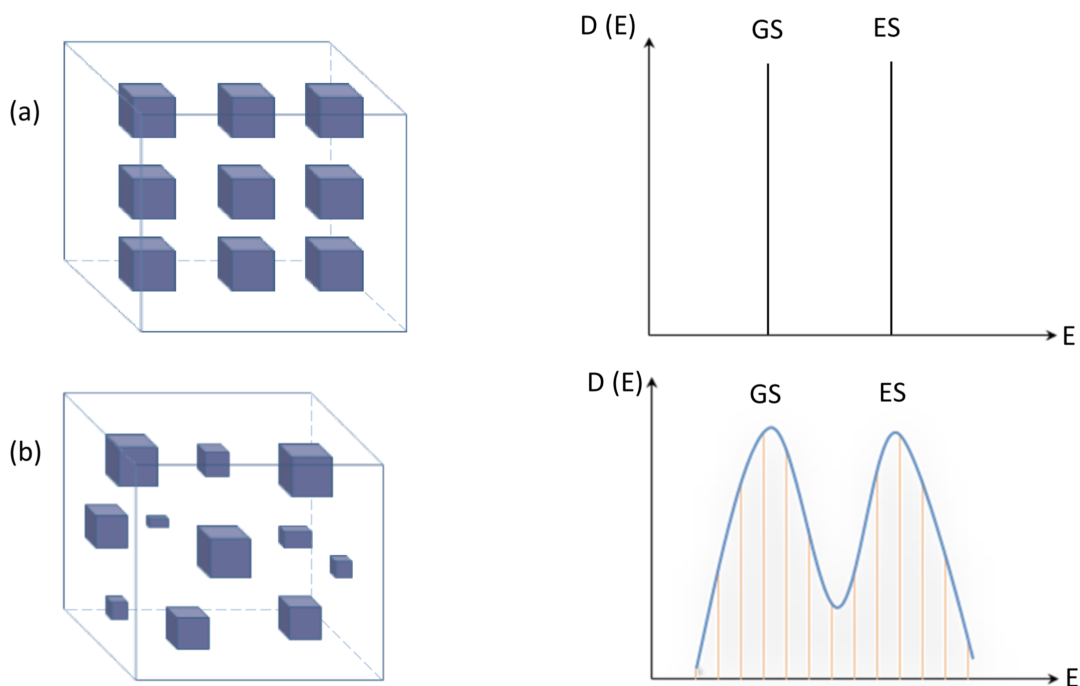

Figure 5.3: The expected density of states for GS and ES as a function of energy for a QD laser material exhibiting the inhomogeneous broadening in case of (a) similar, (b) dissimilar dot sizes.

The line widths of the GS and ES optical transitions in this case would depend upon the uniformity of dot sizes. More homogeneous (same dimension/similar sizes/similar

composition) dots would result in reduced inhomogeneous line widths of the individual transitions (GS and ES). Measurements of the spontaneous emission [5.4] and absorption spectra [5.5] of a laser device can provide a comparative measurement of inhomogeneous linewidth with and without free carrier effects.

5.4: Homogeneous Broadening

The increase in temperature or excitation level (average number of electron-hole (e-h) pairs per QD) influences the entire dot ensemble by increasing the line width of the individual quantum dots. Resultantly, the line width of the overall spontaneous emission and gain spectrum is increased. This is known as homogeneous broadening.

The mechanism and influence of the homogeneous broadening upon the QD laser emission can be explained as follows: For a laser device, by increasing the current/temperature the homogeneous line width of individual dots increases. At some point, as shown in Figure 5.4, the overall homogeneous broadening may become comparable with the inhomogeneous broadening. At low temperatures and current densities (low Γ_{hom}) various QDs act independently to lase with a broad spectral line width. For larger Γ_{hom} (higher temperatures and current densities) QDs spatially and spectrally isolated from lasing QDs may now contribute to lasing. This process results in a reduction in lasing line width with increasing Γ_{hom}.

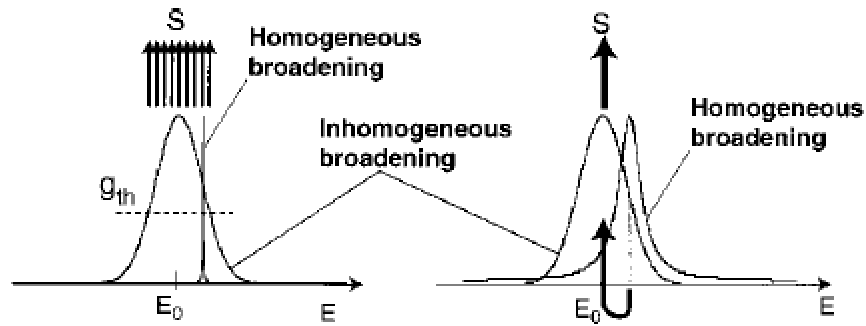

Figure 5.4: The lasing spectra, of a QD laser device as a function of homogeneous broadening which connects the spatially isolated dots, resulting in an emission via narrow lasing line [5.6].

In order to compare two quantum dot devices with similar homogeneous broadening, it is essential to compare them at the same population inversion level i.e. at the same percentage of their corresponding saturated modal gain and the heat-sink temperature.

5.5: Spectral Hole Burning

Spectral hole burning is a process which may usually occur for Fabry-Pérot laser devices. Its effect on lasing line width can be explained as follows:

Figure 5.5 (a) plots a schematic of the Fabry-Pérot mode reflectivity as a function of wavelength. The gain spectrum is shown schematically in Figure 5.5 (b). The ideal lasing spectrum is shown in Figure 5.5 (c), considering perfect gain clamping. However, the increase in photon density with increasing drive current will denude the lasing QDs of carriers as the stimulated recombination rate and carrier supply rate to these states becomes similar. This creates a “Spectral hole” centred on this lasing mode (see Figure 5.5 (d)). As the laser is operating at a current significantly higher than threshold, as lasing from the main mode quenches so gain increases resulting in lasing from neighbouring modes may lase as a consequence of this process. These instantaneous effects result in a time-integrated increase in lasing line width with increasing laser power.

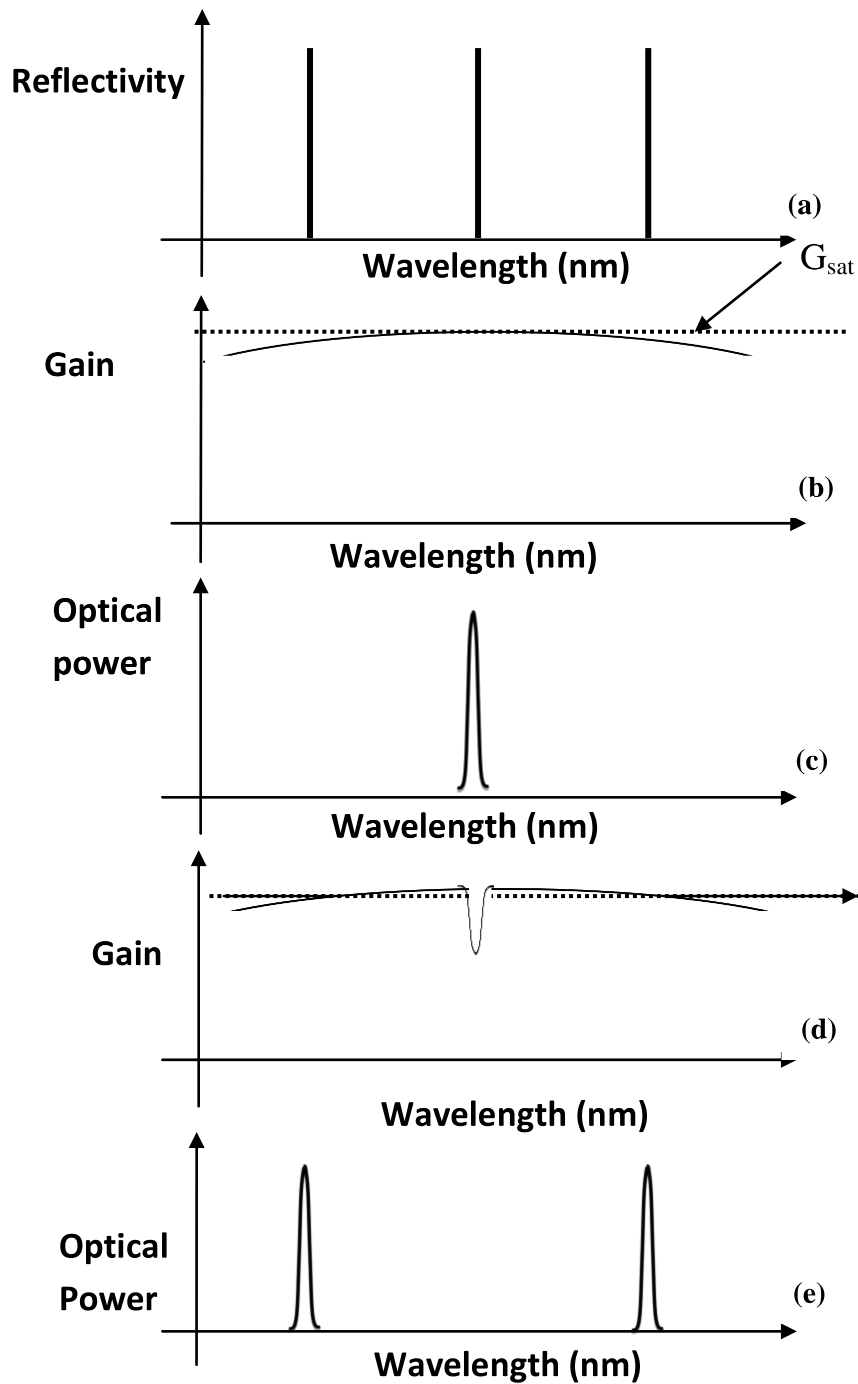

Figure 5.5: (a) Fabry-Pérot longitudinal modes, (b) time integrated gain response (c) lasing via single mode, (d) the spectral dip in the gain spectrum, (e) lasing via neighbouring modes.

5.6: Outline

In this chapter the 3-dB lasing line widths of two quantum dot laser devices are compared under continuous wave operation, at a constant heat-sink temperature of 30°C. One of the selected devices is fabricated from the commercial Innolume epitaxial material and is composed of 10 QD layers while the other is fabricated from QD bi-layer material comprising 5 bi-layers. Both devices are realised as single mode Fabry-Pérot lasers. The laser cavity lengths are selected, such that at lasing both devices should operate at approximately the same inversion level. By doing this, we try to maintain the same homogeneous broadening in the two devices.

The 3-dB lasing spectral line width is measured and compared as a function of output power, and in an attempt to make spectral-hole burning effects similar, this is also discussed in terms of output optical power/QD. This is discussed with reference to the line widths of the spontaneous emission and gain spectra which provide a measure of inhomogeneous broadening.

5.7: Material Characteristics

In this section various material characteristics of the Innolume and bi-layer devices are discussed. The segmented contact method [5.7] is employed to estimate the inhomogeneous line widths via spontaneous emission and modal gain results of the corresponding devices. The devices are characterised as a function of current density at 30°C constant heat-sink temperature, under continuous wave operation.

5.7.1: Inhomogeneous Line width Measurement

5.7.1.1: Significance and Measurement Methods

In our case, the significance of measuring the inhomogeneous line width is to check the homogeneity of the QDs for each of the materials being tested, as a reduced inhomogeneous line width corresponds to more dots of the same sizes. Therefore, it is expected that it would lead to higher density of states for GS/ES of QD ensemble. The spectrum would be broadened homogeneously with a small increase in 3-dB line width of the lasing spectrum as function of current density offering reduced mode competition.

Different techniques are employed to estimate the inhomogeneous line width of a laser device, such as photoluminescence measurement [5.8], using a high energy laser as a pump source or by absorption measurement [5.5]. However, in our case we purpose that, via spontaneous emission measurements, it can also be estimated at very low current/carrier densities by keeping the heat-sink temperature fixed at a value. In this case the measured inhomogeneous line width corresponding to a particular heat-sink temperature would not change as a function of current density. In the following, the measurements are carried out at room temperature, so thermal energy, providing some homogeneous line width is present in all cases.

5.7.1.2: Experimental Results

In our case two materials, the Innolume and bi-layer are compared through inhomogeneous line widths at room temperature. Figure 5.6 (a, b) plots the normalized spontaneous emission spectra as a function of current density, by employing the segmented contact method (eq. 2.6), for the Innolume (5mmx3μm) and bi-layer (10mmx7μm) devices at 30°C constant heat-sink temperature, under continuous wave drive. The minimum achievable carrier densities

correspond to ~ 0.03 and ~ 0.04 e-h pairs per QD for the Innolume and bi-layer devices, respectively. It can be observed that for the given range of current densities as shown in the Figure 5.6(a, b) for each of the devices the full width half maximum of the spontaneous spectra does not change. Hence, it is deduced that the line width of the individual dots does not vary for the corresponding carrier densities. The overall contribution of homogeneous broadening to the intrinsic inhomogeneous line width due to thermally induced broadening mechanisms is already given in literature as ~ 8-10meV [5.9] which will be included in this estimate.

The spontaneous emission line widths were measured to be ~40±1meV and ~27±1meV for the Innolume and bi-layer devices, respectively which in each case includes the intrinsic inhomogeneous line width and the additional broadening due to the room temperature. The smaller line width of spontaneous emission spectra of the bi-layer device is suggestive of the majority of its dots mainly being of the same size in comparison to the Innolume laser device.

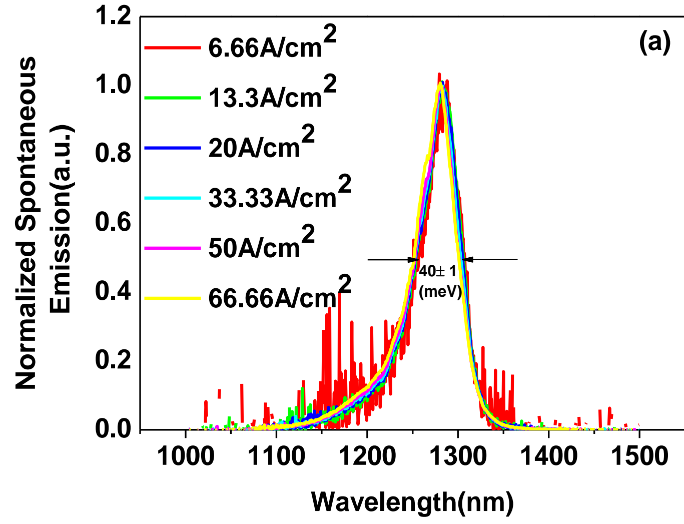

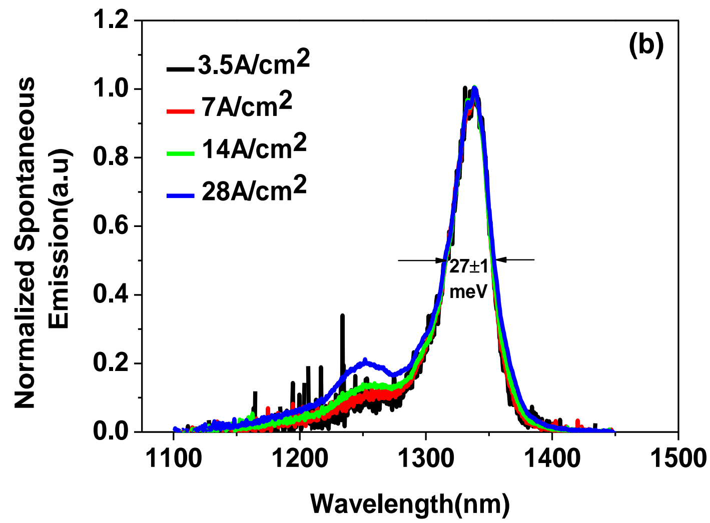

Figure 5.6: Normalised spontaneous emission spectra as a function of current density at 30°C constant heat-sink temperature for (a) Innolume (5mmx3μm,) (b) bi-layer (10mmx7μm) devices, measured via segmented contact method under continuous wave condition.

5.7.2: Modal Gain Measurement

5.7.2.1: Measurement and Significance

The modal gain measurement can be used to retrieve the information about the inhomogeneous linewidth and to explore other broadening mechanisms in the laser device. In our case, by measuring the line width of the modal gain spectra of the Innolume and bi-layer devices, the homogeneity of the dots may be compared again but we would also be including free carrier effects (increasing the homogeneous broadening) as well. As the gain measurement is an important factor, such a measurement is also instructive.

5.7.2.2: Experimental Results

Figure 5.7 plots the normalised modal gain spectra for the Innolume and bi-layer devices. The modal gain spectra for the Innolume (5mmx3µm) and the bi-layer (10mmx7µm) devices were retrieved at 30°C constant heat-sink temperature by the segmented contact method (eq.2.5). To perform a comparison of line widths, the spectral gain results in each case were normalised to their corresponding GS saturated modal gain (Innolume: $24cm^{-1}$, bi-layer: $8cm^{-1}$: section: 5.7.3.2) value. As sown in the Figure 5.7, the line widths of the Innolume and bi-layer devices are measured to be ~ 50±1meV and ~ 34±1 meV respectively. A reduced line width in case of bi-layer device is quite obvious.

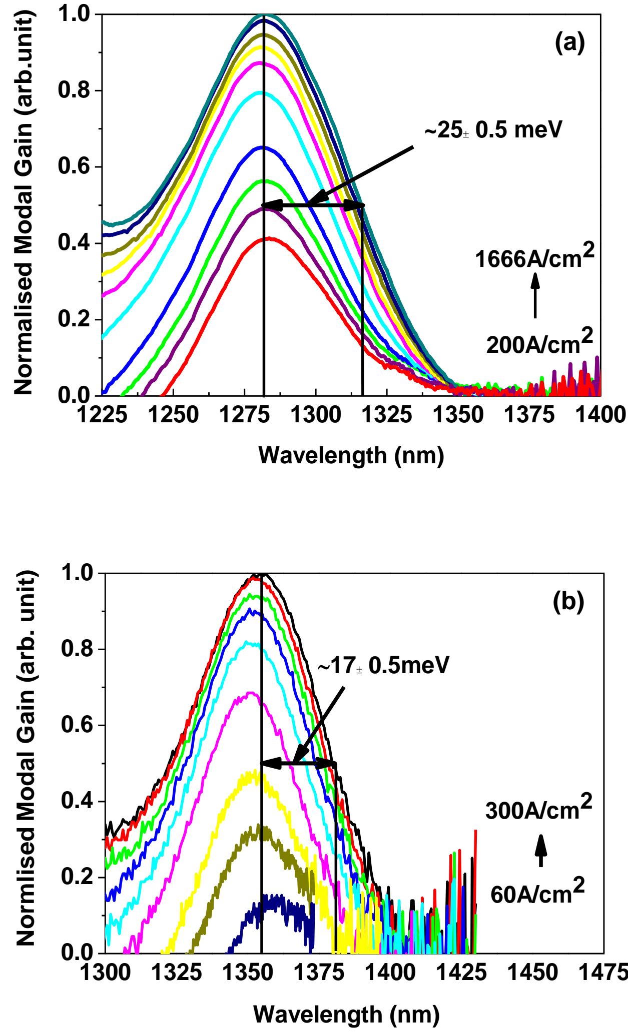

Figure 5.7: Normalized modal gain spectra with respect to the GS saturated modal gain as a function of current density for QD, (a) Innolume (5mmx3µm), (b) bi-layer (10mmx7µm) devices at 30°C constant heat-sink temperature obtained via segmented contact method.

5.7.2.3: Discussion

The measured line width of the modal gain spectrum in each case is due to the contribution of inhomogeneous line width, thermally induced additional broadening and the Poisson carrier distribution. The inhomogeneous line widths of the GS, Innolume and bi-layer devices as already measured by us are ~ 40±1meV and ~ 27±1meV respectively which already include an homogeneous line width due to thermal energy of ~ 8-10meV. The difference between the

measured modal gain line width and the inhomogeneous line width is estimated as ~ 30meV and ~ 21meV for the Innolume and bi-layer respectively. This difference is attributable to the broadening due to the poisson carrier distribution as already discussed in chapter 3(section: 3.10). It is a time averaged response of probable dot occupancies as a function of mean dot occupancy. It is noteworthy that the ratio of the line widths measured by spontaneous emission at low current density (27:40 = 0.68) is almost identical to that measured for gain at high current density (34:50 = 0.68).

5.7.3: Device Length Selection

5.7.3.1: Significance of Device Length Selection

For our analysis, the 3-dB, GS lasing spectral line width of the devices are to be analysed under the same population inversion condition. The main purpose is, to try maintaining the same homogeneous broadening (due to free carrier and thermal effects) at each excitation level. In this way we are able to observe solely, the effects of different inhomogeneous line width of each of the device material on their respective 3-dB lasing line width. For this purpose, the GS gain-current density (G-J) curves for each of the devices are inspected carefully. Laser cavity length selection is based upon selecting devices operating at the same percentage of their respective saturated modal gain.

5.7.3.2: Length Selection

The single pass gain measurements were performed via the segmented contact method at a heat-sink temperature of 30°C, in order to select device (Innolume and bi-layer) lengths for 3-dB, GS lasing spectral line width comparison. The modal gain as a function of current density was determined in each case. Figure 5.8 (a, b) plots the normalised gain as a function of current density curves with respect to the maximum GS gain for each of the devices at 30°C.

The squares (open and closed) represent the experimental data. An empirical fit [5.10] was employed to determine the saturated modal gain values in each case, which were 24±1cm^{-1} and ~8±1 cm^{-1} in case of Innolume and bi-layer devices respectively. The selected devices were operating at 63% of their respective saturated modal gain value. This corresponds to the lengths, 1mm and 4mm for Innolume and bi-layer laser devices respectively.

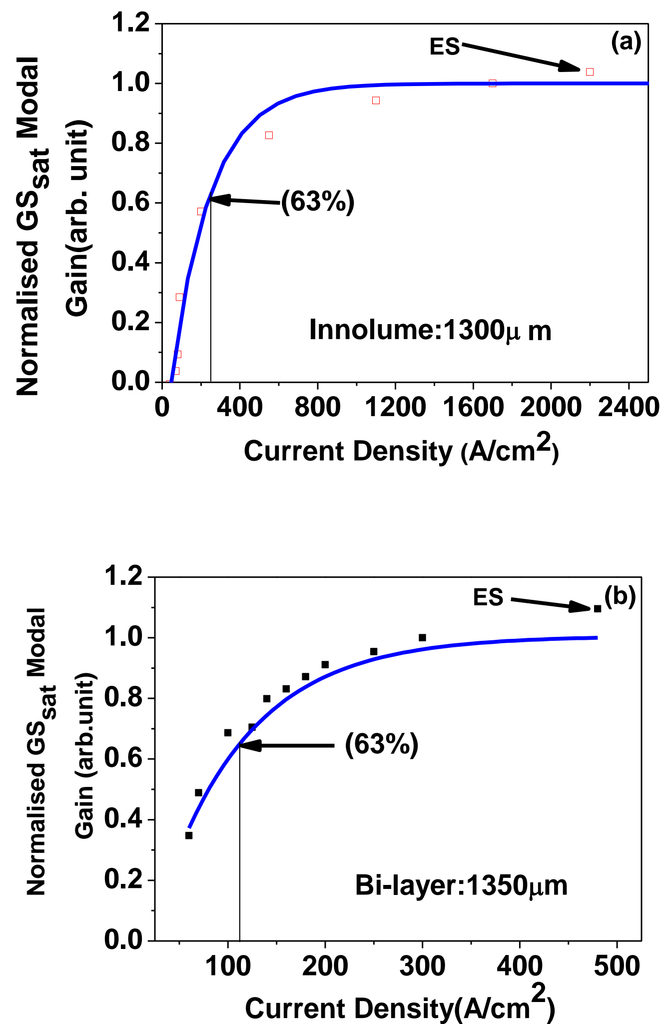

Figure 5.8: The GS normalised (with respect to maximum GS modal gain) modal gain as a function of current density (G-J characteristics) for QD, (a) Innolume (5mmx3μm), (b) bi-layer (10mmx7μm) devices at 30°C by segmented contact method, under continuous wave measurement condition.

5.8: Device Characteristics

5.8.1: Significance of Single Mode Device

A single mode laser device is advantageous, as higher order modes have different effective refractive indexes they will have a different spectral position leading to an apparent broadening of the emission linewidth. A single mode device is expected to lase via fewer modes i.e. it would exhibit a lower 3-dB lasing spectral line width than a multi mode device [5.3]. A single lateral mode device is also generally needed for fibre coupling as the presence of higher order modes may result in a reduction in coupling efficiency of the laser.

5.8.2: Modal Behaviour of Innolume and Bi-layer Devices

A high resolution spectroscopy technique is generally used to resolve the electroluminescence spectra, in order to ensure single mode behaviour of the devices. An Advantest 8384 optical spectrum analyser was used for this purpose and electroluminescence spectra were resolved with 10pm resolution in each case to observe the Fabry-Pérot longitudinal modes as clearly as possible. The spectra were analysed over various wavelength ranges. Figures 5.9 (a, b) plots the resolved electroluminescence spectra as a function of wavelength, at 30°C heat-sink temperature under continuous wave measurement condition, for the Innolume (1mmx3µm) and bi-layer (4mmx5µm) laser devices.

According to the Figure 5.9 (a, b), in each case the mode position was predicted from the inspection of one of the spectra and was then predicted for the other two, to confirm the single mode behaviour. Mode beating for a second lateral mode was not observed for both devices and this was confirmed via inspection.

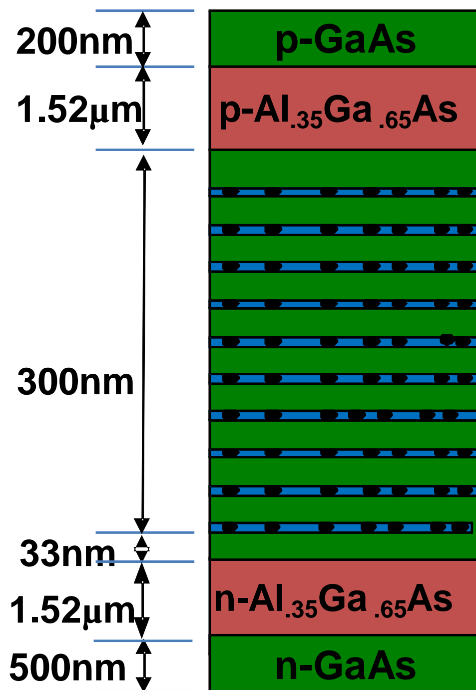

(a)

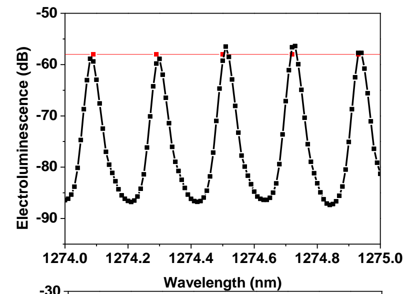

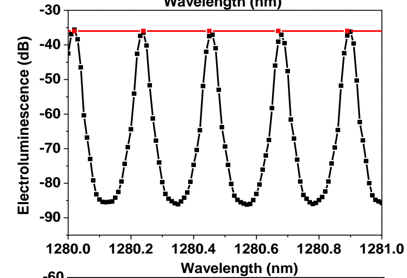

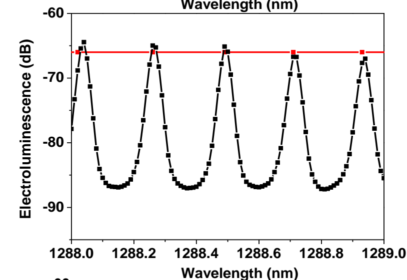

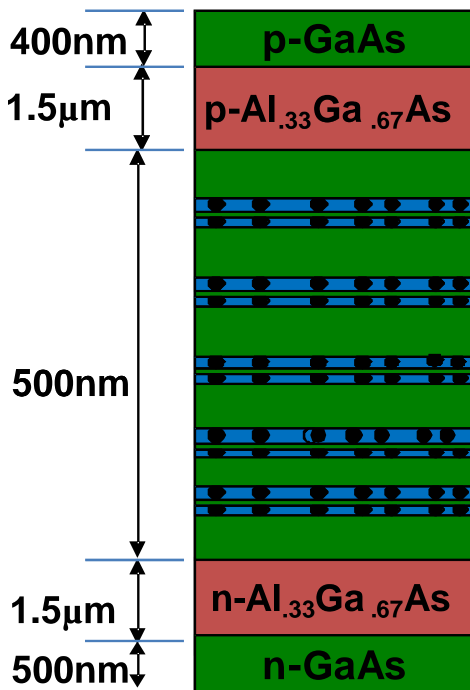

(b)

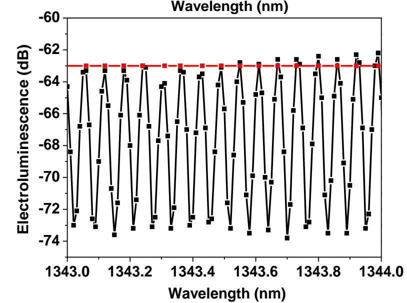

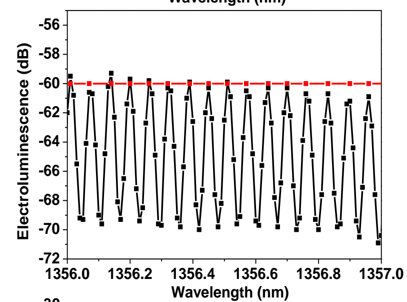

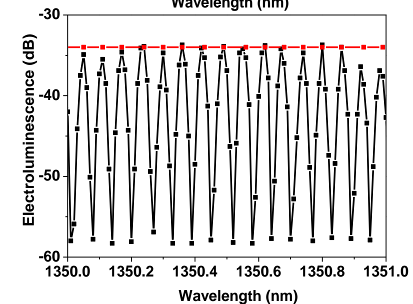

Figure 5.9: The schematic and electroluminescence spectra for (a) Innolume (1mmx3µm)**,** (b) bi-layer (4mmx5µm) QD laser devices showing single mode behaviour after lasing at 30°C heat-sink temperature under continuous wave operating mode.

5.9: 3-dB Line width Comparison

5.9.1: Light-Current Density Characteristics

In our case optical power as a fnction of current density was used to determine, the threshold current density and the external differential efficiency for each laser device.

5.9.1.1: Significance and Measurement of External Differential Efficiency

One of the basic and essential steps as a part of the characterisation of any laser device is to determine the external differential efficiency i.e. η_d. It is a measure of the efficiency of a laser device to convert electrical energy into output optical power. Theoretically, with an injection of 'q' coulombs within a particular time slot, the output optical power (photons emitted) produced for the same time interval is given by hc/λ (h: Plank's constant, c: velocity of light in vacuum, λ: wavelength of the photon) . Therefore, the η_d is calculated as hc/qλ.

It can be determined empirically via light-current density characteristics (L-J) of a laser device i.e. from the slope of the linear section above J_{th}. In this case the external differential efficiency for both facets is determined by eq.5.2:

$$\eta_d = 2\frac{dP}{dI}\left[\frac{q\lambda}{hc}\right] \qquad (5.2)$$

Where *P* is the optical out put power, *I* is the injection current, and the factor of 2 is for both facets. Here (eq. 5.2) in order to calculate the external differential efficiency of a device, we always compare the slope of L-J characteristics of the device (2dP/dI) with the slope (hc/qλ) of a 100% efficient device.

The η_d can also be calculated for a particular device length by eq.5.3.

$$\eta_d = \eta_i \frac{\alpha_m}{\alpha_m + \alpha_i} \qquad (5.3)$$

Where α_m is the mirror loss. The α_i is the internal loss: the characteristic of the device material. The η_i is the internal quantum efficiency of the laser.

5.9.1.2: Results

The internal loss (α_i) in each case was measured to be ~1.5cm^{-1} via net modal gain analysis as described in the section: 5.7.2. The mirror loss in each case was calculated by using the eq. 5.4:

$$\alpha_m = \frac{1}{2L} \ln\left(\frac{1}{R_1 R_2}\right) \qquad (5.4)$$

Where L is length of the laser device. R_1 and R_2 are the reflectivities of the both facets assumed to be 32% in each case.

For the 1mm Innolume and 4mm bi-layer laser devices the α_m was calculated as 11.4cm^{-1} and 2.8cm^{-1} respectively by eq. 5.4. Therefore, by using the information (α_i and α_m), values of external differential efficiencies were calculated (eq. 5.3) as 0.88η_i, for 1mm long Innolume and 0.65η_i, for 4mm bi-layer devices.

Figure 5.10 (a, b) plots, the light-current density characteristics for Innolume (1mmx3μm) and bi-layer (4mmx5μm) devices, at 30°C heat-sink temperature. The experimentally determined external differential efficiency values, by eq.5.2, were 20% and 18%, for Innolume (1mm) and bi-layer (4mm) devices respectively.

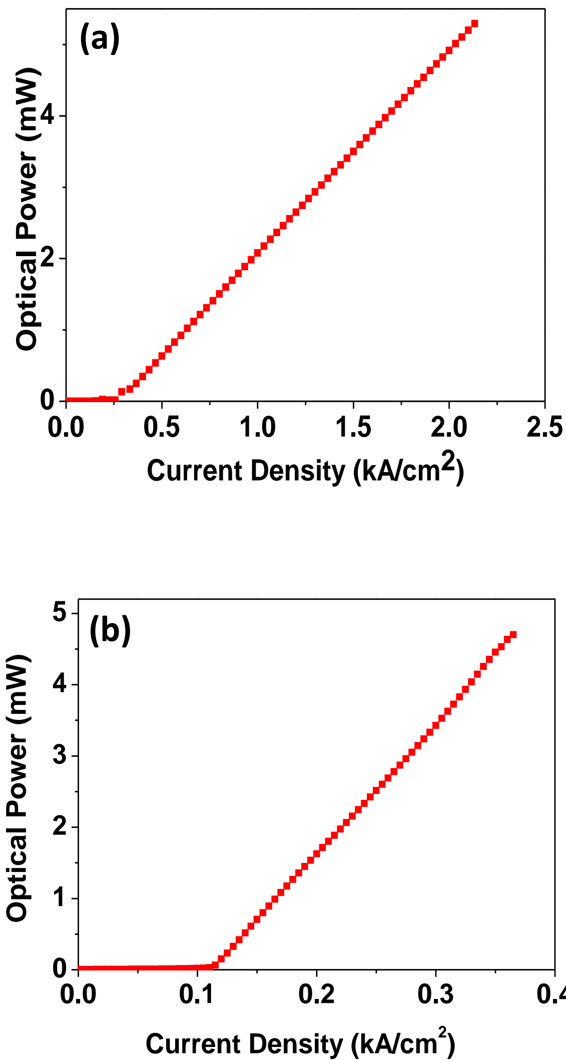

Figure 5.10: Light-current density characteristics (a) Innolume (1mmx3μm), (b) bi-layer (4mmx5μm) devices at 30°C heat-sink temperature, under continuous wave measurement condition.

5.9.1.3: Discussion

A low value for the experimentally determined differential efficiencies is observed for both devices. These reduced values of external differential efficiencies for both devices may be attributable to devices operating at ~ 63% of their maximum saturated modal gain values where gain cannot be described as being linear as a function of current density, as shown in Figure 5.8. At this point of operation, it is expected that the increase in photon density as a

function of current density starts deviating from the expected exponentially increasing behaviour.

5.9.2: 3-dB Line Width Comparison

5.9.2.1: Experimental Conditions

The 3-dB line width of the GS lasing spectrum was measured for the Innolume (1mmx3µm) and bi-layer (4mmx5µm) devices as a function of the same incremental steps of output optical power to analyse the effect of spectral hole burning in each case. The heat-sink temperature was kept constant at 30°C and devices were operated under continuous wave condition. The 10pm resolution adjustment was used to resolve the intensity spectrum properly.

5.9.2.2: Innolume Laser Device

5.9.2.2.1: Experimental Results

Figure 5.11 (a) plots the GS lasing spectra as a function of output optical power for the Innolume (1mmx3µm) device at 30°C under continuous wave operation condition. Figure 5.11 (b) plots the same GS lasing spectra as function of output optical power with a 10dB offset for each trace, in order to clearly observe the evolution of lasing spectrum as a function of output power. The 3-dB lasing spectral line width measurements were performed up to an optical power of 4.5mW and two important mechanisms can be noticed. Firstly, after 3.5mW the GS electroluminescence spectrum shows a dip in the middle of the lasing spectrum and secondly, the lasing spectra showed a red shift and a broadening with increased out put power levels.

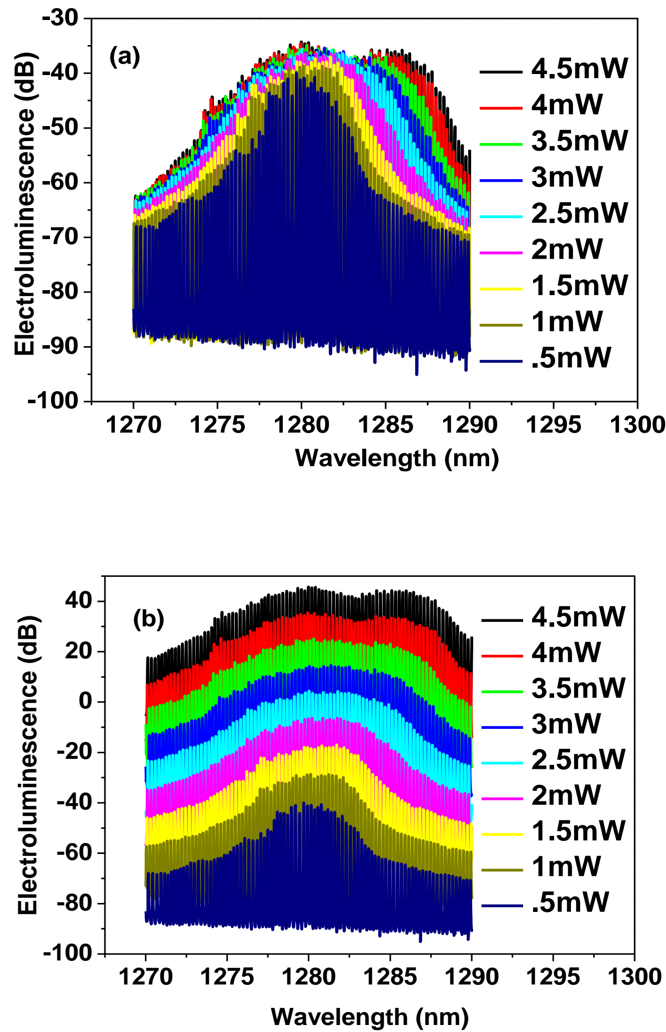

Figure 5.11: GS electroluminescence spectra as function of output optical power for Innolume (1mmx3μm) laser device (a) lasing (b) offset by 10 dB, at 30°C constant heat-sink temperature under continuous wave operation mode

5.9.2.2.2: Homogeneous Line Width of the Innolume Laser Device

Figure 5.12 (a) plots the measured, 3-dB lasing spectral line width as a function of output optical power for the Innolume (1mmx3μm) laser device at 30°C heat-sink temperature, under continuous wave operating. The blue line represents the data of the measured 3-dB line width after the dip in the middle of the GS lasing spectra was observed.

Figure 5.12 (b) plots the GS lasing spectrum at 4.5mW for the same experimental conditions as mentioned previously. From the Figure 5.12 (a), a dip in the middle of the GS lasing spectrum at 4mW was observed. Any further increase in the current density manifested itself as a decrease in the intensity of the central lasing modes and an increase in the intensity of the lasing modes on either sides of the dip. The difference between the peaks as shown in Figure 5.12 (b) on the either side of the dip at 4.5mW output optical power is quite obvious and was measured to be ~6nm(4±0.5meV).

5.9.2.2.2.1: Experimental Results and Discussion

The observed dip is attributable to the mechanisms which are already discussed in the literature [5.3] i.e. when homogeneous broadening becomes comparable with the inhomogeneous broadening then a laser device starts lasing via central lasing mode and all dots with in the range of homogeneous line width via carriers and photons contribute to the lasing and resultantly device lases via few modes. However due to the gain saturation, at current densities higher than the threshold after the gain saturation, when the carriers relaxation rate for the dots contributing to the central lasing mode becomes lesser than their stimulated emission rate, the corresponding mode looses the intensity and a dip equal to the line width of the mode/QD is observed. Then lasing process shifts to the other neighbouring modes and other lasing peaks are observed.

Such a dip with increase in excitation level has already been observed experimentally as well in the case of 1.3μm QD lasers [5.3]. Therefore, the observed difference between the peaks (4± 0.5meV) of the lasing spectrum in our case indicates the homogeneous linewidth of the QD, Innolume laser device.

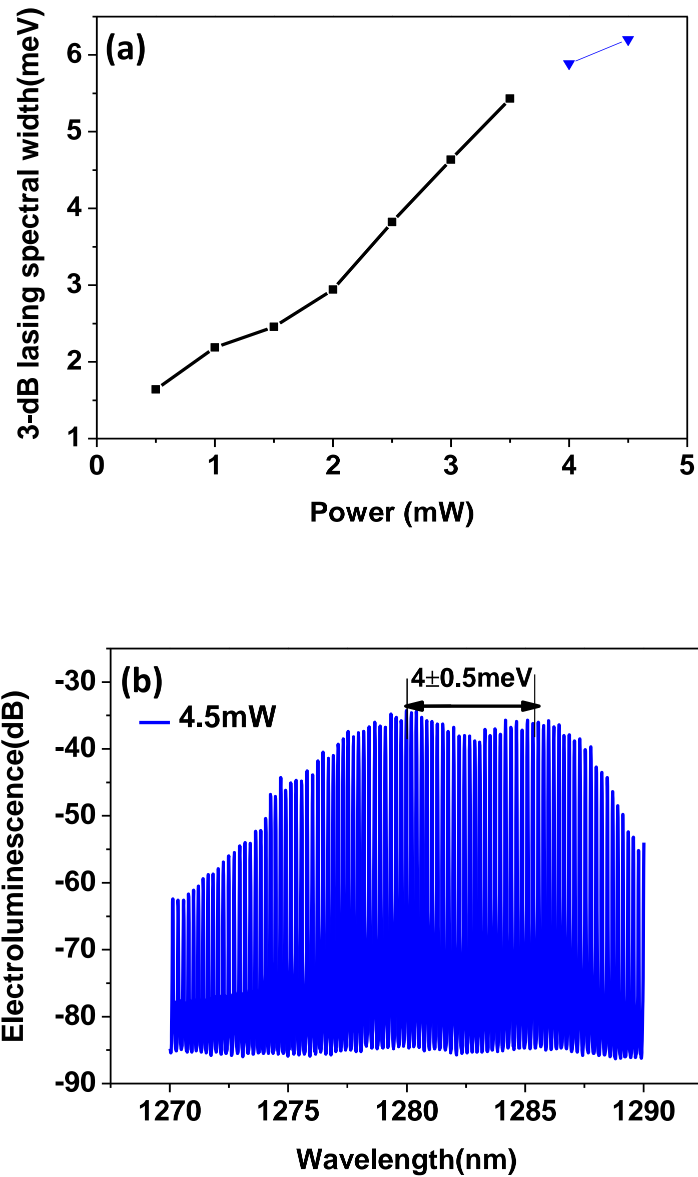

Figure 5.12: (a) GS, 3-dB lasing spectral line width as a function of power. (b) electroluminescence spectrum as a function wavelength at 4.5mW, 30^0C heat-sink temperature for Innolume (1mmx3μm) laser device under continuous wave measurement condition .

5.9.2.3: Bi-layer Laser Device

Figure 5.13 (a) plots the GS lasing spectral results for a bi-layer (4mmx5µm) laser device as a function of output optical power at 30°C constant heat-sink temperature, under continuous wave measurement conditions. Figure 5.13(b) plots the offset (10dB per trace), lasing spectra for the same device under the same experimental conditions, in order to observe the evolution of the lasing spectra. Figure 5.13(c) plots, the increase in 3-dB lasing spectral line width as a function of output optical power as was measured from Figure 5.13 (a, b).

An increase in GS 3-dB lasing spectral line width at 30°C under continuous wave measurement conditions for the bi-layer (4mmx5µm) laser device was measured as ~ 3nm (2meV) at 5mW. A red shift and a broadening with increasing output power were observed. In case of the bi-layer laser device, a dip similar to that of the Innolume (1mmx3µm) laser device was not observed for the GS, even up to 5mW.

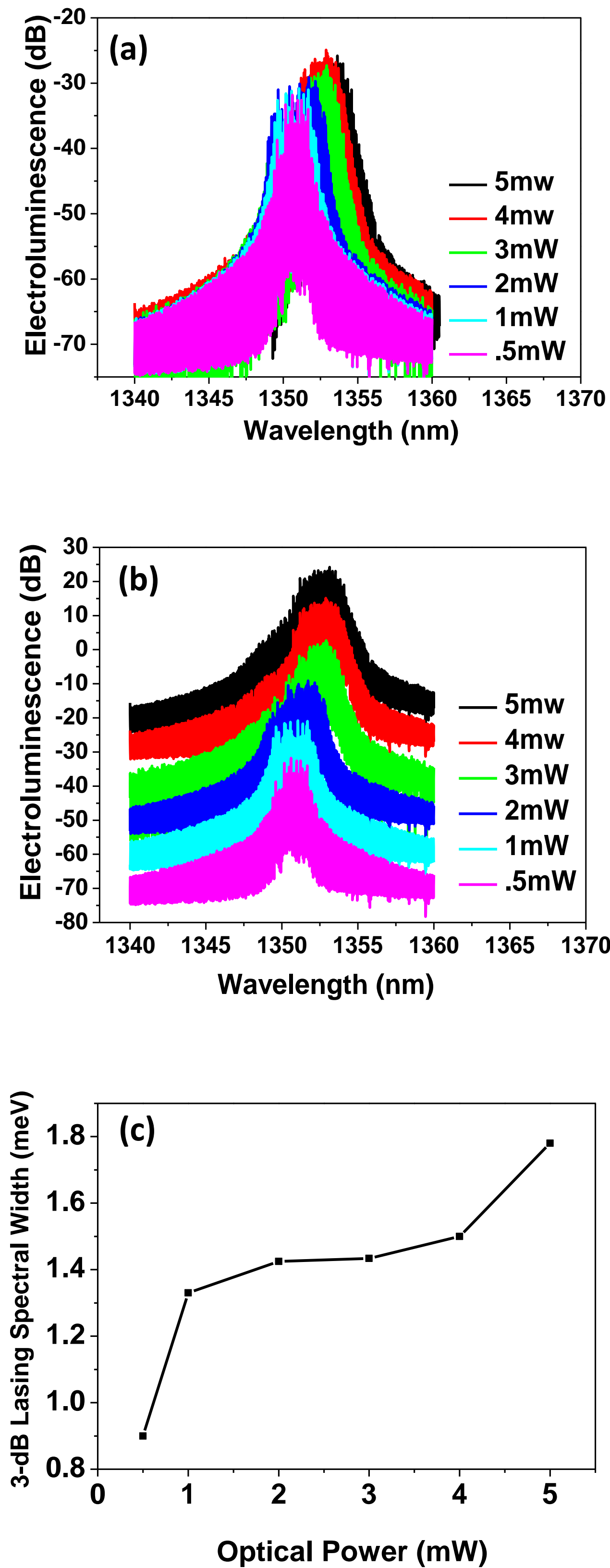

Figure 5.13: (a) GS , lasing spectra as a function of out put optical power, (b) GS, lasing spectra off set by 10dB, (c) 3-dB lasing spectral line width of GS for bi-layer (4mmx5μm) laser device at 30°C heat-sink temperature.

5.9.2.4: Comparison of 3-dB Lasing Spectral Line width

Figure 5.14 (a, b) allows a comparison of the devices by plotting the GS, 3-dB lasing line width for both devices (Innolume: 1mmx3µm, bi-layer: 4mmx 5µm) at 30°C heat-sink temperature. Figure 5.14 (a) plots the 3-dB lasing spectral line width as a function of the output optical power for each device, in order to try to make spectral hole burning effects similar. Figure 5.14 (b) plots the 3-dB lasing spectral line width of each device as a function of optical output power per quantum dot. The dot densities in the case of the Innolume and bi-layer materials are ~ $4x10^{10}/cm^2$ and $2.7x10^{10}/cm^2$ respectively. This is done in an attempt to normalise the removal of carriers from the lasing QDs.

5.9.2.5: Results and Discussion

The differential device resistances in both cases of the Innolume (~ 4ohms) and bi-layer (~ 3ohms) laser devices may cause different self heating effects which may influence their corresponding homogeneous broadenings. The analysis would be more reliable if the self heating effects are entirely removed by maintaining the junction temperature at a constant value by the method already described (Chapter: 3). However, the lasing spectra for the Innolume (1mmx3µm) and bi-layer (4mmx5µm) laser devices show approximately similar red shifts in lasing electroluminescence spectra (~ 3nm ±1). It is attributed to similar self heating effects due to the devices operating at same inversion level.

From Figure 5.14 (a) it can be observed that with an increase in output optical power for both of the devices, the 3-dB mode packet line width goes on increasing. For the same steps of increase in output optical power, the increase in the 3-dB lasing spectral line width and the rate of increase for the Innolume device is greater in comparison to the bi-layer device.

Figure 5.14 (b) plots the 3-dB lasing spectral linewidth as a function of output optical power/dot (photons/dot)). The purpose here is to try to make the spectral hole burning effects as similar as possible in both cases.

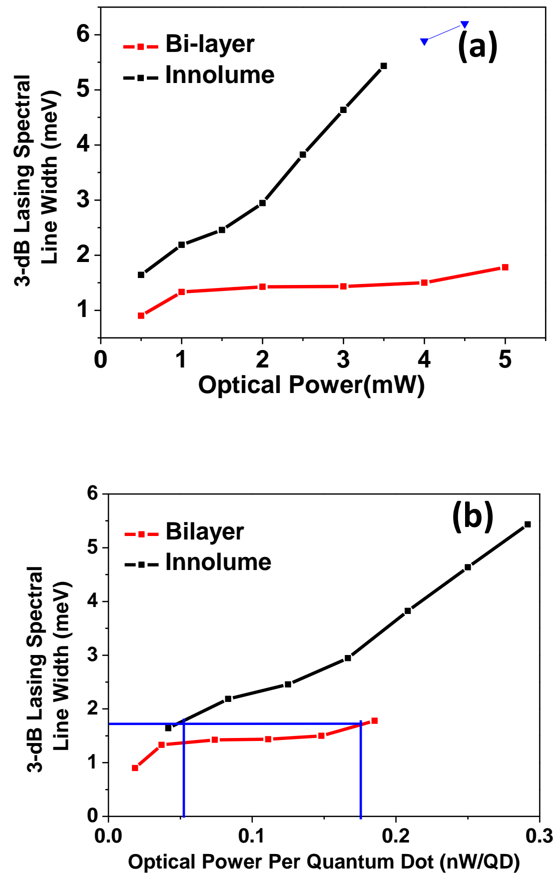

Figure 5.14: (a) 3-dB lasing spectral line width as a function of output optical power, (b) optical power/dot (photons/dot) for Innolume (1mmx3µm) and bi-layer (4mmx5µm) devices at 30°C heat sink temperature under continuous wave operation condition.

5.10: Summary

Bearing in mind the attempts made to maintain similar levels of homogeneous line-width and the effects of spectral hole-burning, the role of a reduced inhomogeneous line-width on reducing the lasing line-width has been highlighted. The results presented, on QD materials with inhomogeneous line-widths (as measured by low current density EL) differing from 40 meV to 27meV show quite different laser line-width characteristics with increasing output power. This is suggestive of inhomogeneous line-width being the key driver for the lasing line width for the Innolume sample. For the narrower bi-layer sample, the reduced lasing line-width, and reduced sensitivity to power within the mode suggests we are moving towards a realm where the homogeneous line-width is dominant. For these samples and conditions, the switch from the line-width being governed by the inhomogeneous line-width, to the homogeneous line-width is occurring in this range of values for inhomogeneous line-width.

5.11: Future Work

The reduction in laser line-width observed for the bi-layer sample is very promising for fibre-optic communications applications. These results point to continued work in developing the epitaxial processes to reduce the inhomogeneous line-width may pay off in large reductions in lasing line-width.

In terms of future experiments, a range of samples where only the inhomogeneity was changed would eliminate uncertainties present in these measurements due to different QD densities, chip lengths, etc. The noise characteristics of the devices would also be of interest.

References

[5.1] IEEE Corporate. (2009). 10Gb/s Ethernet Passive Optical Network [Online]. Available http://www.ieee802.org/3/av/ Accessed 5th October 2012.

[5.2] A. V. Savelyev, I. I. Novikov, M. V. Maximov, Yu. M. Shernyakov, A. E. Zhukov, "Temperature and current dependences of the lasing spectrum's width of quantum dot lasers" , Semiconductor Vol. 43, 12,1597 - 1601(2009).

[5.3] M. Sugawara, N. Hatori, H. Ebe, M. Ishida, Y. Arakawa, T. Akiyama, K. Otsubo, and Y. Nakata, "Modeling room-temperature lasing spectra of 1.3μm self-assembled InAs/GaAs quantum-dot lasers: Homogeneous broadening of optical gain under current injection", J. Appl. Phys. 97, 043523 (2005).

[5.4] A. Markus, M. Rossetti, V. Calligari, J. X. Chen, and A. Fiore, Role of thermal hopping and homogeneous broadening on the spectral characteristics of quantum dot lasers, J. Appl. Phys. 98, 104506 (2005).

[5.5] L. Harris, D. J. Mowbray, M. S. Skolnick, M. Hopkinson, and G. Hill, "Emission spectra and mode structure of InAs/GaAs self-organized quantum dot lasers", Appl. Phys. Lett. Vol. 73, 969 (1998).

[5.6] Mitsuru Sugawara, Kohki Mukai, Yoshiaki Nakata, and Hiroshi Ishikawa,"Effect of homogeneous broadening of optical gain on lasing spectra in self-assembled In_xGa_{1-x} As/GaAs quantuum dot lasers", Phys. Rev. B Vol. 61, 7595 - 7603(2000).

[5.7] Blood Peter, Gareth M. Lewis, Peter M. Smowton, "Characterization of Semiconductor Laser Gain Media by the Segmented Contact Method", IEEE J. sel. Top. In Quant. Elect. Vol. 9, 1275 - 1282(2003).

[5.8] K. Mukai et al, "Self-formed InGaAs Quantum Dots on GaAs substrates emitting at 1.3 μm", Jpn. J. Appl. Phys. Vol. 33, L1710(1994).

[5.9] K. Matsuda, K. Ikeda, T. Saiki, H. Saito, and K. Nishi, "Carrier–carrier interaction in single $In_{0.5}G_{0.5}As$ quantum dots at room temperature investigated by near-field scanning optical microscope", Appl. Phys. Lett. Vol. 83, 2250(2003).

[5.10] A. E. Zhukov, A. R. Kovsh, V. M. Ustinov, A. Yu. Egorov, N. N. Ledentsov, "Gain characteristics of quantum dot injection lasers", Semicond. Sci. Technol., Vol. 14, 18 - 123(1999).

Chapter 6: Conclusion & Future Work

The main aim of the thesis was to characterise 1.3μm QD laser devices in terms of their static performance via different gain measurement techniques. These devices are currently being commercialised in telecommunication and medical fields and have found their place in sensing devices and displays. Therefore, there is a need to improve upon their performance via understanding the physics of the devices. Gain measurement is a major technique to accomplish this. By gain measurement, we can determine the static and dynamic performance of a laser device and hence can optimise the device designs to improve their performance.

In chapter 2 initially a historical review of gain measurement techniques is presented, which is then followed by a technical review of three gain measurement techniques. The purpose mainly was to point the important aspects to be taken care off while selecting and then successfully implementing a technique. The methodology of comparison and analysis of the techniques presented here can further be used to evaluate any new gain measurement technique in terms of S/N ratio, low and high current density measurement and resolution requirements.

The chapter 3 presents the empirically obtained gain data obtained under the strict conditions of constant heat sink and constant junction temperature conditions. Therefore presents an excellent comparison of spectral gain measurements with and without self heating effects. The origin of negative differential gain is explored due to the free carrier effects. This can further lead to designing high speed switching laser devices. The concept of Poisson carrier distribution and corresponding shift and asymmetric broadening of the gain spectrum has been explained fully. This can lead to futuristic low threshold devices having a reduced inhomogeneous line width. The physics of carrier dynamics at high current densities

explained in this chapter can lead to understanding the behaviour of dual state lasing devices and SOAs.

In chapter 4 the gain characterisation at very low carrier density was made possible by demonstrating an integrated amplifier. The noise due to the integrated amplifier in the gain spectra was less and 3-dB amplification was achieved without any spectral mismatch with the signal getting amplified. This low carrier density analysis can further be used to explore the carrier distribution (Fermi/random) among dots, in case, if more optically efficient materials are available. The analysis would be more reliable if self heating effects are entirely removed via method explained in chapter3.

Chapter 5 discusses the effect of inhomogeneous linewidth on lasing spectral line width of the laser devices. It shows that for the laser device having more value of inhomogeneous line width the lasing line width is controlled via inhomogeneous line width. However for the devices with very less inhomogeneous line width the lasing line width remain small and independent of the output optical power and spectra broadens homogeneously. The analysis was accomplished empirically by comparing a bi-layer laser device with a commercial Innolume material. In this case spectral hole burning and homogeneous line width of the two materials were kept constant to make a fair comparison and to infer the interdependence of inhomogeneous line width and lasing line width. However the carrier life time may be another point to be considered while comparing the materials in future, as it can effect the lasing line width as well.